GENERATION AND DYNAMICS OF OPTICAL DISSIPATIVE SOLITON

A Thesis Submitted
in partial fulfillment of the requirements
for the degree of
Doctor of Philosophy

by
Gurkirpal Singh Parmar
(Regn. No. 901212012)

Under the Supervision of

Dr. Soumendu Jana
(Associate Professor)

THAPAR INSTITUTE
OF ENGINEERING & TECHNOLOGY
(Deemed to be University)

to

SCHOOL OF PHYSICS AND MATERIALS SCIENCE
THAPAR INSTITUTE OF ENGINEERING AND TECHNOLOGY, PATIALA-147004
INDIA
January 2018

DECLARATION

I, Gurkirpal Singh Parmar, hereby certify that work presented in this thesis entitled "*GENERATION AND DYNAMICS OF OPTICAL DISSIPATIVE SOLITON*" submitted in partial fulfilment of the requirement for the award of degree of DOCTOR OF PHILOSOPHY in the School of Physics and Materials Science, Thapar Institute of Engineering and Technology, Patiala is an authentic record of my own work carried out under supervision of Dr. Soumendu Jana. The matter embodied in this thesis has not been submitted in part or full to any other university or institute for the award of any degree.

Gurkirpal Singh Parmar

Gurkirpal Singh Parmar

This is to certify that the above statement made by the candidate is true to the best of my knowledge.

Soumendu Jana

Dr. Soumendu Jana
Associate Professor
School of Physics and Materials Science
Thapar Institute of Engineering and Technology
Patiala

ACKNOWLEDGEMENTS

First of all, I express my sincere gratitude to my thesis supervisor Dr. Soumendu Jana for his support, valuable advice and encouragement throughout the course of this thesis. It would have been difficult to complete this work without his help.

I thank Dr. O. P. Pandey, Dean of Research and Sponsored Projects, for his support at different stages. I also thank Prof. N. K. Verma and Prof. Kulvir Singh, School of Physics and Materials Science, TIET, Patiala for always motivating me.

I acknowledge Head of SPMS, Dr. M. K. Sharma for his support. I thank all members of my doctoral committee- Dr. B. C. Mohanty, Dr. Debabrata Deb and Dr. Mahesh Kumar Sharma for having valuable discussions with them and their suggestions. A special thanks to Dr. Debabrata Deb for his help. I am very grateful to Prof. Boris Malomed, Tel Aviv University, Israel,for his valuable support.

Financial support from Technical Education Quality Improvement Program(TEQIP) and Thapar Institute of Engineering and Technology is thankfully acknowledged.

I would also thank to my all friends from whom I learn the art of happiness and never give up approach. I would like to give special acknowledgement to my fellow research scholars Ajitpal Singh, Baldeep Kaur, Jaspreet Kaur, Indu Gupta and Neeraj Sharma for making my campus and lab time enjoyable.

I would like to express my sincere and deep gratitude to my parents and sisters for their love, encouragement, care and support. I am indebted forever to my dear wife Chandni Parmar for supporting me at every step.

Above all, praise to the Almighty for everything.

Gurkirpal Singh Parmar

PUBLICATIONS

I. SCI Journals:

1. *Bistable Dissipative Soliton in Cubic-Quintic Nonlinear Medium with Multiphoton Absorption and Gain Dispersion.*
   Gurkirpal Singh Parmar and Soumendu Jana, Journal of Electromagnetic Waves and Applications **29**, 1410-1429 (2015).

2. *Dissipative Soliton Fiber Lasers with Higher-Order Nonlinearity, Multiphoton Absorption and Emission, and Random Dispersion.*
   Gurkirpal Singh Parmar, Soumendu Jana and Boris A. Malomed, Journal of Optical Society of America B **34**, 850-860 (2017).

3. *Dispersion-Managed Soliton Fiber Laser with Random Dispersion, Multiphoton Absorption and Gain Dispersion.*
   Gurkirpal Singh Parmar, Rajib Pradhan, Boris A. Malomed and Soumendu Jana, Journal of Optics, **20**, 105501 (2018).
   .

4. *Dissipative Soliton Fiber Laser with Higher Order Dispersive and Nonlinear Effects.*
   Gurkirpal Singh Parmar, Boris A. Malomed and Soumendu Jana, (submitted).

Relevent Research Papers (Not included in thesis):

5. *Evolution of Bell-Shaped Dissipative Optical Solitons from Super- Gaussian Pulse in Parabolic Law Medium with Bandwidth Limited Amplification.*
   Soumendu Jana, Shivani, **Gurkirpal Singh Parmar**, Baldeep Kaur, Qin Zhou, Anjan Biswas and Milivoj Belic, Optoelectronics and Advanced Materials-Rapid Communications **10 (3-4)**, 143-150 (2016).

6. *Dispersion Managed Dissipative Solitons with Higher Order Nonlinearity and Frequency-Selective Feedback.*
   Kadam Bhambri, **Gurkirpal Singh Parmar**, Neena Gupta, Debabrata Deb and Soumendu Jana, Optical and Quantum Electronics **49**, 376(1-21) (2017).

II. International Conferences:

1. *Pulse propagation in cubic-quintic nonlinear medium under the influence of gain dispersion, two-photon absorption and three-photon absorption*
   Gurkirpal Singh Parmar and Soumendu Jana, 12^{th} International Conference on Fiber Optics and Photonics (Photonics-2014) held at IIT Kharagpur, West

Bengal, India (December 13-16, 2014).

2. *Dissipative Soliton in optical fiber with multiphoton absorption and random dispersion*
Gurkirpal Singh Parmar and Soumendu Jana, Workshop on Recent Advances in Photonics (WRAP-2015), IISC Bangalore, India (December 16-17, 2015).

3. *Generation and interaction of dispersion- managed dissipative soliton in optical fiber with multiphoton absorption and higher order nonlinearity*
Gurkirpal Singh Parmar and Soumendu Jana, 13^{th} International Conference on Fiber Optics and Photonics (Photonics-2016) held at IIT Kanpur, Uttar Pradesh, India (December 4-18, 2016).

III. National Conferences:

1. *Spatio-Temporal Soliton in Inhomogeneous Nonlinear Media*
Soumendu Jana, **Gurkirpal Singh Parmar** and Kanupriya Garg, DAE-BRNS National Laser Symposium (NLS-22) held at Manipal University, Manipal, Karnataka, India (January 8-11, 2014).

2. *Dispersion- Managed Dissipative Soliton in Higher Order Nonlinearity*
Gurkirpal Singh Parmar and Soumendu Jana, National Conference on Photonics and Materials Science (NCPMS-2015) held at Guru Jambheshwar University of Science and Technology, Hisar, Haryana, India (November 17-18, 2015).

3. *Super- Gaussian dissipative soliton in higher order nonlinear medium with frequency selective feedback*
Soumendu Jana, Shivani, **Gurkirpal Singh Parmar** and Baldeep Kaur, DAE-BRNS National Laser Symposium (NLS-24) held at RRCAT, Indore, Madhya Pradesh, India (December 2-5, 2015).

ABSTRACT

Optical fiber based laser has emerged as a big contender in industrial as well as experimental laser. Their performance can be improved by employing the concept of soliton. This thesis presents theoretical investigations on the generation, stability and interaction of optical dissipative solitons in semiconductor doped fiber laser cavity under the influence of various higher order nonlinear and dispersive effects. The soliton conditions are established and the roles of the dispersive as well as nonlinear effects on the dissipative solitons are found using a variational method based analytical approach. The analytically results are verified by split-step Fourier method based numerical approach. Phase controlled and temporal separation controlled soliton switching are investigated through interaction of two dissipative solitons.

Optical dissipative soliton is generated in a lossy fiber with cubic-quintic nonlinearity, multi-photon absorption and gain dispersion. Rayleigh's dissipative function in conjugation with variational method is used to analytically solve the governing complex cubic-quintic Ginzburg-Landau equation and validated numerically. Impacts of two photon and three photon absorptions that arise due to positive imaginary parts of third and fifth order susceptibility respectively are found to be detrimental on the pulse as well as soliton. The negative imaginary part of fifth order susceptibility may lead to three photon emission, which provides an alternative gain mechanism for the stable dissipative solitons, provided that it is not too strong, to avoid the onset of the blowup.

Real fibers may feature a variety of imperfection like shape variation, inhomogeneous refractive index and dopant concentration, bending effects etc. These effects are random in nature and manifest themselves through random variations of the group velocity dispersion. Dissipative solitons are generated in such random dispersive optical fiber laser cavity with cubic-quintic nonlinearity, multi-photon absorption and gain dispersion. They also remain stable under the action of perturbation in the form of the random dispersion as well as noise. The dissipative solitons generated in both random and non-random environment are bistable, with two different pulses, low- and high-amplitude ones, found for a given width. In the presence of the nonlinear gain,

the low-amplitude dissipative soliton is stable, while its high-amplitude counterpart is subject to the blowup instability. Interactions between the dissipative solitons lead to fusion of high-amplitude solitons into breathers, and periodic merger-splitting sequences for low-amplitude ones. Relative-phase-controlled switching is obtained by the interaction of two dissipative solitons.

Dispersion management, a technique for soliton stabilization is used for generation of dissipative soliton in a fiber laser cavity with cubic-quintic nonlinearity, multiphoton absorption and gain dispersion. Each of the anomalous and normal fiber segments of the dispersion map is having some random dispersion fluctuation. The dispersion-managed dissipative breather solitons are robust against certain level of noise. Soliton switching between low to high speed regime is achieved by varying the temporal separation as well as relative phase between the dispersion-managed dissipative solitons.

Due to the ultrashort duration, dissipative solitons in fiber laser cavities are subject to higher order dispersion and nonlinear perturbations, particularly, third order dispersion and intrapulse Raman scattering. Stable dissipative solitons are generated in such systems. Roles of the perturbations on dissipative solitons are shown in a doped fiber cavity with cubic-quintic nonlinearity, multi-photon absorption and gain dispersion.

The results reported in the thesis suggest new experiments on dissipative soliton fiber laser and dispersion-managed dissipative soliton laser, all-optical switching devices, all-optical data processing and all-optical delay lines.

CONTENTS

LIST OF FIGURES

Chapter 1

Introduction

During last several decades soliton remained as a very active topic of research. Solitons are localized structure that retain their shape even after collision with another soliton [1]. When the broadening of a wave is restricted by nonlinearity induced contraction, one may get a solitonic structure. Although first observed long back in 1834 by John Scott Russell, soliton research attracted adequate attention only after the middle of the last century. As of now it is a well explored and matured field. Soliton research involves multidisciplinary research knowledge, in turn has applications in various fields of Physics, Chemistry, Engineering and Biology and even in Social Science [1–5]. In fact, it is now believed by scientific community that if there is a wave, there is a possibility of soliton formation.

Optical solitons are self-confined beams or pulses that retain their shape during propagation. They originate as a result of interaction between two counteracting phenomena: broadening due to group velocity dispersion (self-diffraction) and contraction due to nonlinearity-induced self-phase modulation (self-focusing) [6–8]. These self-organized and self-maintained solitons are remarkably robust against various perturbations. In view of confinement in space or time domain two broad categories of solitons can be formed. Any laser beam, due to their small aperture tends to diffract, which results in broadening of the beam (self-diffraction). If such laser beams, which has for example, Gaussian intensity and hence refractive index profile (along transverse

direction) is propagating through nonlinear medium, then by virtue of nonlinearity it may tend to be self-focused. When self-focusing perfectly compensates self-diffraction, the beam propagates as a self-trapped beam (i.e. no change is observed in spatial dimensions of the beam) or a spatial soliton [9–11]. The other kind of soliton is temporal soliton, which arises due to their confinement in time. Optical temporal solitons are formed due to the balance between dispersion induced pulse broadening and nonlinearity-induced pulse contraction (i.e., self-phase modulation) [12–14]. A third category, named spatio-temporal soliton can also be generated, which is confined both in spatial and temporal domain [6,9,12]. Spatiotemporal solitons are popularly referred as 'light bullet'. Taking into account their properties, the solitons appears as the best candidate for transport and processing of information [15], all-optical signal processing and all-optical computation.

However, the concept of soliton originate generally in conservative systems, i.e., lossless environment. In contrast, most of the practical systems are lossy in nature. The concept of soliton can be extended to those lossy or dissipative systems also. Dissipative solitons (DS), broadly speaking, are those self-confined structures which originate in lossy nonlinear systems. In the vast diversity of DS, the optical dissipative solitons (ODS) acquired appreciable attention from both theoretical as well as experimental research fields [16–20]. The DS can be viewed as an addition to the conventional solitons of conservative. DSs are observed in an open system that is far from equilibrium. In such systems, energy as well as matter can enter and leave the system through its boundaries [1]. Since the system is dissipative, pumping is very essential in formation as well as maintaining DS. Thus, in dissipative systems, in addition to the balance (which is common in conservative solitons) of diffraction/dispersion with nonlinearity, another balance, i.e., loss by gain is very much essential. Mathematically, conservative solitons corresponds to integrable (usually by means of inverse scattering method) systems, while those of DS and ODS are mostly nonintegrable. Due to only one fold

balance the conservative systems have single parametric family of soliton solutions (Figure 1.1 a). But in dissipative system, the additional gain-loss balance leads to fixed point solutions (Figure 1.1 b). The following figure, suggested by Akhmediev et al. [1] will be helpful to understand the fact.

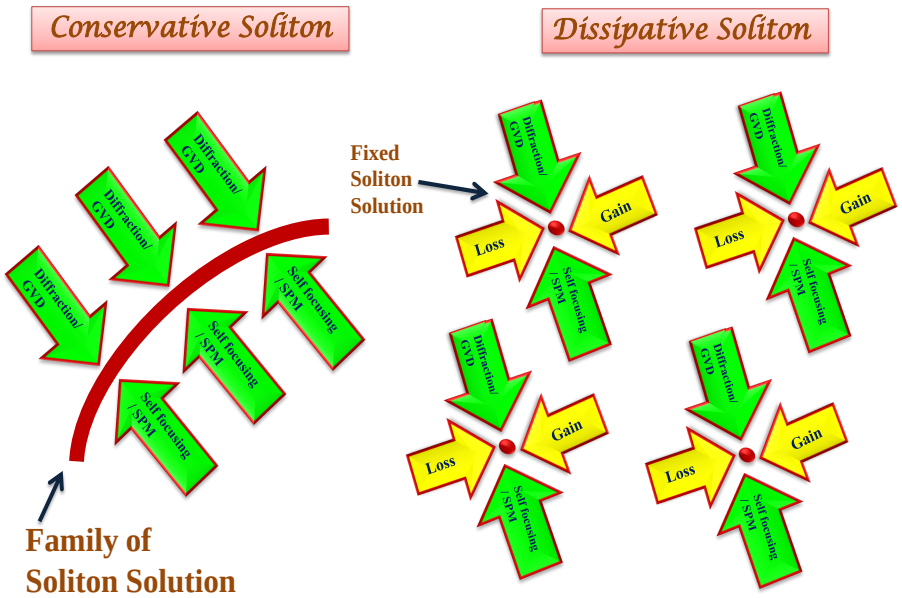

Fig. 1.1: Qualitative differences between the solitons in conservative and dissipative systems.

The amplitude, width and shape, of DS are well defined and these depend on the equation parameters. DS can acquire different shapes. It shows a number of periodic and chaotic changes. Dissipative systems have regions from where they absorb energy from an outside source and also the regions from where energy is lost to the environment [2]. In most of the dissipative solitons, energy flow from centre to the tails. In view of the supply of external energy (or matter in some case) to keep the dissipative soliton sustained, they can be considered as a 'living thing'.

Soliton in complex nonlinear dissipative systems are now attracting extensive research interest [21]. They can be found in a wide variety of systems: nonlinear optics [1, 2], chemistry [5], fluid dynamics [16], biology [17], ferrofluids [18], granular media [19] and gas discharge etc. [22]. DSs can exist in nature as well as they can

be created in laboratories. Some other interesting examples of DSs in nature are the tsunami waves, sand dunes in deserts, morning glory or rolling cloud, which can be long up to hundreds of mile [2]. The theory for naturally occurred DSs is extremely complex. Examples in optics include ultra-short pulses, spatial structures and soliton propagation found in mode-locked lasers, wide-aperture laser systems and long-haul all-optical transmission systems, respectively. For the stable operation of these systems, the continuous supply of energy and proper choice of parameters is necessary. Like other DSs, an essential balance between energy supplied and loss is required for ODS also [23]. To prevent overheating or cooling of the system, this equilibrium must be exact. The nonlinear dynamics of the system are associated with this exact balance. This means that DSs have to be self-localized. Nevertheless, for given external conditions, their amplitude, width and shape are unique.

ODS study connects three novel concepts, namely, the basic soliton theory, the nonlinear dynamics and the concepts of pattern formation [1, 2]. This requires a great deal of mathematical modelling and thus attracted a vast mathematical research community too. This large family of DS systems can be modelled by either complex Ginzburg Landau equation (CGLE) [1–5, 23], or complex Swift-Hohenberg equation (CSHE) [1] or Lugiato-Lefever equation (L-L) [24]. Most of the models are non-integrable, can be solved generally following numerical methods. However, variational method based analytical approach, though approximate, is developed for simulation and to avoid tiresome numerical computations essential to find out the stability domain [25]. It should be remembered about the dissipative systems that although the systems are lossy, they doesn't have only decaying solutions. Another interesting aspect of this research is its connection with pattern formation. Most of the DS systems are explained by using nonlinear partial differential equations. Different kind of transformations i.e. either smooth or in form of divisions or bifurcations, of DS can be observed.

1.1 Development of DS Over Decades

Within last few decades the research on DS as well as ODS has become very enriched. A major portion of DS research is theory driven. Several mathematical models have been developed to address the problems related to DS. Neil Akhmediev and co-workers [1,2, 23], Boris Malomed and co-workers [21, 22], Govind Agrawal and co-workers [6, 26]are among the pioneer research groups working for the growth and development of this dynamic field.

There are various models that support the generation of DS in optics. The basic model which describes nonlinear phenomena in a system, which is far from equilibrium is complex Ginzburg Landau equation (CGLE) [27]. CGLE describes the dissipative systems near subcritical bifurcations [28]. Corresponding solitons are called DS in CGLE. A large variety of solitons can be formed in CGLE, e.g., stationary solitons, sources, sinks, moving solitons and fronts with fixed velocity [29]. Thual and Fauve observed stable pulse-like solutions of the quintic CGLE [30]. The minimum requirement for their stability were also calculated [31]. The stable solutions of the 1D-CGLE were presented and analyzed by Akhmediev and co-workers [32]. The energy and momentum balance equations determine the distance and the phase difference between the soliton pulses. A 2-D phase plane was introduced for studying the general dynamics and stability criteria of the system [29]. Crespo et al. reported a pulsating soliton in CGLE that periodically modifies its shape with time [33]. These solitons can be excited for a wide range of parameters and are subjected to restructuring to finally develop into stationary solitons [34] and thus are considered to be stable limit cycles in the finite-dimensional dynamical system [35, 36]. It was observed that when ripples increases, the soliton cracks into pieces, eventually results in the generation of erupting solitons [37]. With the changes in parameters, a rectangular pulse and a sink was observed. Then the solitons formed were called creeping solitons [33]. These solitons

generated by solving CGLE were also observed in mode locked lasers [38]. The pulsating solitons were classified into two categories namely plain pulsating soliton having single period of pulsations and quasi-periodic soliton with several periods. An another class of pulsating soliton is known as exploding soliton, in which the evolution starts from a stationary localized structure having a perfect soliton shape but with time, pulse get covered with seemingly chaotic structure [33]. A linear stability analysis of exploding solitons of CGLE equation was performed [39]. A set of perturbation eigen values for these solitons were found numerically and scenario for chaotic soliton dynamics was given based on this analysis.

Akhmediev et al. demonstrated collisions of groups of DSs in a fibre laser cavity by using numerical as well as experimental methods [40]. Two models namely the continuous CGLE and the CGLE with parameter management, were considered for studying the system and proper parameters were chosen to study the interaction behaviour between the solitons in fiber laser cavity [1]. The results obtained could be helpful in understanding the interactions when the number of solitons in the laser. The work was considered helpful in understanding more complicated interactions of DSs, when more than three solitons are present in the fibre laser cavity [41].

Ankiewicz et al. obtained the exact solutions of CGLE for dissipative system, by using Lagrangian minimization technique and were found to be in agreement with the solutions obtained by using moment method [42]. Stability of one, two, and three dimensional CQGLE (cubic-quintic Ginzburg Landau equation) were established using variational method based on the Lagrangian approach [43]. The input pulse parameters were found that finally results in a stable DS. The treatment of (3+1)-dimensional CQGLE was done analytically by variational method and also numerically [44]. Light bullets generated in this case were very robust and even resisted the successive increase of amplitude during its formation. Two kinds of stationary stable solitons namely solitons and antisolitons having opposite internal energy flux directions and opposite

chirp were observed [45]. At certain values of the system parameters, the energy of the soliton can increase indefinitely due to dissipative soliton resonance (DSR) which can be very useful in the design of high-energy ultra-short pulses [46, 47]. The idea of DS has remarkably influenced the dynamics of passively mode-locked lasers that some systems are now called as dissipative soliton lasers [47–50]. It was observed that physical properties like pumping power, mode-locking mechanism and the sign of chromatic dispersion, have no significant effect on large variety of DSs [48]. A dual-wavelength DSs in net-normal dispersion regime were experimentally observed in figure-eight passively mode locked fibre laser [51]. Luo et al. investigated polarization-insensitive figure-eight fiber laser for the vector characteristics of the pulse operating DSR region [52]. The two polarization components were observed to be having different spectral distributions. The external continuous wave (CW) effect was studied on the motion of CGLE solitons. When amplitude of CW is small, soliton motion is induced [53]. It was observed that active mode-locking in super long lasers has many advantages over passive mode-locked laser such as self-triggering, stability of single-pulse lasing, synchronisation of the pulse repetition rate [54]. Primarily soliton was demonstrated in a system with anomalous dispersion gradually, normal dispersion come into the picture. Not only anomalous dispersion, the normal dispersion is also used for DS generation. Pulse operation in all-normal-dispersion dissipative soliton fiber laser mode-locked by nonlinear polarization rotation were demonstrated [55]. Through adjustment of the pump power and orientations of the wave plates, harmonic mode-locking, bound states, and dual-wavelength dual-pulse states were obtained. This work gives a more clear understanding on the characteristics of all-normal dispersion dissipative soliton fiber lasers. Also DS have been observed in complex Swift- Hohenberg equation (CSHE) [56]. On solving CSHE numerically, several types of stationary and moving solitons were observed to be stable and they have existence for wider range than those for CGLE. It was also noted that by changing the parameters of the nonlinear gain, different types

of soliton pairs can be generated [56]. Similar localized patterns were also observed by solving Lugiato-Lefever equation [L-L] [24]. It was observed that small DS bifurcated from the trivial equilibrium [57].

Very robust gain guided solitons in dispersion-managed (DM) fibers with net positive group velocity dispersion (GVD) have been observed [58]. DM soliton fiber ring laser operation at near zero cavity GVD in a passively mode locked erbium doped fiber shows the Gaussian like profile of the soliton spectrum of the laser without spectral sidebands [59]. The nonlinearity of the fiber laser cavity can be managed by relating the output coupling position and strength in an erbium doped mode-locked fiber laser which helps in generating high peak power pulses [60]. Antisymmetric DM solitons have been observed with a strong dispersion map in ytterbium-doped fiber laser at a particular net cavity dispersion [61]. The chirped fiber Bragg grating was used to get net normal dispersion value in an antimonide- based saturable absorber that has been used to generate a dissipative DM soliton in thulium-holmium mode locked fiber laser [62].

1.2 Motivation

Although significant work has been done in ODS in fiber, still there is a great scope of further development. Most of the investigations use the basic model which are somewhat simplified. With the introduction of ultrashort pulses and nonlinear fiber materials, the higher order nonlinear effects are readily observable in optical fiber even at moderate light intensity. More attention can be paid to explore ODS with such higher order nonlinear effects. In our case, emphasis will be given to make the model more realistic by studying the generation of ODS in the presence of higher order nonlinear phenomenon and their effect in soliton dynamics in fiber laser cavity.

Generally most of the theoretical models refer optical fiber. Ideal fiber model generally consists of constant core diameters and thus does not include any kind of imperfec-

tions in the fiber geometry. Thus to make our system more realistic, a random system is preferred to study the generation of DS in fiber laser cavity. Due to small core diameters and with the usage of high intensity pulses, these fiber lasers generally show higher order effects which can have both detrimental as well as advantageous effects on the DS. Also, less attention has been paid to the dynamics of the individual ODSs. Their interaction, which is yet another important aspect, has not been explored properly. Thus, investigation of the dynamics of individual DS and interaction between them is on demand. Also to get a complete knowledge of the behavior of the DSs the interaction dynamics is very crucial. Apart from being a topic of fundamental research interest the soliton dynamics has potential application in developing all-optical switching devices, all-optical data processing, all-optical delay lines and optical communication links.

1.3 Objectives

The objectives of our PhD proposal are as follows:

1. To find the parametric region of existence of optical dissipative solitons in semiconductor doped fiber laser cavity.

2. To find the stability criteria of the optical dissipative solitons in semiconductor doped fiber laser cavity.

3. To study the dynamics of the optical dissipative solitons.

1.4 Outline of the Thesis

The layout of the thesis is as follows:

Chapter 1 describes the introductory part of the thesis. It includes the basic introduction to soliton and dissipative Soliton. The historical perspective of theoretical, analytical and numerical study and growth of DS is provided. A review of literature and motivation behind the presented work are also presented.

Chapter 2 includes the basic knowledge of different phenomena that are pivotal for the understanding of the DS. This chapter provides the information of different types of linear and nonlinear optical phenomena that are Common in optical fiber cavities. Difference between dissipative and conservative soliton is presented. Fiber laser is also described. The mathematical schemes, both analytical and numerical, required for the study of DS are also discussed.

Chapter 3 contains an investigation on the generation of DS in doped fiber in higher nonlinear media under the effect of multi-photon absorption and gain dispersion. The analytical model for soliton evolution is designed using CGLE. The analytical solutions of the system are obtained using variational method in conjugation with Rayleigh's dissipative function. The results obtained analytically are verified numerically by using split-step Fourier method (SSFM). Stability zone for dissipative soliton generation is also presented.

Chapter 4 presents the generation of DS in fiber laser cavity under the combined effect of cubic-quintic nonlinearity, multiphoton absorption and/or multiphoton emission and gain dispersion. To make the system more realistic randomly varying GVD along the length is also introduced. The conditions for stable operation of the laser in the DS regime are found. The observed DSs are found to be bistable, high- and low- amplitude ones for the same width. Stability of DSs in the presence of perturbation in form of the random GVD and noise is also checked. Interaction and switching dynamics of the DSs are also explored.

Chapter 5 describes another important technique of soliton generation; the dispersion-management, is described. The generation and interaction dynamics of dispersion-managed dissipative soliton (DMDS) in a doped fiber laser with cubic-quintic nonlinearity, multiphoton absorption and gain dispersion has been presented. Like a real practical fiber, each of the anomalous and normal fiber segments of the

dispersion map is having some random dispersion fluctuation. Role of temporal separation as well as phase difference between the interacting dispersion-managed dissipative solitons and switching phenomena have been studied.

Chapter 6 Higher order dispersive and nonlinear effects impose great challenge against the soliton formation and its stability. In the preceding chapters up to second order dispersion is considered. In this chapter, we consider the third order dispersion (TOD) and intrapulse Raman scattering in optical fiber laser in presence of cubic-quintic nonlinearity, two-photon absorption, three-photon absorption, gain dispersion and loss. The role of TOD and impact of intrapulse Raman scattering in soliton generation has been investigated. Dissipative soliton interaction has also been discussed.

Chapter 7 summarizes the work carried out. It also discusses scope for future work.

Chapter 2

Essentials of Dissipative Solitons

Any soliton and hence dissipative Soliton (DS) is an important example of beneficial use of optical nonlinearity. DS is formed as a result of balance of nonlinearity of the medium and dispersion/diffraction present in the system along with an additional gain-loss balance. So optical nonlinearity plays a very important role in generation and further more in stability of DS. In fact, optical nonlinearity as wide spread impact; leads to a separate field of study called nonlinear optics. Nonlinear optics has been a growing field since 1960's [63–65]. It all started with the finding of second-harmonic generation by Franken et al. in 1961 [64], shortly after the presentation of the first working laser by Maiman in 1960 [63]. It is a phenomenon that occurs as a result of modification of optical properties of the material when exposed to highly intense light. There are several mechanism of generation of nonlinear polarization and hence optical nonlinearity. Besides electron cloud deformation, intramolecular motion are also responsible for nonlinear polarization.

2.1 Optical Nonlinearity

The fundamental linear theory of light-matter interaction is based on the electronic polarization of the material prompted due to the electric field of the (i.e. linear) light. In conventional optics, at low-light intensity, the induced polarization is linearly

proportional to the applied electric field (E) of the radiation having relation [6],

$$\vec{P}(r,t) = \epsilon_0 \chi^{(1)} \vec{E}(r,t) \tag{2.1}$$

where, ϵ_0 is the electric permittivity of free space and $\chi^{(1)}$ is the electric susceptibility of the medium. But for laser radiation, it was observed that the simple assumptions and conclusions drawn in linear optics were no longer sufficient to describe the conditions that arise due to the usage of intense laser beam on certain type of optical materials [9]. Thus, researchers realized that the new effects arising due to intense laser light can be explained only by modified formula. The high intensity ($\sim 2.5kW/cm^2$) of the laser light make the polarization relation non-linear with respect to the applied field [8]:

$$\vec{P}(r,t) = \epsilon_0 \left[\chi^{(1)} \vec{E}^1(r,t) + \chi^{(2)} \vec{E}^2(r,t) + \chi^{(3)} \vec{E}^3(r,t) + \chi^{(4)} \vec{E}^4(r,t) + \chi^{(5)} \vec{E}^5(r,t) + ... \right] \tag{2.2}$$

where, $\chi^{(2)}$, $\chi^{(3)}$, $\chi^{(4)}$, and $\chi^{(5)}$ are known as the second, third, fourth and fifth order nonlinear optical susceptibilities, respectively. The term $\vec{P}^{(2)}(t) = \epsilon_0 \chi^{(2)} \vec{E}^2(r,t)$ is called the second-order nonlinear polarization, $\vec{P}^{(3)}(t) = \epsilon_0 \chi^{(3)} \vec{E}^3(r,t)$, is the third-order nonlinear polarization, $\vec{P}^{(4)}(t) = \epsilon_0 \chi^{(4)} \vec{E}^4(r,t)$ is forth-order nonlinear polarization and $\vec{P}^{(5)}(t) = \epsilon_0 \chi^{(5)} \vec{E}^5(r,t)$ is fifth-order nonlinear polarization. The nonlinear part of polarization leads to several nonlinear optical phenomenon [9, 66, 67]. $\chi^{(2)}$, gives rise to second harmonics generation (SHG) and sum frequency generation (SFG) effects . Kerr effect, stimulated Raman scattering (SRS) and stimulated Brillouin scattering (SBS) are third order nonlinear effects. Three photon absorption/emission are the fifth order nonlinear effects that depends on fifth-order of nonlinear optical susceptibility. Optical fibers do not exhibit second order polarization, as optical fiber materials (i.e. silica glass) are centrosymmetric (i.e.,they shows inversion symmetry at molecular level). So the even order polarization terms in the Eqn. (2.2) can be neglected for optical fiber.

Nonlinear effects in optical fibers are an important area of research both academi-

cally and industrially. The use of single mode fibers (SMF) for data transmission using ultrashort pulses have made the study of nonlinear optics very attractive. The basic nonlinearities and their effects are discussed below.

2.1.1 Kerr (Third Order) Nonlinearity and Kerr Nonlinear Effects

The $\chi^{(3)}$ gives rise to many phenomena like third-harmonic generation, four-wave mixing, and nonlinear refraction. The lowest-order nonlinearity that can occur in optical fiber is due to the third order susceptibility i.e. $\chi^{(3)}$. The corresponding nonlinearity is called Kerr or cubic nonlinearity. Kerr nonlinearity is one of the simplest forms of nonlinearity experienced in optical fibers and is based on the intensity dependence of refractive index. The refractive index of a Kerr nonlinear medium can be expressed as [8, 68]

$$n(\omega, \mid E \mid^2) = n_0(\omega) + n_2 \mid E \mid^2 = n_0(\omega) + n_2 I \tag{2.3}$$

where, n_0 is the linear refractive index of the material, ω is the frequency of the incident radiation, $\mid E \mid^2$ (i.e., I) is the optical intensity of the radiation and n_2 is Kerr/cubic nonlinearity coefficient and is given by

$$n_2 = \frac{3}{2{n_0}^2 c\epsilon_0} Re\chi^{(3)}, \tag{2.4}$$

where $Re\chi^{(3)}$ is the real part of $\chi^{(3)}$ and n_2 denotes the strength of optical nonlinearity. This intensity dependence of refractive index gives rise to the phenomena of self-focusing,self phase modulation etc. [69, 70].

Due to the small core diameter, intensity of optical field inside the optical fiber increases significantly. Also the use of inline fiber amplifiers has resulted in the increase of absolute value of power in the optical fiber. These factors give rise several nonlinear effects in the optical fiber that affect the propagation of light both constructively as well as destructively [7, 9]. Here we discuss some of the common nonlinear effects that arise inside the optical fiber due to Kerr type nonlinearity.

2.1.1.1 Self-Phase Modulation

At higher intensities, the refractive index of a medium depends on the intensity of light. In a Kerr nonlinear medium it is given by Eqn. (2.3), i.e.

$$n = n_0 + n_2 I \tag{2.5}$$

where, n_0 is the refractive index of the medium at low intensity and n_2 is a nonlinear refractive index coefficient and I represents the intensity of the light pulse. Even though the change in refractive index is minute but as the pulse propagates in the optical fiber over a long distances, cumulative effects can be significant. This variation of refractive index results in change in phase of the light pulse itself. This phenomenon is called self-phase modulation (SPM) [12]. The change in phase of optical field is given by $\phi = \tilde{n} k_0 L = (n + n_2 \mid E \mid^2) k_0 L$, where $k_0 = \frac{2\pi}{\lambda}$ and L is fiber length. The nonlinear phase, $\phi_{NL} = n_2 k_0 L \mid E \mid^2$, is due to SPM. The phase at the centre of the pulse will be different from the leading and trailing edges of the pulse, and hence the instantaneous frequency throughout the pulse will be different from the central frequency. If the instantaneous frequency moves toward the lower frequency region, that is called down chirping or red shift. Conversely, if the instantaneous frequency move towards the high frequency region, that is called up chirping or blue shift.

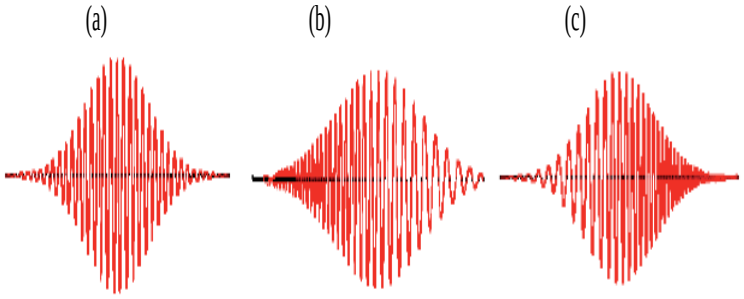

Fig. 2.1: (a) Original Pulse (b) Red shift pulse (c) Blue shift pulse.

2.1.1.2 Two Photon Absorption

Two-photon absorption (TPA) is a third order nonlinear effect and was first predicted theoretically by Maria Goeppert-Mayer in 1931 [71] and observed experimentally by Kaiser and Garrett in 1961 [72]. In this process, an atom or a molecule absorbs a pair of photons simultaneously and the sum of energy of photons is equal to the transition energy. The TPA coefficient is related to third order susceptibility. $\chi^{(3)}$ is a complex

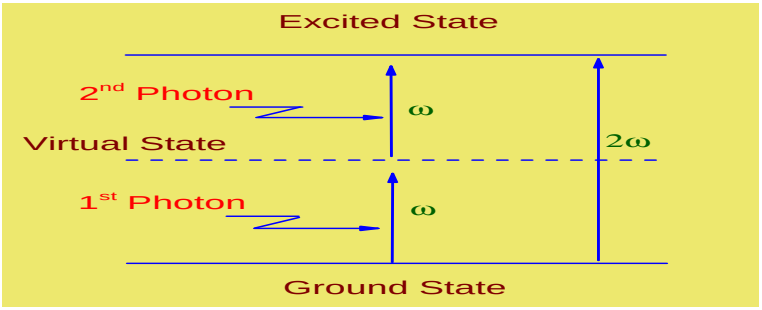

Fig. 2.2: Schematic diagram of energy levels involved in two photons absorption.

quantity. While the real part of $\chi^{(3)}$ gives rise to Kerr nonlinearity and the imaginary part of $\chi^{(3)}$ gives rise to TPA with the coefficient:

$$\alpha_2 = \frac{3\omega Im(\chi^{(3)})}{2{n_0}^2 c^2 \epsilon_0}. \tag{2.6}$$

Here, ω is the frequency and ϵ_0 is the vacuum permittivity, n_0 is the refractive index and c is the velocity of light. In TPA, the optical loss can be described by the relation: $\frac{dI}{dz} = -\alpha I - \alpha_2 I^2$, where, $\frac{dI}{dz}$ is the change in beam intensity along the propagation direction in the sample, α is the linear absorption coefficient due to impurities and α_2 is the TPA coefficient. The TPA coefficient α_2 is dependent on the TPA cross section σ_2 according to the relation: $\sigma_2 = \frac{\hbar\omega\alpha_2}{N}$, where N is the number density of the molecules in the system and $\hbar\omega$ is the energy of the photons in the incident optical field.

2.1.2 Quintic (Fifth order) Nonlinearity and Quintic Nonlinear Effects

Kerr effect is the lowest nonlinear effect experienced in optical fiber. However, with the advent of highly nonlinear material and with the use of high power ultra-short pulses, the fifth order nonlinear phenomena become relevant. So the study of quintic or fifth order nonlinearity becomes pivotal.

At high intensities and also at moderate intensity for some optical materials, upto fifth order susceptibility becomes important. This leads to cubic-quintic optical nonlinearity. Such cubic-quintic nonlinearity can be written as [12, 73]:

$$n(I) = n_0 + n_2 I + n_4 I^2 \tag{2.7}$$

where, n_2 is cubic nonlinear coefficient that creates self-focusing while n_4 corresponds to self-defocusing effect in a beam. For pulse, they also have intriguing effects which will be discussed in the proceeding chapters. n_4 is a fifth order nonlinear coefficient as it corresponds to fifth order nonlinear susceptibility throuth the relation: $n_4 = \frac{5}{16 n_0}\chi^{(5)}$. This type of nonlinearity is also called competing nonlinearity as there is a kind of competition between the focusing and defocusing nonlinearities [74]. It is important to note that the quintic nonlinearity is very much weaker in comparison to the cubic one, but still it not only significantly modifies the existing nonlinear phenomena but may also gives rise to some totally new phenomena. The cubic-quintic nonlinearity is also called parabolic nonlinearity. Quintic nonlinearity has a positive role in stabilization of soliton pulses.

2.1.2.1 Three Photon Absorption

Three-photon absorption (3PA) is a fifth order nonlinear effect. It involves a transition of an atom or molecule from the ground state to the higher energy state by simultaneous absorption of three photons from an incident radiation field [75]. The imaginary part

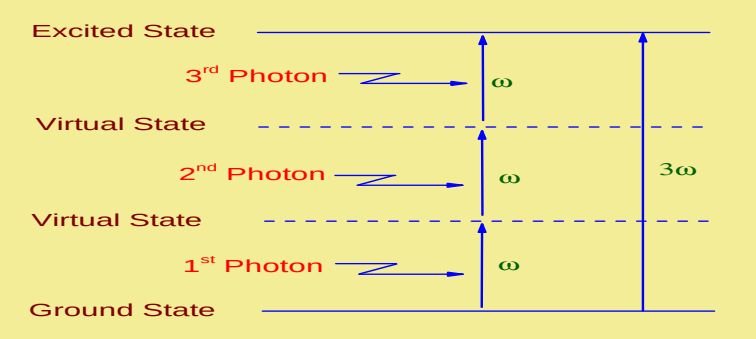

Fig. 2.3: Schematic diagram of energy levels involved in three photons absorption.

of $\chi^{(5)}$ gives rise to 3PA with the coefficient:

$$\alpha_3 = \frac{5\omega Im(\chi^{(5)})}{2{n_0}^3 c^3 \epsilon_0^2}. \tag{2.8}$$

In 3PA, the optical loss can be described by the relation: $\frac{dI}{dz} = -\alpha I - \alpha_3 I^3$, where, $\frac{dI}{dz}$ is the change in beam intensity along the propagation direction in the sample, α is the linear absorption coefficient and α_3 is 3PA coefficient.

2.2 Dispersion

Other than nonlinearity in optical fibers, dispersion is an important issue. In a single mode fiber, different frequency components of the optical pulse travel at different speed. So they do not arrive simultaneously at the output ; hence broadening of the pulse takes place. Various dispersion mechanism responsible for pulse broadening in optical fiber are given below:

2.2.1 Material Dispersion

The effect of dispersion in optical fiber can be described by Taylor series expansion of mode propagation constant β about frequency ω_0 given as:

$$\beta(\omega) = n(\omega)\frac{\omega}{c} = \beta_0 + \beta_1(\omega - \omega_0) + \frac{1}{2}\beta_2(\omega - \omega_0)^2 + \frac{1}{6}\beta_3(\omega - \omega_0)^3 + ..., \tag{2.9}$$

where, $\beta_m = (\frac{d^m\beta}{d\omega^m})_{\omega=\omega_0}, (m = 0, 1, 2, ...)$ [6]. The broadening is governed by the group velocity dispersion (GVD) coefficient, β_2, related to the dispersion parameter (D) of

the fiber, as $D = \frac{-2\pi c}{\lambda^2}\beta_2$. Depending on the sign of β_2, the dispersive medium can be considered as normal ($\beta_2 > 0$) or anomalous ($\beta_2 < 0$). This is also called as intramodal or chromatic dispersion. Material dispersion occurs due to the variation of refractive index of the core of the fiber as a function of wavelength. As the result, since group velocity is a function refraction index of the fiber the different frequency components will travel at different speed. This will result in the broadening of the pulse. The material dispersion can be given as [76]:

$$\sigma_{mat} = \sigma_\lambda L \mid D_{mat}(\lambda) \mid, \tag{2.10}$$

where, σ_{mat} is pulse spread, σ_λ is spectral width, L is the unit length and D_{mat} is material dispersion.

2.2.2 Waveguide Dispersion

In a single mode optical fiber, a major part of the optical power ($\sim 80\%$) propagates through the core of the fiber and the rest part ($\sim 20\%$) travels through the cladding. As refractive index of the cladding is slightly less than that of core, the pulse propagating through the cladding travels faster than that travelling through the core. At the receiving end of the fiber these two modes will arrive at different times depending on the group delay. Thus the spreading of the pulse occurs. This is called waveguide dispersion (Fig. 2.4).

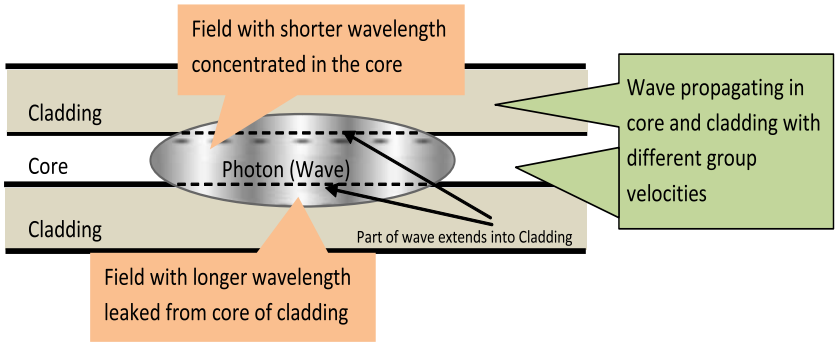

Fig. 2.4: Pulse broadening in optical fiber due to waveguide dispersion.

The waveguide dispersion arises due to wavelength dependence of mode propagation constant. So, different wavelength component of source will have different propagation constant travelling with different velocities. The group delay i.e., the time required for a mode to travel along a fiber of length L can be expressed in terms of normalized propagation constant 'b' as

$$b = \frac{\beta^2/k^2 - {n_2}^2}{n_1^2 - n_2^2} \tag{2.11}$$

For small value of index difference, $\Delta = (n_1 - n_2)/n_1$, above expression is written as

$$b = \frac{\beta/k - n_2}{n_1 - n_2} \tag{2.12}$$

On solving for β, we get

$$\beta = n_2 k(b\Delta + 1) \tag{2.13}$$

By assuming that n_2 is not a function of wavelength, we find that the group delay τ_{wg} due to waveguide dispersion is

$$\tau_{wg} = \frac{L}{c}\frac{d\beta}{dk} = \frac{L}{c}\left[n_2 + n_2\Delta\frac{d(kb)}{dk}\right] \tag{2.14}$$

The modal propagation constant β is obtained from the eigenvalue equation and is generally given in terms of the normalized frequency V. We shall therefore use the approximation

$$V = ka\left({n_1}^2 - {n_2}^2\right)^{1/2} = kan_1\sqrt{2\Delta} \tag{2.15}$$

Which is valid for small values of Δ, to write the group delay in terms of V instead of k yielding

$$\tau_{wg} = \frac{L}{c}\left[n_2 + n_2\Delta\frac{d(Vb)}{dV}\right] \tag{2.16}$$

This is the required expression for group delay due to waveguide dispersion. Waveguide dispersion can be ignored in the multimode fibers as it is generally very small but in single mode fiber its effect is significant.

2.2.3 Polarization-Mode Dispersion

Even in a single mode optical fiber, the signal pulse at same wavelength has two orthogonal polarization states or modes (x and y polarization mode). Initially, these two polarization modes are fully aligned with each other. But for long distance the varying birefringence (refractive index dependence on polarization and propagation direction of light) will make each mode to travel at slightly different velocity. Resulting difference in propagation times $\Delta\tau_{PMD}$ between two orthogonal modes will result in spreading of the pulse (Figure 2.5). This is called polarization-mode dispersion (PMD)

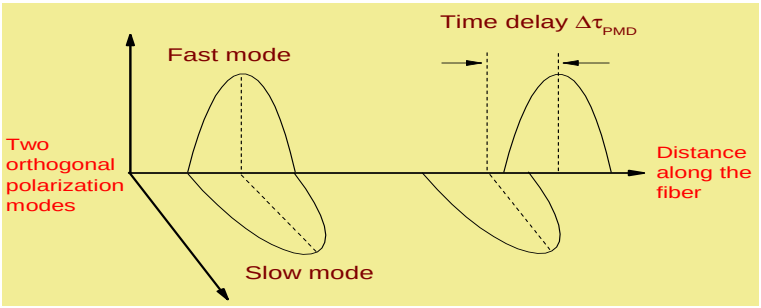

Fig. 2.5: Polarization-mode time delay as pulse propagates in the fiber with varying birefringence along its length.

[77]. If v_{gx} and v_{gy} are the group velocities of two orthogonal polarization modes, then during the propagation of the pulse over the length L, the differential time delay is given as:

$$\Delta\tau_{PMD} = \left| \frac{L}{v_{gx}} - \frac{L}{v_{gy}} \right| \tag{2.17}$$

The value of PMD varies with time as the perturbations causing birefringence effects vary with temperature and stress dynamics [76]. In practical systems, these perturbations show up as a random, time-varying fluctuations in the value of PMD.

2.2.4 Third Order Dispersion

Although the contribution of second order dispersion is most dominating group velocity dispersion (GVD) term in optical fibers but if the pulse wavelength gets close to zero-

dispersion wavelength, then contribution of third order dispersion (TOD) becomes dominant factor in GVD effects. TOD plays an important role only if dispersion length associated with it is less than the dispersion length associated with second order dispersion [6]. TOD tend to distort the pulse shape. Pulse becomes asymmetric with an oscillatory structure near one of its edges. The sign of TOD also plays a significant role in oscillations. If sign of TOD is positive, oscillations develop near the trailing edge of the pulse and for negative TOD, leading edge develops oscillations. The general equation with TOD term can be written as:

$$i\frac{\partial U}{\partial z} = \frac{\beta_2}{2}\frac{\partial^2 U}{\partial T^2} + \frac{i\beta_3}{6}\frac{\partial^3 U}{\partial T^3} \tag{2.18}$$

where, U is the normalized envelop of the field, z is the normalized distance of propagation, β_2 is GVD coefficient and β_3 is TOD coefficient.

2.3 Intrapulse Raman Scattering (IRS)

In optical fiber, IRS is an important higher-order nonlinear effect. It becomes relevant when ultrashort pulses ($T_0 < 1\ ps$) are used in the fiber [6]. IRS results in the shifting of ultrashort optical pulse frequency towards the longer wavelength while propagating through the fiber. The lower frequency component of the pulse get amplified by high frequency component. So transferring of energy towards red shift side takes place through stimulated Raman scattering [9]. This shift in frequency increases with the distance. The general nonlinear Schrödinger equation having IRS term can be written as:

$$i\frac{\partial U}{\partial z} + \frac{1}{2}\frac{\partial^2 U}{\partial T^2} + \mid U \mid^2 U = T_R U \frac{\partial \mid U \mid^2}{\partial t^2} \tag{2.19}$$

where, first term represents evolution of pulse envelop with propagation, second term is the GVD term, third term represents cubic nonlinearity and T_R is IRS coefficient.

The broadening of the pulse takes place as it propagates along the fiber. However, a fascinating phenomena using the fiber nonlinearities takes place through optical soliton, which are formed as a result of interplay between dispersive and nonlinear effects. The detailed discussion is as follows.

2.4 Soliton

Solitary waves or commonly known as 'Solitons' have been a topic of enormous theoretical and experimental studies in various fields like optics [1, 6], plasma physics [78], hydrodynamics [79], communication technology [9], gas discharge [80] and biology [17]. The localized states of waves, which are capable of traveling with a self-similar shape and behave like a particle during interaction, are called soliton. In fact, if there is a wave there is a possibility of soliton formation. Soliton research was initiated long back in 1834 by a Scottish engineer John Scott Russell, who observed first shallow water soliton while working in Glasgow-Edinburgh channel. John Scott Russell reproduced such waves later on studied them extensively and reported his work naming these waves as the 'wave of translation'. Such waves were later named as solitary waves. Its properties were completely explored only after the introduction of suitable mathematical models and inverse scattering was developed in 1960's. The name soliton was given in order to reflect the particle like nature that remained intact even after a collisions. The trajectories of two solitons can change after collision with respect to the trajectories without the collision [8]. So, the interaction can result in the little phase change of the two waves.

2.4.1 Temporal Soliton

As the name suggests temporal solitons are pulses those neither broaden nor contract in time [6, 81, 82], i.e., the pulse is confined in time domain. In nonlinear dispersive medium, the propagating pulse undergoes chirping because of both dispersion and non-

linearity induced SPM. In anomalous dispersive media, the chirping due to dispersion opposite to the chirping due to nonlinearity induced SPM. If the opposite chirps cancel each other, the pulse propagates with constant temporal as well as spectral width. Such localised pulse is known as temporal soliton. For example, let us consider a propagating

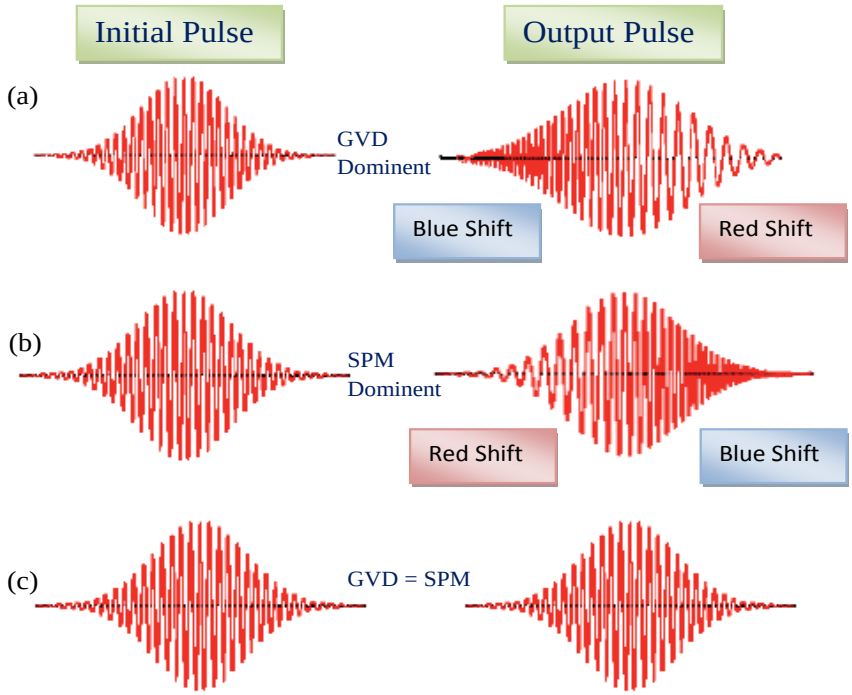

Fig. 2.6: Generation of temporal soliton. (a)red shifted pulse due to GVD dominance, (b) blue shifted pulse due to SPM, and (c)Localized pulse due to GVD and SPM inter-balance.

optical pulse in a self-focussing anomalous dispersive Kerr nonlinear medium. When dispersion is dominant, leading edge of the pulse gets blue shifted and the trailing edge of pulse gets red shifted. This causes a temporal spreading of the pulse. On the other hand, when nonlinearity is dominant, a chirp develops due to self-phase modulation, which is opposite in nature as compared to GVD induced chirp. A perfect balance between these two chirps keeps both spectral and temporal widths invariable that lead to formation of temporal solitons as shown in Fig (2.6).

2.4.2 Dispersion-Managed Soliton

A dispersion-managed (DM) soliton is a periodically localised structure that occur in a systems having alternate sections of anomalous and normal fiber systems as shown in the dispersion map (Fig 2.7). The concept of DM soliton was first introduced in 1990

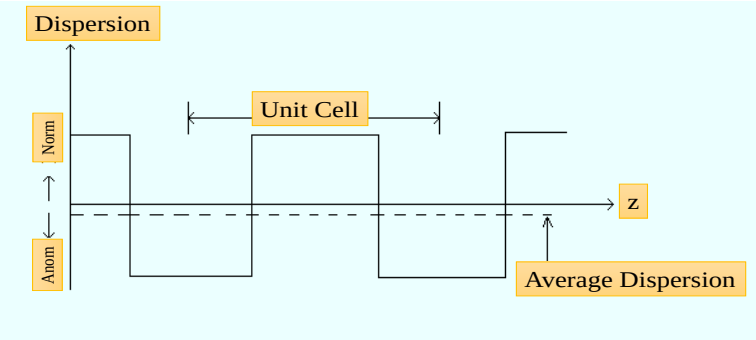

Fig. 2.7: Periodic dispersion map with average anomalous dispersion.

and since then it has become very interesting topic for optical communications and fiber laser. The DM soliton generally exist in average anomalous dispersion, however average normal dispersion can also lead to DM [83, 84]. The main characteristics of DM soliton is that (unlike the fundamental soliton), it periodically changes its shape, width or peak power, but eventually remains confined. Because of this characteristics, DM soliton is also called as breathing soliton. One of the feature that differentiate DM soliton from conventional soliton lies in its highest peak power requirements for sustaining. Actually in comparison to a constant dispersion map, a periodic dispersion map can balance higher values of nonlinearity. The large energy of the DM solitons benefits the system by improving the signal-to-noise ratio (SNR) and thus reducing the timing jitter. Also, by the proper choice of system parameters, both Gordon-Haus effect (arises due to the fluctuations in center frequency) and four-wave mixing (originates due to interactions of two or three wavelengths to generate one or two new wavelengths) can be significantly reduced, thus proving nearly error-free transmission. The important application of the DM system is in the upgradation of the existing

terrestrial network employing standard fibers.

2.5 Fiber Laser

The fiber laser is a laser in which the active medium is an optical fiber [85–88]. Usually the core of this fiber is doped with rare earth material like erbium, ytterbium, thulium etc. On both sides of the 'active' fiber, fiber Bragg gratings (FBG) are placed/formed. These FBGs having high and low reflectivity act as a resonator mirrors, thus reflect lights of specific wavelength. The reflected light from the FBGs causes the induced

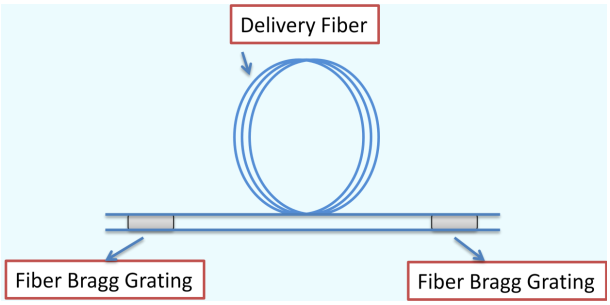

Fig. 2.8: Simple model of fiber laser.

emission in the resonator along with spontaneous emission. This induced light will further leads to the induced emission in the resonator as it is reflected from FBGs again and again. These multiple reflections from FBGs will eventually results in the emission of laser light from lower reflecting FBG. The superiority of fiber laser over other lasers is now-a-days well established in many aspects such as energy efficiency, beam quality, space efficiency, stability and reliability. These qualities of fiber laser are making it major player in laser processing field.

2.5.1 Dispersion-Managed Fiber Laser

The alternate segments of normal and anomalous GVD segment can be effectively used for constructing fiber lasers [89, 90]. This variation of dispersion known as dispersion map helps in maintaining the nonlinear phase accumulation. In anomalous GVD por-

tion, the pulse shape is solitonic. In order to avoid pulse breaking, a pulse must have a monotonic frequency sweep or chirp as it propagates along the fiber [91]. By taking positive GVD value (i.e. normal dispersion), the monotonically chirped pulse can avoid pulse breaking at high intensities. By using the dispersion-management technique, the fiber laser supports stable self-similar pulses at higher energies. Thus pulse energy can be increased by using dispersion segment from large and anomalous to zero and then large and normal dispersion value.

2.6 Methodology

Pulse propagation along the fiber can be studied using analytical or direct numerical methods. Here in our work, we take help of analytical approach to study the dynamics of the system. The analytically obtained results are then verified by using direct numerical solutions as discussed in following subsection.

2.6.1 Governing Equation

Pulse propagation through an optical fiber in the presence of nonlinear and dissipative effects can be described by complex Ginzburg-Landau equation (CGLE) [1, 2] or perturbed nonlinear Schrödinger equation (NLSE) [6]. The main models, used to study the dissipative solitons comprises of a complex Ginzburg-Landau equation (CGLE) or a nonlinear Schrödinger equation (NLSE) with addition of dissipative terms. For our system CGLE will be modified to capture the effect of cubic-quintic nonlinearity and other linear and nonlinear phenomena. The basic complex Ginzburg-Landau equation (CGLE) [1] representing the dissipative system is given by,

$$iE_z + \frac{D}{2}E_{tt} + \mid E \mid^2 E + \gamma \mid E \mid^4 E = i\delta E + i\beta E_{tt} + i\epsilon \mid E \mid^2 E + i\nu \mid E \mid^4 E, \qquad (2.20)$$

where E is the normalized envelope of the field, z is the normalized distance of propagation, t is the retarded time, D is the group velocity dispersion coefficient, with

$D = \pm 1$, depending on whether the group velocity dispersion (GVD) is anomalous or normal, respectively, γ is quintic nonlinearity coefficient, δ is the linear gain-loss coefficient, $i\beta E_{tt}$ accounts for gain dispersion or spectral filtering, $i\epsilon \mid E \mid^2 E$ represents the nonlinear loss or gain depending upon the sign of imaginary part of $\chi^{(3)}$. The term with ν represents loss or gain depending upon the sign of imaginary part of $\chi^{(5)}$. Another equation that support soliton formation is nonlinear Schrödinger equation (NLSE), but as we will use lossy system so we will use NLSE for perturbed system which is given by,

$$i\frac{\partial E}{\partial z} + \frac{D}{2}\frac{\partial^2 E}{\partial t^2} + \mid E \mid^2 E + \gamma \mid E \mid^4 E = iR(E, E^*), \tag{2.21}$$

where, E is the normalized envelope of the field, z is the normalized distance of propagation, t is the retarded time, D is the group velocity dispersion coefficient, with $D = \pm 1$, depending on whether the group velocity dispersion (GVD) is anomalous or normal, respectively, γ is quintic nonlinearity coefficient, R is the perturbation parameter and $R = 0$ for conservative system. In fact, CGLE can be considered as the perturbation of NLSE. The analytical method we will use is variational method (with some modification due to lossy medium).

2.6.2 Analytical Method

Many form of CGLEs are not completely integrable by the inverse scattering method [92]. Such systems are generally solved following numerical methods. However, analytical approach, even approximate one, is very important as it gives very useful understanding of the system. The moment method [93], and variational method in conjugation with Rayleigh's dissipative function have been used in such schemes. In optical fibers, to describe the nonlinear pulse propagation in a dissipative environment, variational method has been widely used [94].

2.6.2.1 Variational Method

The variational method is used in several areas of classical and quantum field and is very helpful in getting a great insight of the system [95]. In 1983, D. Anderson in his milestone work applied the variational method to study the nonlinear pulse propagation in optical fibers [91]. This method is a strong tool to study the dynamics of pulse propagation and soliton generation in the optical fibers, and other systems [96, 97].

As our system is described by CGLE or perturbed NLSE, we will use variation method in conjugation with the Rayleighs dissipative function (RDF). The benefit of this approach is that it gives us explicit evolution for individual system parameters. It can be noted that the left-hand side of Eqn. (2.20) is conservative part, while the right hand side of the equation is dissipative part. The analytical method involves Lagrangian formulation for the conservative part and RDF generation for the dissipative part. Then by using a suitable trial wave function, we obtain the reduced Lagrangian and reduced RDF. The choice of trial function is crucial for the success of this method. There after by using $L_g = \int_{-\infty}^{\infty} L dt$, and $R_g = \int_{-\infty}^{\infty} R dt$, we find the total Lagrangian and RDF. Using the following Euler-Lagrangian equation,

$$\frac{d}{dt}\left(\frac{\partial L_g}{\partial \dot{q_j}}\right) - \frac{\partial L_g}{\partial q_j} + \frac{\partial R_g}{\partial \dot{q_j}} = 0, \tag{2.22}$$

(where, $\dot{q_j} = \frac{dq_j}{dt}$ and q_j represents the pulse parameters). This yields the evolution equations for each pulse parameters. The schematic representation of variational method can be described as:

Finally and essentially in many case, the analytical results are verified and further extended using rigorous numerical simulations. We will use split-step Fourier method (SSFM), a pseudo spectral method, for the purpose of numerical simulation.

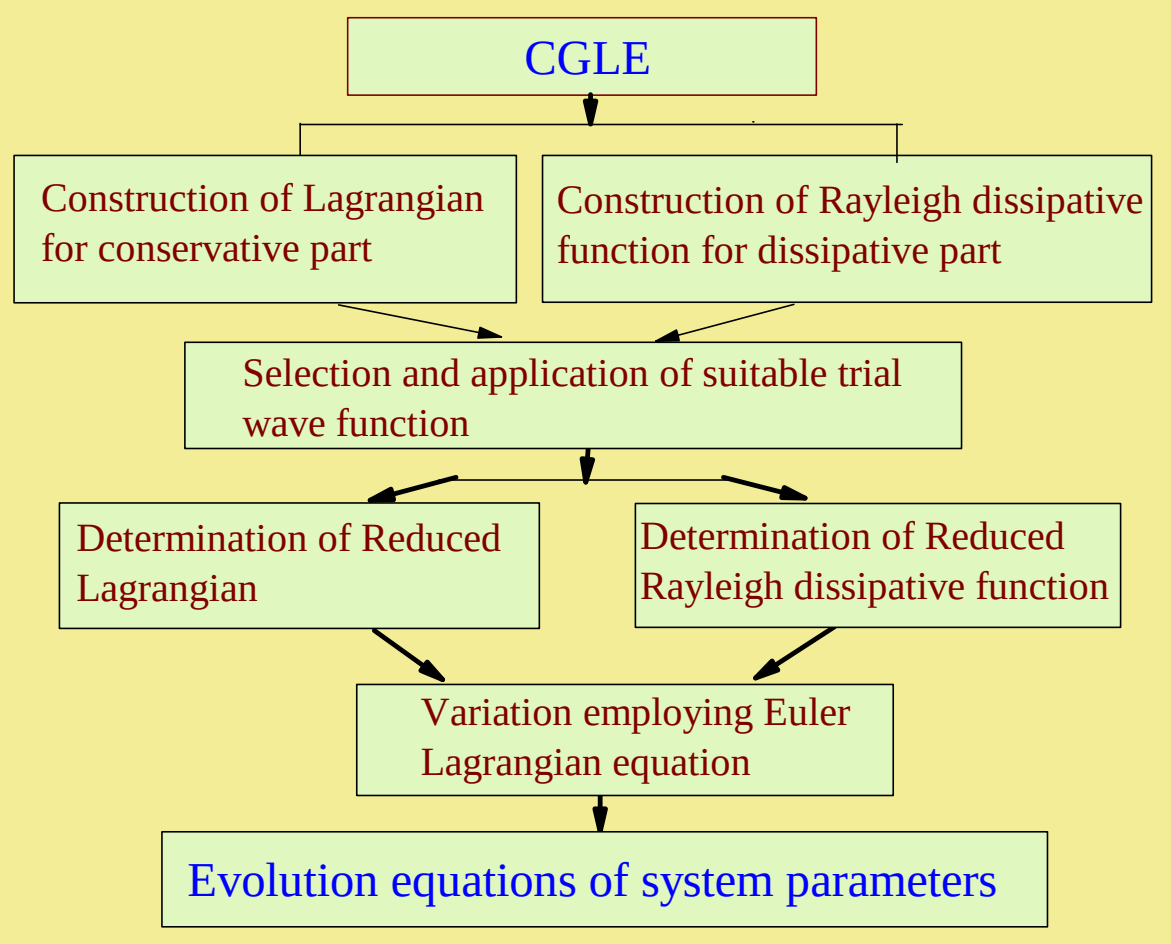

Fig. 2.9: Schematic diagram of analytical methodology.

2.6.3 Numerical Method

For the understanding of pulse dynamics in CGLE or perturbed NLSE systems, a numerical approach is extremely necessary. Numerical methods can be classified into two major categories; finite difference and pseudo-spectral methods. The pseudo-spectral methods are found to be relatively faster than other methods. Split-step Fourier method (SSFM) is a pseudo-spectral methods that is widely used to study the pulse or beam dynamics in nonlinear dispersive media [98]. This method is used extensively in physics and engineering applications. SSFM provides an excellent methodology to solve the time dependent partial differential equation.

2.6.3.1 Split-Step Fourier Method (SSFM)

The basic theory of SSFM involves the division of original equation or problem into two sub-problems. These sub-problems are relatively simpler than the original one. The solutions of these sub-problems are used to obtain the approximate solution of the original problem as discussed below by using cubic-quintic nonlinear Schrödinger equation (CQNLSE): We consider the CQNLSE as:

$$\frac{\partial E}{\partial z} = -\frac{i\beta_2}{2}\frac{\partial^2 E}{\partial t^2} + i \mid E \mid^2 E + i\gamma \mid E \mid^4 E, \tag{2.23}$$

This can be written as,

$$\frac{\partial E}{\partial z} = \Big(-\frac{i\beta_2}{2}\frac{\partial^2}{\partial t^2} + i \mid E \mid^2 + i\gamma \mid E \mid^4 \Big) E, \tag{2.24}$$

The above equation can be rewritten in terms of linear and nonlinear operators as,

$$\frac{\partial E}{\partial z} = (\hat{D} + \hat{N})E, \tag{2.25}$$

where, $\hat{D}$ is a differential operator that accounts for dispersion and losses within the medium and $\hat{N}$ is a nonlinear operator that governs the effect of fiber nonlinearities on pulse propagation. These operators are given by,

$$\hat{D} = -\frac{i\beta_2}{2}\frac{\partial^2}{\partial t^2}, \tag{2.26}$$

$$\hat{N} = i \mid E \mid^2 + i\gamma \mid E \mid^4, \tag{2.27}$$

In real fibers, both dispersion and nonlinearity act simultaneously. In SSFM, the whole fibre segment is divided into small parts each of distance h, and these effects are considered to act independently as shown in Figure 2.10. Generally, propagation from z to $z + h$ is executed in two steps:

Step 1 Nonlinearity acts alone, and $\hat{D} = 0$ in Eqn. (2.25)

Step 2 Dispersion acts alone, and $\hat{N} = 0$ in Eqn. (2.25).

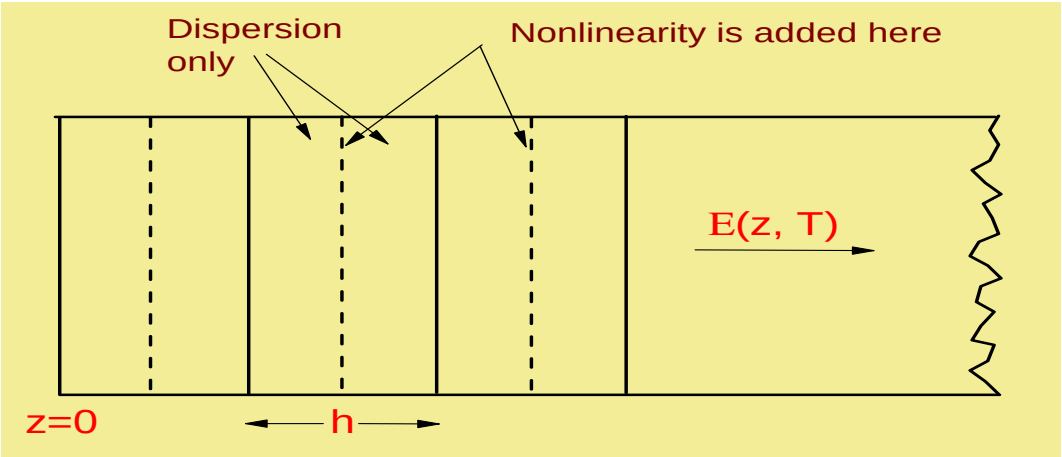

Fig. 2.10: Schematic diagram of the split-step Fourier method used for numerical simulations. The whole fiber length is divided into a large number of parts of width h. The nonlinear effect is included at the centre of each part as shown by a dashed line.

Above process is clear from Figure 2.10. Mathematically,

$$E(z+h,t) \approx exp(h\hat{D})exp(h\hat{N})E(z,t), \tag{2.28}$$

The exponential operator $exp(h\hat{D})$ can be evaluated in the Fourier domain using

$$exp(h\hat{D})B(z,t) = {F_T}^{-1}exp[h\hat{D}(-i\omega)]F_T B(z,t), \tag{2.29}$$

where F_T denotes the Fourier-transform operation, $\hat{D}(-i\omega)$ is obtained from Eqn. (2.26) by replacing the operator $\frac{\partial}{\partial t}$ by $-i\omega$, where, ω is the frequency in Fourier domain. As $\hat{D}(i\omega)$ is just a number in the Fourier space, the evaluation of Eqn. (2.29) is easy.

To check the accuracy of split-step Fourier method, the field envelop on moving the system from z to $z+h$, can be written as:

$$E(z+h,t) = exp[h(\hat{D}+\hat{N})]E(z,t), \tag{2.30}$$

Now for non-commutating operator, $\hat{a}$ and $\hat{b}$, Baker–Hausdorff formula is given as,

$$exp(\hat{a})exp(\hat{b}) = exp[\hat{a}+\hat{b}+\frac{1}{2}[\hat{a},\hat{b}]+\frac{1}{12}\Big[\hat{a}-\hat{b},[\hat{a},\hat{b}]]+....\Big] \tag{2.31}$$

If error introduced by ignoring the non-commutating value of $\hat{D}$ and $\hat{N}$ is negligible. Then Eqn. (2.30) can be written as,

$$E(z+h,t) = exp(\hat{D}h)exp(\hat{N}h)E(z,t), \tag{2.32}$$

The accuracy of the method can be further increased by reducing the step size h, so

$$E(z+h,t) = exp\Big(\hat{D}\frac{h}{2}\Big)exp\Big(\hat{N}\frac{h}{2}\Big)E(z,t), \tag{2.33}$$

The final outcome for field envelop, can be obtained after n-times integration, given as

$$E(z) = exp\Big(\frac{h}{2}\hat{D}\Big)exp(h\hat{N})exp\Big(\frac{h}{2}\hat{D}\Big).....exp(h\hat{N})exp\Big(\frac{h}{2}\hat{D}\Big)E(0). \tag{2.34}$$

The use of FFT algorithm makes numerical evaluation of Eqn. (2.29) relatively easy. This is the main reason for the SSFM is faster than from most of the finite-difference schemes.

Chapter 3

Bistable Dissipative Soliton in a Doped Fiber with Cubic-Quintic Nonlinearity, Multi-photon Absorption and Gain Dispersion

---

In this chapter, we study the generation and dynamics of optical pulse and soliton in a dissipative cubic-quintic nonlinear doped fiber with multi-photon absorption and gain dispersion. Variational method in conjugation with Rayleigh's dissipative function is used to analytically solve the governing complex cubic-quintic Ginzburg-Landau equation and verified by SSFM. Effect of (i) two photon absorption, (ii) three photon absorption and (iii) both two and three photon absorption have been studied. Two and three photon absorptions, are functions of positive imaginary parts of third and fifth order susceptibility respectively. Both of them cause pulse decay and pulse broadening. Conversely, negative imaginary part of fifth order susceptibility may lead to three photon emission, which have been studied. By virtue of a suitable gain, both pulse broadening and decay have been arrested to yield dissipative solitonic pulses.

3.1 Introduction

In modern optical communication system and all-optical device fabrication, the dynamics of optical pulse through nonlinear dispersive media has shown substantial impor-

tance [6]. During the last few decades, a large volume and quality of theoretical research on nonlinear pulse dynamics in optical fiber have attained a significant progress [12]. Generally, in fiber materials, the most prominent nonlinear effects arise due to the third order susceptibility $\chi^{(3)}$. It's real part results in focusing cubic/Kerr nonlinearity through cubic /Kerr nonlinear coefficient $n_2 = \frac{3Re(\chi^{(3)})}{8n_0}$, where n_0 is the linear refractive index. Kerr nonlinearity in turn can suppress the group velocity induced pulse broadening. Temporal soliton are formed due to a perfect counter balancing of the group velocity dispersion and the nonlinearity induced self-phase modulation [81, 82]. Imaginary part of $\chi^{(3)}$ gives rise to two photon absorption (TPA) in the material through the TPA coefficient $\alpha_2 = \frac{3\omega Im(\chi^{(3)})}{2n_0{}^2c^2\epsilon_0}$, where ω is the frequency and ϵ_0 is the vacuum permittivity [99]. TPA technology has applications in imaging, microscopy, lithography and even in data storage. Most of the background linked with the image can be eliminated by TPA. TPA also has detrimental effects as it can also cause damage of the optical materials. Since it constitutes a nonlinear loss mechanism, it can limit the efficiency of optical switches. Under the effect of TPA, reshaping and broadening of primary soliton in case of fiber optics takes place. An input pulse can be simultaneously amplified and compressed in the presence of TPA, even though the compression factor is small. The amplified pulse splits into several chirped solitons and their number depends on the gain and length of the fiber amplifier [100]. Effect of TPA has been investigated in breaking up of higher order solitons into two or more primary solitons [101]. However, in a fiber optic system it introduces significant loss [102]. Thus TPA is considered to have a detrimental effect on the pulse propagation in optical fiber. Higher nonlinearity is required in some applications, e.g., switching, to reduce the operating power. The fifth order nonlinear phenomena become relevant with the advent of highly nonlinear fiber material. In some fiber material the fifth order susceptibility $\chi^{(5)}$ is traceable even at moderate laser intensity; please see [103] and the references therein. The fifth order effects are considerable for highly intense ultra-short pulses. The quintic non-

linear coefficient arises due to the real part of $\chi^{(5)}$ through the relation $n_4 = \frac{5Re(\chi^{(3)})}{16n_0}$. Quintic nonlinearity can significantly modify the pulse dynamics even-though, it is usually very small in comparison to the cubic one. Intriguing dynamics of the optical signal have been observed through the combination of self-focusing Kerr nonlinearity and self-defocusing quintic nonlinearity [104]. Stability of the pulse increases in the presence of the higher order nonlinearity [105]. Besides, a positive valued imaginary part of $\chi^{(5)}$ gives rise to three photon absorption (3PA) with the coefficient $\alpha_3 = \frac{5\omega Im(\chi^{(5)})}{2{n_0}^3 c^3 {\epsilon_0}^2}$. For example, at a wavelength of 1.55 μm, in As_2S_3-based glass, the value of 3PA coefficient has been found to be 2.0×10^{-27} m^3W^{-2} [106]. For fibers made from such glass, 3PA significantly modifies the soliton condition, propagation dynamics and the factor of merit for all-optical switching. For operating wavelengths corresponding to photon energies below half of the electronic band gap the influence of 3PA is notable [107]. Since 3PA is proportional to the cube of the field intensity, it leads to a higher degree of spatial confinement. 3PA has potential applications in wavelength shifting, pulse reshaping and stabilization at communication wavelength in short pulse fiber communication system [108, 109]. The influence of TPA and gain dispersion on pulse propagation has been studied [110]. But 3PA is not given proper attention in the context of fiber optic communication. Moreover, the situation with a negative valued imaginary part of $\chi^{(5)}$ has never been discussed in this context. Such negative imaginary part of $\chi^{(5)}$ may give rise to an effect opposite to 3PA, which can be considered as three photon emission (3PE) and provides a gain to the system. It is interesting to note the interplay between TPA induced loss and 3PE induced gain on pulse propagation. Also, the effect of quintic nonlinearity has been rarely studied in optical fiber [111].

Thus we investigate the pulse propagation in a cubic-quintic nonlinear dissipative medium under the influence of TPA and 3PA in a fiber laser cavity. Three different cases of multiphoton absorption have been considered: (i) two photon absorption,

(ii) three photon absorption and (iii) both two and three photon absorption. We consider gain dispersion in our model since it is prominent for an ultra-short pulse propagating through a gain medium. The power spectrum for femto-second and few pico-second pulses is so wide that it become inevitable to neglect the effect of finite gain bandwidth [112]. In the wide spectrum, different spectral components experience different gain i.e., dispersion in gain occurs. The pulse dynamics and energy profile gets significantly modified under the combined effect of gain dispersion and group velocity dispersion. It can be further noted that the system loss can be minimized by adding a suitable gain, thus gives rise to dissipative soliton. We demonstrated the generation of such dissipative soliton in fiber laser for all three cases of multiphoton absorption. Due to the coexistence of third and fifth order effects in the system, the solitons are found to be bistable.

To model our system mathematically, we consider a complex cubic-quintic Ginzburg-Landau equation (CQGLE). The presence of loss/gain terms make the system dissipative as well as nonintegrable one. One can transform the CQGLE to a nonlinear Schrdinger equation (NLSE) by neglecting the dissipative terms. Such NLSE and its modified version have been solved by using several analytical methods. For example, inverse scattering method [92], AKNS method [113, 114], Bäcklund transformation technique [115], Hirota bilinear method [116, 117], Lux pair method [118]. In early stage of theoretical investigation, exact soliton solution were obtained by mostly using the aforesaid methods. The lower order soliton solution is simple and exact in nature. Higher order soliton solutions are also derived successfully using these methods, but commonly in form of complicated functions. For integrable systems, the exact analytical methods have been found to be more successful. With the advancement of theoretical research, to capture the real effects of a system, a much more complex equations (e.g., some modified NLSE and CQGLE) are being proposed. Although otherwise strong, the exact methods either fail or become too tedious to solve such

'realistic' equations, which are mostly nonintegrable. In this context, a number of approximate analytical methods have been proposed. Variational method and moment method are of this category. For the current investigation we used variational approach in conjugation with Rayleigh's dissipation function [119]. This is basically a combination of Lagrangian based variational method [91] and perturbation method that has been successfully used to determine the pulse dynamics in a dissipative system [120]. Variation method leads to a solution which is very close to the exact solution. Moreover, it yields the evolution equation of the beam/pulse parameters that provides more insight into the dynamics of the system. The advantage of variational method is best felt for a system with no exact solution.

The layout of this chapter is as follows. Section 3.2 contains the mathematical model and analytical method for obtaining pulse evolution equations. Dissipative pulse propagation is discussed in section 3.3, wherein subsection 3.3.1 illustrates the analytical results. To validate the analytical results a split-step Fourier method based numerical scheme is employed in subsection 3.3.2. Section 3.4 shows generation of dissipative soliton both analytically and numerically. Section 3.5 shows the effect of initial chirp on the soliton propagation. The findings have been summarized and potential applications are presented in the concluding section 3.6.

3.2 Mathematical Formulation

Propagation of ultra-short pulse in a lossy dispersive fiber cavity having cubic-quintic nonlinearity, gain dispersion, two and three photon absorption, we consider the following complex cubic-quintic Ginzburg-Landau equation:

$$i\frac{\partial E}{\partial z}+\frac{1}{2}\frac{\partial^2 E}{\partial t^2}+\mid E\mid^2 E+\gamma\mid E\mid^4 E=\frac{i}{2}g_o E+\frac{id}{2}\frac{\partial^2 E}{\partial t^2}-\frac{i}{2}\alpha E-iK\mid E\mid^2 E-i\nu\mid E\mid^4 E \tag{3.1}$$

where E is the normalized field distribution, z is the normalized distance of prop-

agation and t is retarded time. The first term in the left hand side of Eqn. 3.1 represents the evolution of the pulse envelope with propagation. The second term is the GVD term. The third and fourth terms represents cubic and quintic nonlinearities respectively. The CQGLE has been normalized so that coefficient of cubic nonlinearity becomes unity. γ is quintic nonlinearity coefficient normalized with respect to the cubic one. If the pulse width is larger than the intraband relaxation time, the gain spectrum $g(\omega)$ can be expanded in Taylor series about the carrier frequency ω_0 [112]. We consider up to second order derivative terms in the expansion and an operating frequency equal to the carrier frequency. This leads to the first two terms in right hand side of Eqn. 3.1. The first term in the right hand side can be inferred as the gain saturation term, which is meaningful for a pulse of energy comparable to the saturation energy of the amplifier. The second term is the second order gain dispersion term that comes into play when the pulse spectral width and the gain bandwidth are comparable. g_0 and d symbolize the coefficients of gain saturation and gain dispersion respectively. The third term accounts for the system loss, which is inherent in the medium. Here, α stands for the dimensionless wave guide loss coefficient. The fourth and fifth terms are due to the TPA and 3PA respectively. K and ν denotes the TPA and 3PA coefficients respectively. Since we choose a self-focusing cubic and defocusing quintic nonlinearity, the sign of the third term in left hand side of Eqn. 3.1 is positive while γ is negative. Sign of both K and ν is positive as they correspond to TPA and 3PA induced losses. At this point, it is worthy to mention that both cubic and quintic nonlinearity can be observed at a given wavelength, but dominance of TPA and 3PA are observed at different wavelengths. Therefore, three possibilities may arise. Firstly, at a shorter wavelength TPA will be prominent, 3PA will not occur. Secondly, at a longer wavelength 3PA will be dominant and TPA will vanish. Thirdly, at an intermediate wavelength both TPA and 3PA can be observed simultaneously. For general mathematical development (and also for the third possibility) we consider both of them and finally discuss the first two

cases by setting either $K = 0$ or $\nu = 0$.

Eqn. 3.1 is not completely integrable by the inverse scattering method. However, with some restriction, it may have a particular solution. Such systems are generally solved by using numerical methods. However, for better understanding of the system an analytical approach, even approximate one, is very important. In this context moment method and variational method in conjugation with Rayleighs dissipative function (RDF) [94] can be named. Particularly, variational method has been widely used to describe the nonlinear pulse propagation in optical fibers, even in such dissipative environment. The evolution of pulse parameters obtained by using this method is in close proximity with those observed by other methods, including direct numerical simulations. The advantage of this approach is that it gives us explicit evolution for individual system parameters. It can be noted that the left hand side of Eqn. 3.1 is conservative part, while the right hand side of the equation is dissipative part. The analytical method involves Lagrangian formulation for the conservative part and RDF generation for the dissipative part. The Lagrangian corresponding to the conservative part of Eqn. 3.1 is given by,

$$L = \frac{i}{2}(EE_z^* - E^*E_z) + \frac{1}{2} \mid E_t \mid^2 - \frac{1}{2} \mid E \mid^4 - \frac{\gamma}{3} \mid E \mid^6 \tag{3.2}$$

whereas, for the dissipative part Rayleighs dissipation function can be constructed as follows:

$$\begin{aligned} R &= \frac{id}{2}(E_{tt}^* E_z - E_{tt} E_z^*) + iK \mid E \mid^2 (EE_z^* - E^*E_z) + i\nu \mid E \mid^4 (EE_z^* - E^*E_z) \\ &- \frac{i}{2}(g_o - \alpha)(EE_z^* - E^*E_z) \end{aligned} \tag{3.3}$$

A CQGLE may lead to a variety of soliton solution profiles, e.g., bright, dark, flat-top, rotational, and chirp-free solution etc. Mostly, a bright bell shaped solution is considered. In the current investigation, a sech ansatz of the following form has been considered:

$$E(z,t) = A(z) sech\left(\frac{t}{W(z)}\right) \exp\left(i\phi(z)\right) \tag{3.4}$$

where $A(z)$, $W(z)$ and $\phi(z)$ denote the complex amplitude, temporal width and phase of the pulse respectively. The reduced Lagrangian and reduced RDF can be establish using the $L_g = \int_{-\infty}^{\infty} Ldt$, and $R_g = \int_{-\infty}^{\infty} Rdt$, in conjugation with the ansatz (i.e., Eqn. 3.4) and take the form:

$$\begin{aligned} L_g &= i(AA_z^* - A^*A_z)W(z) + 2W(z) \mid A(z) \mid^2 \frac{\partial\phi(z)}{\partial z} + \frac{1}{3}\frac{\mid A(z) \mid^2}{W(z)} \\ &- \frac{2}{3} \mid A(z) \mid^4 W(z) - \frac{16}{45}\gamma \mid A(z) \mid^6 W(z) \end{aligned} \tag{3.5}$$

$$\begin{aligned} R_g &= \frac{id}{3W(z)}\left[(AA_z^* - A^*A_z) - 2i \mid A(z) \mid^2 \frac{\partial\phi(z)}{\partial z}\right] + \frac{4i}{3}KW(z) \mid A(z) \mid^2 (AA_z^* - A^*A_z) \\ &+ \frac{8}{3}K \mid A(z) \mid^4 W(z)\frac{\partial\phi(z)}{\partial z} + \frac{32}{15}\nu \mid A(z) \mid^6 W(z)\frac{\partial\phi(z)}{\partial z} \\ &+ \frac{16i}{15}\nu \mid A(z) \mid^4 W(z)(AA_z^* - A^*A_z) \\ &- (g_o - \alpha)W(z)\left[2 \mid A(z) \mid^2 \frac{\partial\phi(z)}{\partial z} + i(AA_z^* - A^*A_z)\right] \end{aligned} \tag{3.6}$$

Now, by employing the Euler-Lagrangian equation we can obtain four equations of motion,

$$\frac{d}{dz}\left(\frac{\partial L_g}{\partial \dot{q_j}}\right) - \frac{\partial L_g}{\partial q_j} + \frac{\partial R_g}{\partial \dot{q_j}} = 0 \tag{3.7}$$

where, $\dot{q_j} = \frac{\partial q_j}{\partial z}$ and q_j is the generalized coordinate, namely, $A(z)$, $A^*(z)$, $W(z)$ and $\phi(z)$. So we get the following four equations:

$$\begin{aligned} -i\frac{d}{dz}\left(W(z)A^*(z)\right) &= iW(z)A_z^*(z) + 2W(z)A^*(z)\frac{\partial\phi(z)}{\partial z} + \frac{1}{3}\frac{A^*(z)}{W(z)} \\ &- \frac{4}{3} \mid A(z) \mid^2 A^*(z)W(z) + \frac{id}{3}\frac{A^*(z)}{W(z)} \\ &+ \frac{4i}{3}KW(z) \mid A(z) \mid^2 A^*(z) - \frac{16}{15}\gamma \mid A(z) \mid^4 A^*(z)W(z) \\ &+ \frac{16}{15}i\nu W(z) \mid A(z) \mid^4 A^*(z) - i(g_o - \alpha)W(z)A^*(z) \end{aligned} \tag{3.8}$$

$$\begin{aligned} i\frac{d}{dz}\left(W(z)A(z)\right) &= -iW(z)A_z(z) + 2W(z)A(z)\frac{\partial\phi(z)}{\partial z} + \frac{1}{3}\frac{A(z)}{W(z)} \\ &- \frac{4}{3} \mid A(z) \mid^2 A(z)W(z) - \frac{id}{3}\frac{A(z)}{W(z)} \\ &- \frac{4i}{3}KW(z)A(z) \mid A(z) \mid^2 - \frac{16}{15}\gamma \mid A(z) \mid^4 A(z)W(z) \\ &- \frac{16}{15}i\nu W(z) \mid A(z) \mid^4 A(z) + i(g_o - \alpha)W(z)A(z) \end{aligned} \tag{3.9}$$

$$i(AA_z^* - A^*A_z) = -2 \mid A(z) \mid^2 \frac{\partial\phi(z)}{\partial z} + \frac{1}{3}\frac{\mid A(z) \mid^2}{W^2(z)} + \frac{2}{3} \mid A(z) \mid^4 + \frac{16}{45}\gamma \mid A(z) \mid^6 \quad (3.10)$$

and

$$\begin{aligned} 2W(z)\left[A(z)\frac{\partial A^*(z)}{\partial z} + \frac{\partial A(z)}{\partial z}A^*(z)\right] & \\ + \; 2 \mid A(z) \mid^2 \frac{\partial W}{\partial z} & \\ + \; \frac{2d \mid A(z) \mid^2}{3W(z)} + \frac{8K}{3} \mid A(z) \mid^4 W(z) & \\ + \; \frac{32\nu}{15} \mid A(z) \mid^6 W(z) - 2(g_o - \alpha) \mid A(z) \mid^2 W(z) & \\ = \; 0 & \quad (3.11) \end{aligned}$$

Equation 3.8 $\times$ $A(z)$ - Eqn. 3.9 $\times$ $A^*(z)$ gives,

$$\begin{aligned} \frac{d}{dz}\left[2 \mid A(z) \mid^2 W(z)\right] &= -\frac{2d \mid A(z) \mid^2}{3W(z)} - \frac{8}{3}KW(z) \mid A(z) \mid^4 \\ &- \frac{32}{15}\nu W(z) \mid A(z) \mid^6 + 2(g_o - \alpha)W(z) \mid A(z) \mid^2 \quad (3.12) \end{aligned}$$

The integrated intensity of the pulse is given by $\int_{-\infty}^{\infty} \mid E(z,t) \mid^2 = 2 \mid A(z) \mid^2 W(z)$. Therefore, Eqn. 3.12 describes the dissipation of energy with propagation. The right hand side of Eqn. 3.12 vanishes in the absence of TPA, 3PA and gain dispersion. This leads to the constant intensity of the pulse befitted for a conservative system.

Again Eqn. 3.8 $\times$ $A(z)$ + Eqn. 3.9 $\times$ $A^*(z)$ gives following equation,

$$i(AA_z^* - A^*A_z) = -2 \mid A(z) \mid^2 \frac{\partial\phi(z)}{\partial z} - \frac{1}{3}\frac{\mid A(z) \mid^2}{W^2(z)} + \frac{4}{3} \mid A(z) \mid^4 + \frac{16}{15}\gamma \mid A(z) \mid^6 \quad (3.13)$$

Comparing Eqn. 3.10 and Eqn. 3.13 we get,

$$\mid A(z) \mid^2 W^2(z) + \frac{16\gamma \mid A(z) \mid^4 W^2(z)}{15} = 1 \quad (3.14)$$

The Eqn. 3.14 remains conserved throughout the propagation distance. For cubic case such condition was referred as 'fundamental soliton condition' (see [110]). It may be noted that although the 'fundamental soliton condition' remains conserved, but due to the dissipative effects it doesn't guarantee zero broadening and decay of the pulse. However, for a conservative system, the aforesaid condition can give rise to a shape

preserving soliton. In a dissipative system one needs to achieve the loss-gain balance to achieve a self-similar solitonic pulse. The above equation gives rise to the evolution equations of amplitude $A(z)$ and pulse width $W(z)$ as follows:

$$\frac{dW(z)}{dz} = \frac{\left[\begin{array}{l} \frac{-d}{3aW}\left(-1+\sqrt{M}\right) - \frac{2KW}{3a^2}\left(-1+\sqrt{M}\right)^2 \\ \quad - \frac{4\nu W}{15a^3}\left(-1+\sqrt{M}\right)^3 + (g_o-\alpha)W\frac{1}{a}\left(-1+\sqrt{M}\right) \end{array}\right]}{\left[\frac{-4}{W^2\sqrt{M}} + \frac{1}{a}\left(-1+\sqrt{M}\right)\right]} \tag{3.15}$$

$$\frac{dA(z)}{dz} = -\frac{A(1+aA^2)}{W(1+2aA^2)} \frac{\left[\begin{array}{l} \frac{-d}{3aW}\left(-1+\sqrt{M}\right) - \frac{2KW}{3a^2}\left(-1+\sqrt{M}\right)^2 \\ \quad - \frac{4\nu W}{15a^3}\left(-1+\sqrt{M}\right)^3 + (g_o-\alpha)W\frac{1}{a}\left(-1+\sqrt{M}\right) \end{array}\right]}{\left[\frac{-4}{W^2\sqrt{M}} + \frac{1}{a}\left(-1+\sqrt{M}\right)\right]} \tag{3.16}$$

where, $M = 1 + \frac{4a}{W^2}$ and $a = \frac{16\gamma}{15}$. The integrated intensity can be obtained by

$$P(z) = \int_{-\infty}^{\infty} \mid u(z,t) \mid^2 dt \tag{3.17}$$

For investigating the dissipative pulse propagation, the coupled equations 3.15 and 3.16 are the key equations. The model can be simplified if the gain saturation can perfectly counter balance the system loss, i.e. $g_0 = \alpha$. For this case the pulse width and amplitude vary as follows:

$$\frac{dW(z)}{dz} = \frac{\left[\frac{-d}{3aW}\left(-1+\sqrt{M}\right) - \frac{2KW}{3a^2}\left(-1+\sqrt{M}\right)^2 - \frac{4\nu W}{15a^3}\left(-1+\sqrt{M}\right)^3\right]}{\left[\frac{-4}{W^2\sqrt{M}} + \frac{1}{a}\left(-1+\sqrt{M}\right)\right]} \tag{3.18}$$

$$\frac{dA(z)}{dz} = -\frac{A(1+aA^2)}{W(1+2aA^2)} \frac{\left[\frac{-d}{3aW}\left(-1+\sqrt{M}\right) - \frac{2KW}{3a^2}\left(-1+\sqrt{M}\right)^2 - \frac{4\nu W}{15a^3}\left(-1+\sqrt{M}\right)^3\right]}{\left[\frac{-4}{W^2\sqrt{M}} + \frac{1}{a}\left(-1+\sqrt{M}\right)\right]} \tag{3.19}$$

Thus we investigate the system under two conditions:

Case I: When gain saturation g_0 is equal to system loss α ($g_0 = \alpha$).

Case II: When gain saturation g_0 is greater than system loss α ($g_0 > \alpha$).

3.3 Dissipative Pulse Propagation:($g_0 = \alpha$)

In this section, we discuss the pulse dynamics for a system when the gain saturation is equal to the system loss, i.e., $g_0 = \alpha$. In spite of this gain-loss balance, the system will still remain dissipative because of the detrimental influence of gain dispersion and multi-photon absorption on pulse dynamics. Besides simplification, the condition $g_0 = \alpha$ will increase the 'visibility' of the gain dispersion, TPA and 3PA.

3.3.1 Analytical Results

To find the dissipative pulse dynamics equations 3.18 and 3.19 are solved. Depending on the wavelength of the pulse we consider three different situations: a shorter wavelength that corresponds to TPA, a longer wavelength that corresponds to 3PA and an intermediate wavelength, which shows both TPA and 3PA. A very recent work reported (see [121]) deals with such cases for wavelengths ranging from 1.15μm to 1.55μm in hydrogenated amorphous silicon. Due to the high nonlinearity, low loss and capacity of high power transmission at telecommunication wavelength, optical fiber core are fabricated using such materials [122]. TPA dominates over 3PA at lower wavelengths, namely, at 1.15μm and 1.25μm. 3PA is dominating at a larger wavelength, i.e., at 1.5μm. The coexistence of TPA and 3PA is observed at the intermediate wavelength 1.3μm,. This situation is indeed interesting as in this state the dominance of TPA or 3PA is intensity dependent. Since TPA and 3PA are proportional to the square and cube of the field intensity respectively, so at low intensity, 2PA dominates nonlinear absorption while 3PA dominates at high intensity. For all three cases of multiphoton absorption, other aspects like gain dispersion and cubic-quintic nonlinearity are present. First, we consider a shorter wavelength where TPA is dominant and 3PA is too small to consider. The effect of 3PA can be rejected by setting $\nu = 0$ in equations 3.18 and 3.19. The variation of peak intensity (i.e., $\mid A \mid^2$) with propagation distance is demonstrated in left hand side column of Figure 3.1, taking quantic nonlinearity (Figure 3.1 (a)), gain

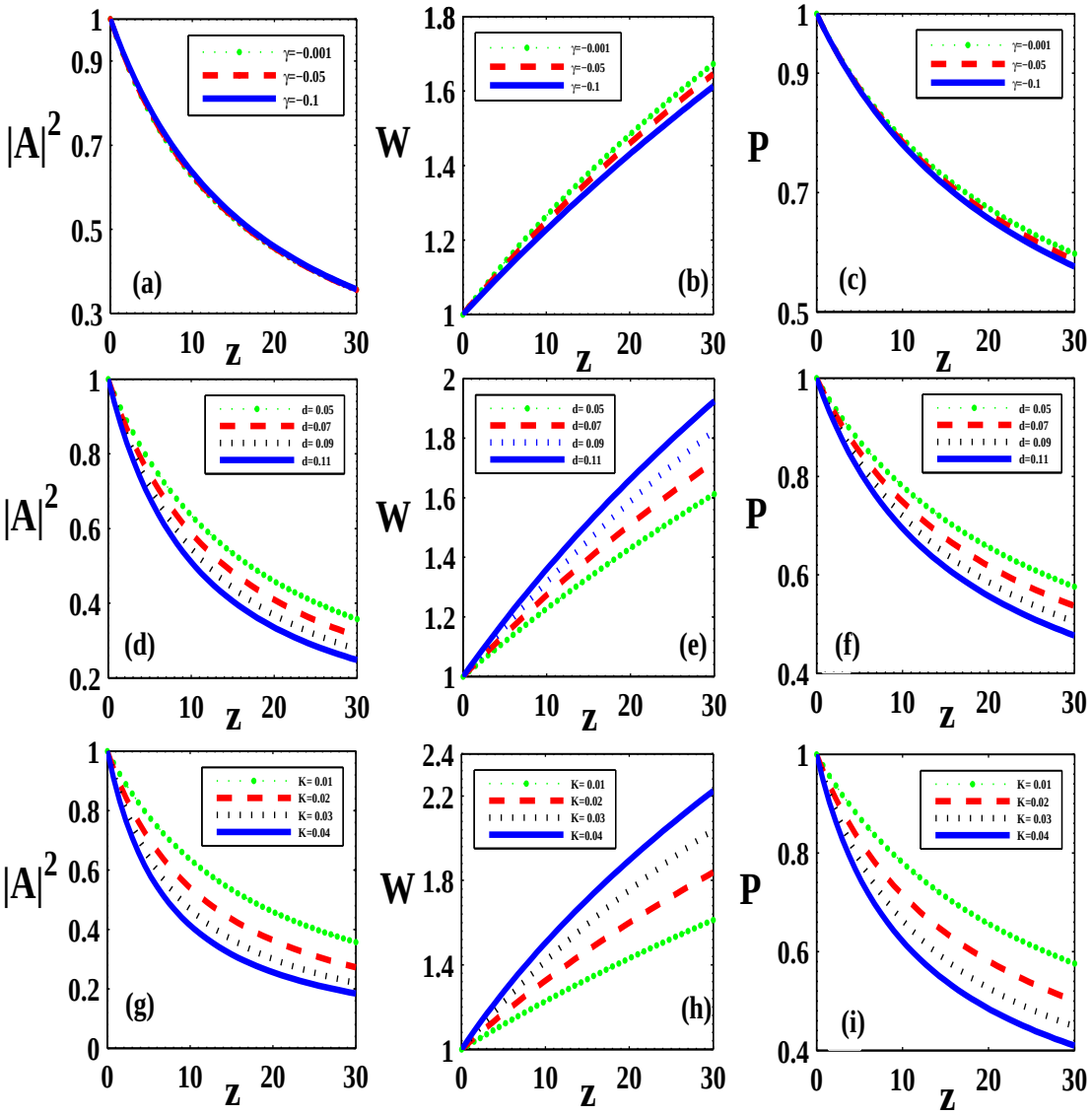

Fig. 3.1: Pulse degradation with normalized propagation distance in presence of TPA. (a) Decay of peak intensity, (b) pulse broadening and (c) integrated pulse intensity decay for different γ, $d = 0.05$ and $K = 0.01$. (d) Decay of peak intensity, (e) pulse broadening and (f) decay of integrated pulse intensity for different d with $\gamma = -0.1$ and $K = 0.01$. (g) Decay of peak intensity, (h) pulse broadening and (i) integrated pulse intensity decay for different K with $\gamma = -0.1$ and $d = 0.05$. For (a)-(i), $\nu = 0$.

dispersion (Figure 3.1 (d)) and TPA (Figure 3.1 (g)) as parameters. Corresponding variation of pulse width with normalized propagation distance is demonstrated in the middle column of Figure 3.1, i.e., in Figure 3.1 (b), 3.1 (e) and 3.1 (h) respectively. Plots in the right hand side columns (i.e., Figure 3.1 (c), 3.1 (f) and 3.1 (i)) portray the

corresponding variation of integrated pulse intensity (P). Due to the detrimental effect of TPA and gain dispersion a common trend of pulse amplitude decay (Figure 3.1 (a), 3.1 (d) and 3.1 (g)) and pulse width broadening (Figure 3.1 (b), 3.1 (e) and 3.1 (h)) is observed with propagation along the fiber length. Similar decay-trend is observed in the integrated pulse intensity too. Further it is noticed in Figure 3.1 (a) that the variation in quintic nonlinearity marginally modifies the pulse decay behaviour. But visible pulse width contraction is noticed with increasing quantic nonlinearity (Figure 3.1 (b)). The integrated pulse intensity decreases with increasing strength of quintic nonlinearity. The influence of the gain dispersion can be understood by noting Figure 3.1 (d), 3.1 (e) and 3.1 (f), wherein the gain dispersion considerably degrades the pulse quality during propagation. With increasing gain dispersion the decay rate of both peak intensity (Figure 3.1 (d)) and integrated pulse intensity (Figure 3.1 (f)) increases. Side by side, pulse broadening becomes faster as displayed in Figure 3.1 (e). TPA is expectedly found to be detrimental to the pulse quality. The rate of pulse decay (Figure 3.1 (g) and 3.1 (i)) and pulse broadening (Figure 3.1 (h)) become faster with stronger TPA. We now investigate the pulse propagation at a wavelength where 3PA is dominant and TPA is negligible. Like the case of TPA in this case also the peak intensity and integrated pulse intensity decay and pulse broadens with propagation as depicted in Figure 3.2. The effects of quintic nonlinearity (Figure 3.2 (a)-(c)) and gain dispersion (Figure 3.2 (d)-(f)) are similar to the TPA case. A careful comparison of these figures with their TPA counterpart in Figure 3.1 (a)-(f) reveals that the pulse decay and broadening rate are significantly slower in 3PA case. Thus shifting from TPA to 3PA wavelength would be beneficial in terms of maintaining pulse quality during propagation. Figure 3.2 (g), 3.2 (h) and 3.2 (i) respectively display the variation of peak intensity, integrated pulse intensity and pulse width with propagation distance, taking as a parameter. Like the case of TPA, increasing strength of 3PA (ν) leads to pulse decay and broadening but at a much smaller rate. A third situation may arise when in

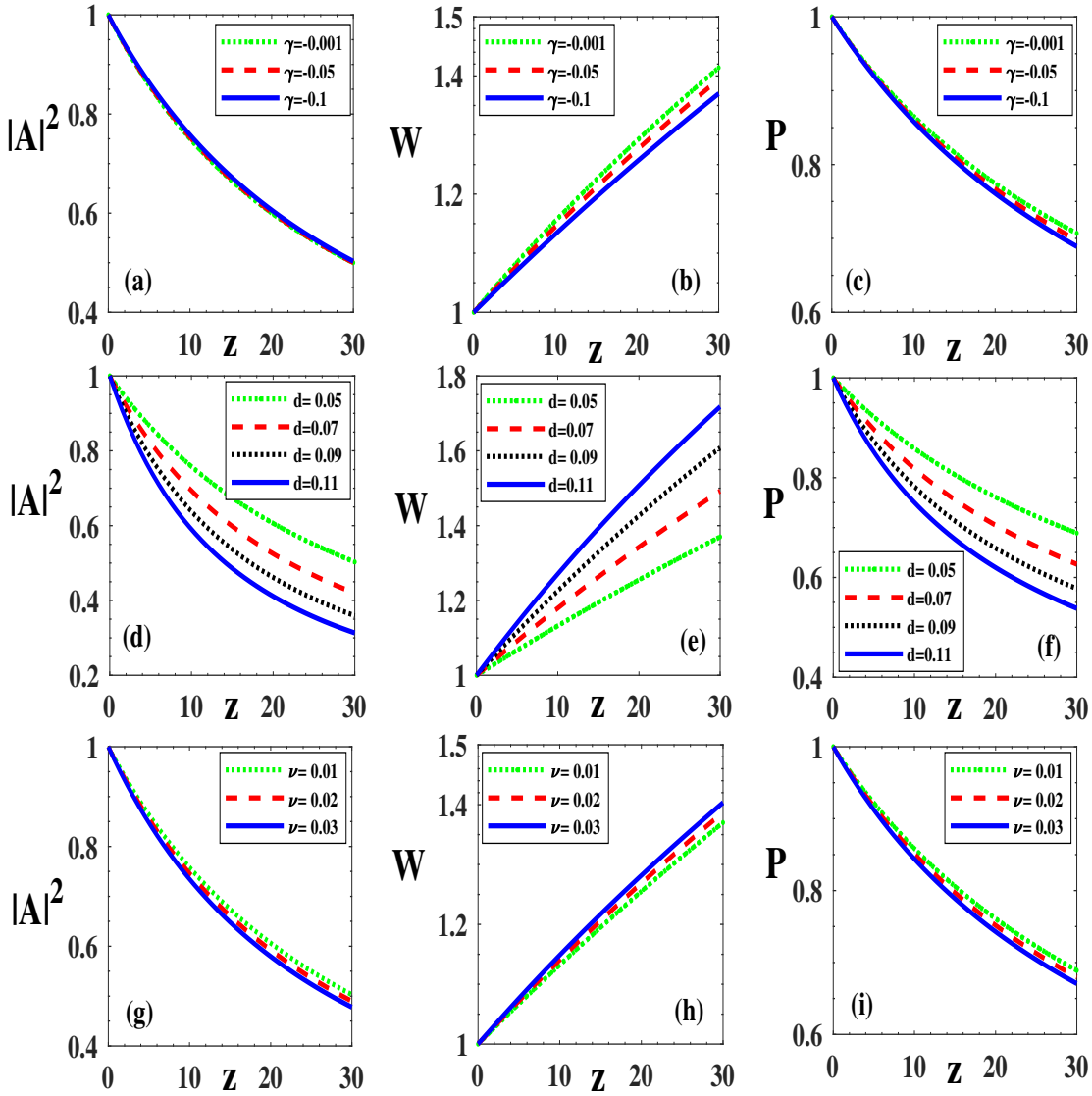

Fig. 3.2: Evolution of pulse parameters with normalized distance of propagation in presence of 3PA. (a) Decay of peak intensity, (b) pulse broadening and (c) integrated pulse intensity decay for different γ with $d = 0.05$ and $\nu = 0.01$. (d) Decay of peak intensity, (e) pulse broadening and (f) integrated pulse intensity decay for different d and γ = -0.1 and $\nu = 0.01$. (g) Decay of peak intensity, (h) pulse broadening and (i) integrated pulse intensity decay for different ν with γ = -0.1 and $d = 0.05$. For (a)-(i), K= 0.

both TPA and 3PA are sizable at an intermediate wavelength. The combined influence of TPA, 3PA and gain dispersion ultimately leads to the decay as well as broadening of the pulse.

The variation of peak intensity, pulse width and integrated pulse intensity with

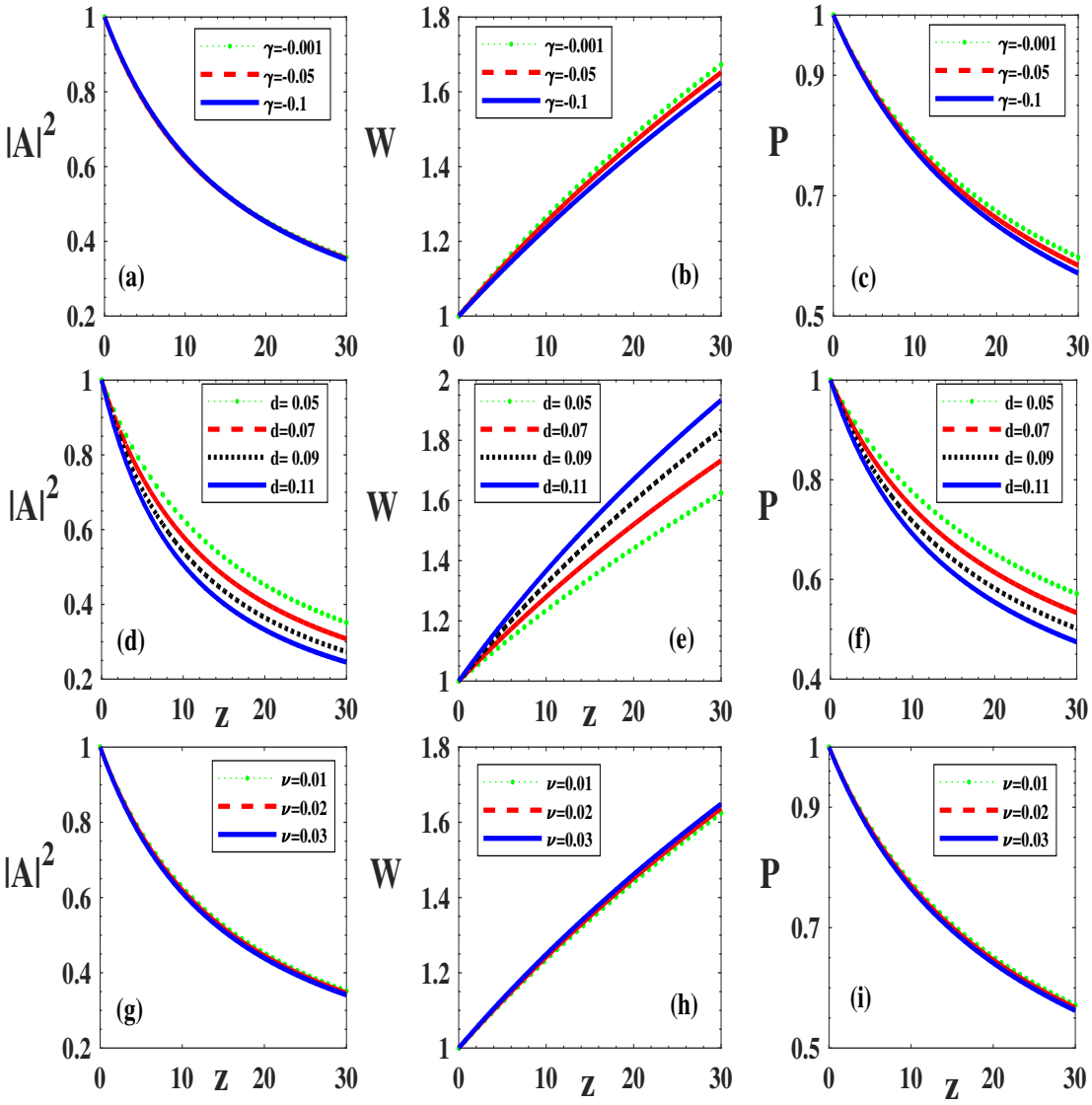

Fig. 3.3: Pulse degradation with normalized distance of propagation under combined influence of TPA and 3PA. (a) Decay of peak intensity, (b) pulse broadening and (c) decay of integrated pulse intensity for different γ with d = 0.05, K = 0.01 and ν = 0.01. (d) Decay of peak intensity, (e) pulse broadening and (f) integrated pulse intensity decay for different d and γ = -0.1, K = 0.01 and ν = 0.01. (g) Peak intensity decay, (h) pulse broadening and (i) decay of integrated pulse intensity for different ν with γ = -0.1, d = 0.05 and K = 0.01.

propagation distance is plotted in Figure 3.3 (a), 3.3 (b) and 3.3 (c) respectively taking γ as a parameter. Corresponding sets of plots are presented in Figure 3.3 (d)-(f) for different d and in Figure 3.3 (g)-(i) for different ν. By comparing Figure 3.3 (a)-(i) with

their corresponding plots in Figure 3.1 (a)-(i) and Figure 3.2 (a)-(i), it can be noted that the major share of the detrimental effect on peak intensity, width and integrated intensity of the pulse goes to TPA. The monotonous decay or broadening profiles turn interesting with a choice of negative value of the imaginary part of $\chi^{(5)}$ and hence a negative ν. This leads to an effect opposite to 3PA, thus can be considered as three photon emission. Since 3PA introduces loss in the system, 3PE should provide gain. Once again, we plot the variation of peak intensity, pulse width and integrated pulse intensity with propagation distance under the influence of gain dispersion, TPA but for different strength of 3PE. It can be noted that increasing strength of 3PE reduces, although slightly, the rate of both pulse decay (Figure 3.4 (a) and 3.4 (c) and the corresponding insets) as well as pulse broadening (Figure 3.4 (b)). Thus 3PE will be favourable for arresting pulse decay and broadening, and hence for the generation solitonic pulse. At this point, it is better to mention that the reports on 3PE are rather rare. However, polarization-correlated 3PE from a positively charged triexciton

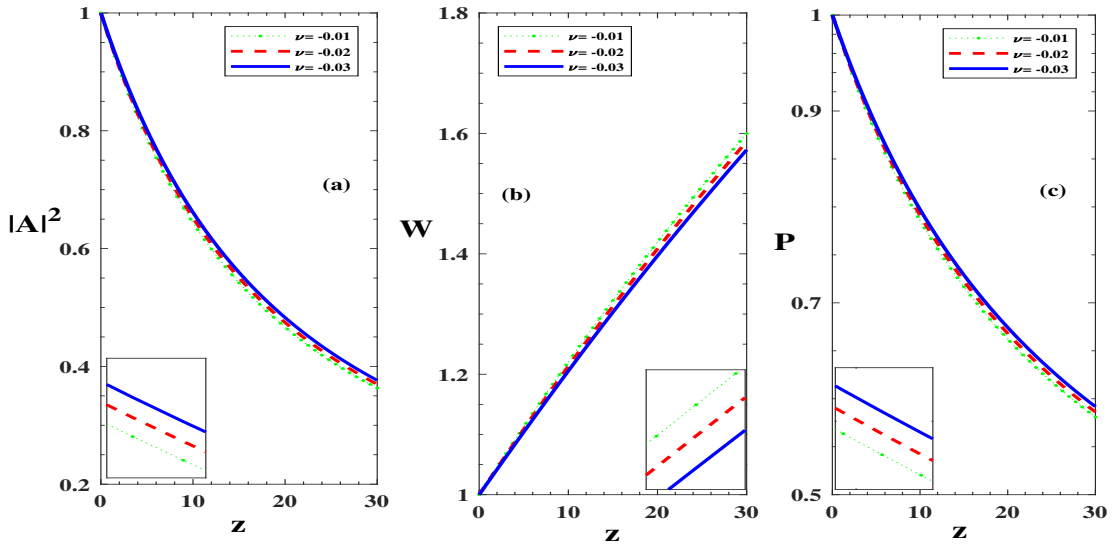

Fig. 3.4: Variation of normalized (a) peak intensity, (b) pulse width and (c) integrated pulse intensity along the fiber in presence of both TPA and 3PE for different values of 3PE coefficient with $d = 0.05$ and $K = 0.01$ and γ = -0.1. The corresponding insets show the blown-up views.

in a self-assembled $GaAs$ quantum dot (QD) has been reported [123]. More reports of multiphoton emission in semiconductor devices are coming out recently. The first experimental observations of two-photon emission (TPE) from semiconductors has been reported in [124], wherein spontaneous and singly stimulated TPE were demonstrated in optically pumped $GaAs$ and in current-driven $GaInP/AlGaInP$ quantum well. However, the experimental realization of 3PE in a semiconductor is yet to come. In this report we intend to provide the mathematical modelling for a fiber link with 3PE and to highlight its advantage for compensating loss in the process of obtaining dissipative solitons.

3.3.2 Numerical Results

The results obtained analytically so far need to be validated by directly solving the governing CQGLE. Figure 3.5 displays the pulse propagation under the influence of gain dispersion and TPA for different strength of quintic nonlinearity. Figure 3.5 (a) corresponds to γ = -0.001, while Fig. 3.5 (b) and 3.5 (c) are plotted for γ = -0.05 and γ = -0.1 respectively. Corresponding peak intensity and pulse width are depicted in the left and right hand side insets respectively. The decay of peak intensity and broadening of pulse width are almost in accordance with the analytical result. Only an additional oscillation in peak intensity and width is present. This seems to be originated due to the counteracting effects of focusing cubic and defocusing quintic nonlinearity. However, because of the approximate nature of the variational method such oscillations are too weak to observe in analytical results. The numerically obtained pulse evolution profile thus qualitatively matches with the analytical one. Pulse propagation is also numerically obtained by taking d and K as parameters. The nature of pulse evolution for those cases too (not shown) qualitatively matches with that found analytically. We then plot the pulse propagation in 3PA wavelength in presence of gain dispersion for different strength of quintic nonlinearity.

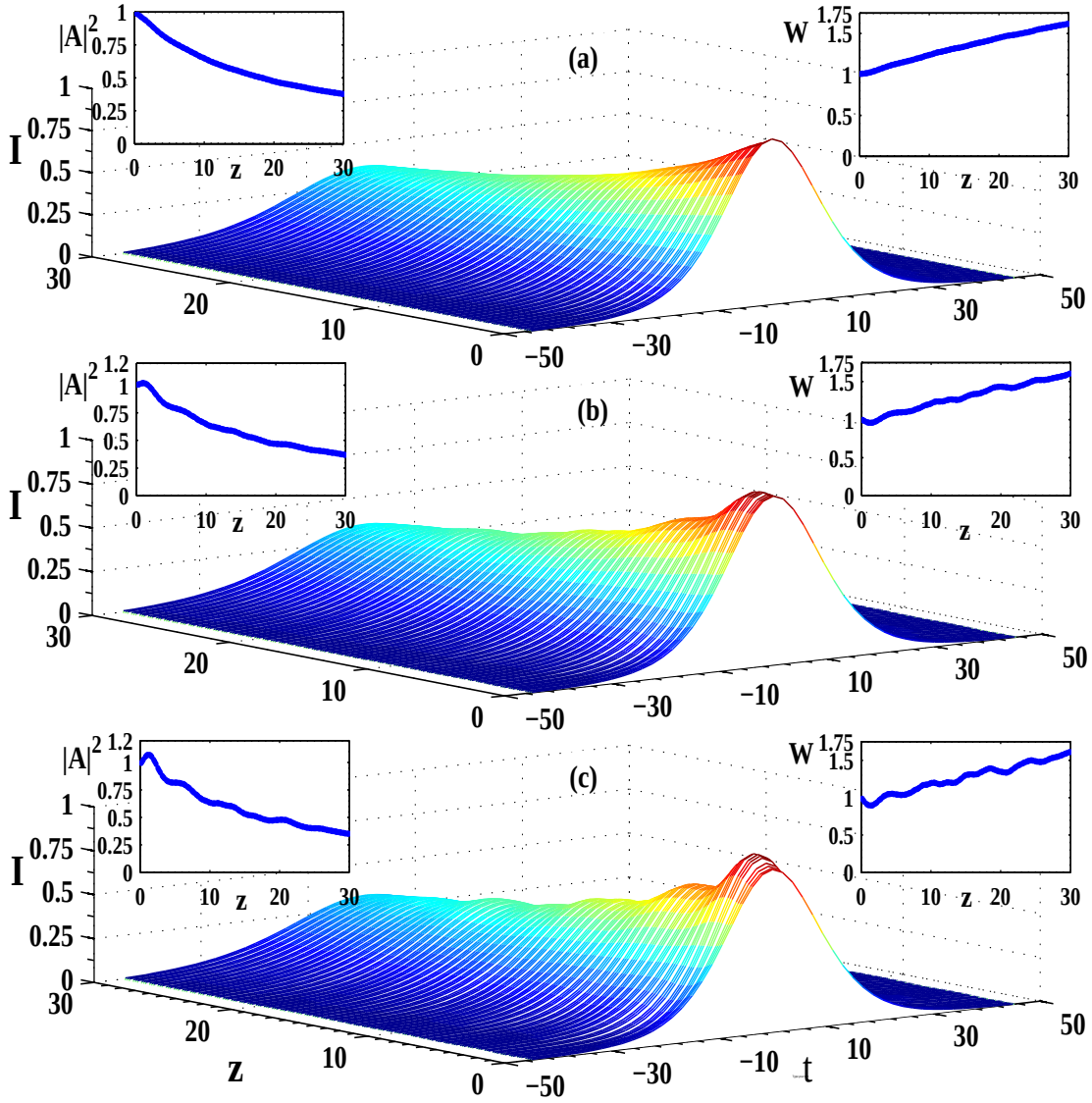

Fig. 3.5: Pulse intensity profile under the effect of TPA and gain dispersion with propagation distance for (a)γ = -0.001, (b)γ = -0.05, (c)γ = -0.1 respectively. Insets on left hand side show the variation of peak intensity and those on right hand side show the variation of normalized pulse width along the fiber. Here K = 0.01, d = 0.05.

Figure 3.6 shows the pulse propagation profile and corresponding variation in peak intensity and pulse width for (a) γ = -0.001, (b) γ = -0.05 and (c) γ = -0.1. The decay and broadening trend is found to be similar to that of the analytical case presented in Fig. 3.2. Similar study under combined influence of TPA and 3PA is presented in Fig. 3.7 for varying strength of γ. This case too resembles with the analytical one

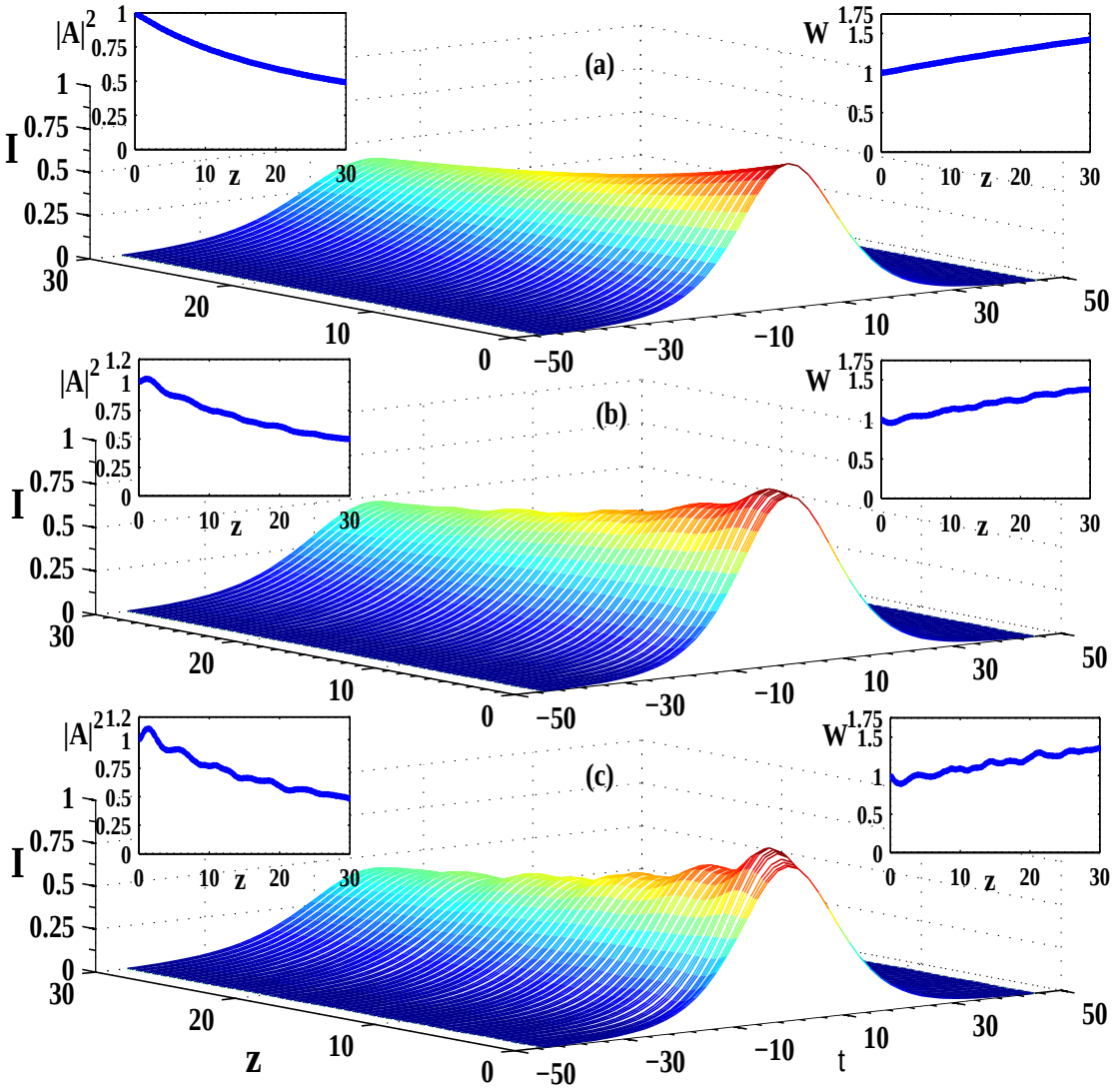

Fig. 3.6: 3D plot showing the effect of 3PA and gain dispersion on pulse propagation along the fiber for (a)γ = -0.001, (b) γ = -0.05, (c) γ = -0.1 respectively. Left hand side insets show the variation of peak intensity and right hand side insets depict the variation of normalized pulse width with propagation. ν = 0.01 and d = 0.05.

depicted in Fig. 3.3. The pulse propagation behaviour has been extensively studied with different values of d and K for both 3PA and combined case of TPA and 3PA. For all cases, the numerical results are found to be identical to the corresponding analytical case, but not shown just to make the chapter less crowded with figures. Furthermore, we numerically verified the case of Fig. 3.4 with 3PE and got matching gain behaviour

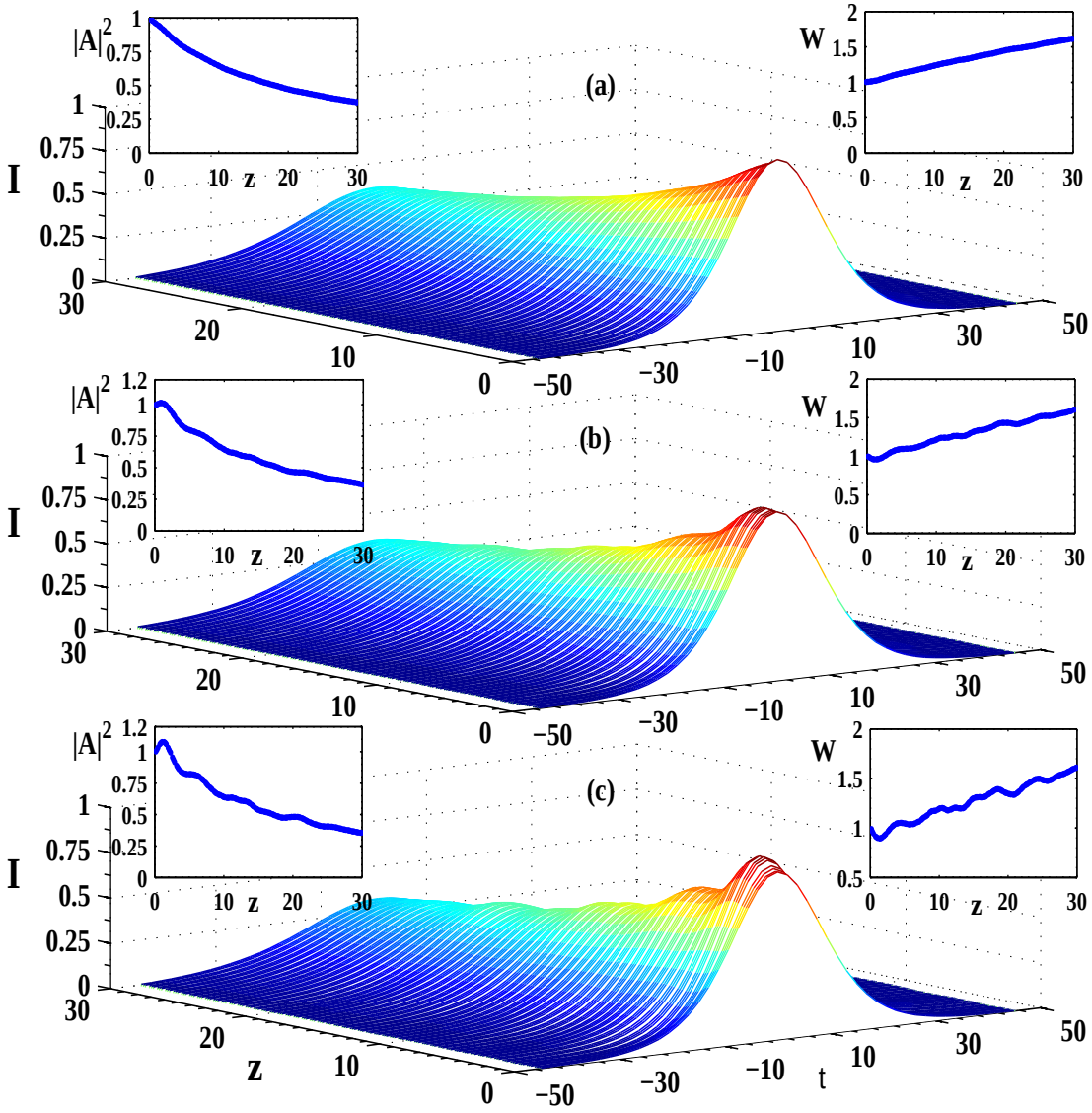

Fig. 3.7: Evolution of pulse intensity profile under the combined effect of TPA and 3PA along the fiber for (a) γ = -0.001, (b) γ = -0.05, (c) γ = -0.1 respectively. Insets on left hand side portray the variation of peak intensity and insets on right hand side show the variation of normalized pulse width along the fiber. Here $K = 0.01$, $d = 0.05$ and $\nu = 0.01$.

of 3PE. This is presented in Fig. 3.8.

3.4 Solitonic Pulse Propagation: ($g_0 > \alpha$)

The investigation in the previous section shows pulse decay and broadening for all three cases of multiphoton absorption. The dissipative nature can be arrested by ap-

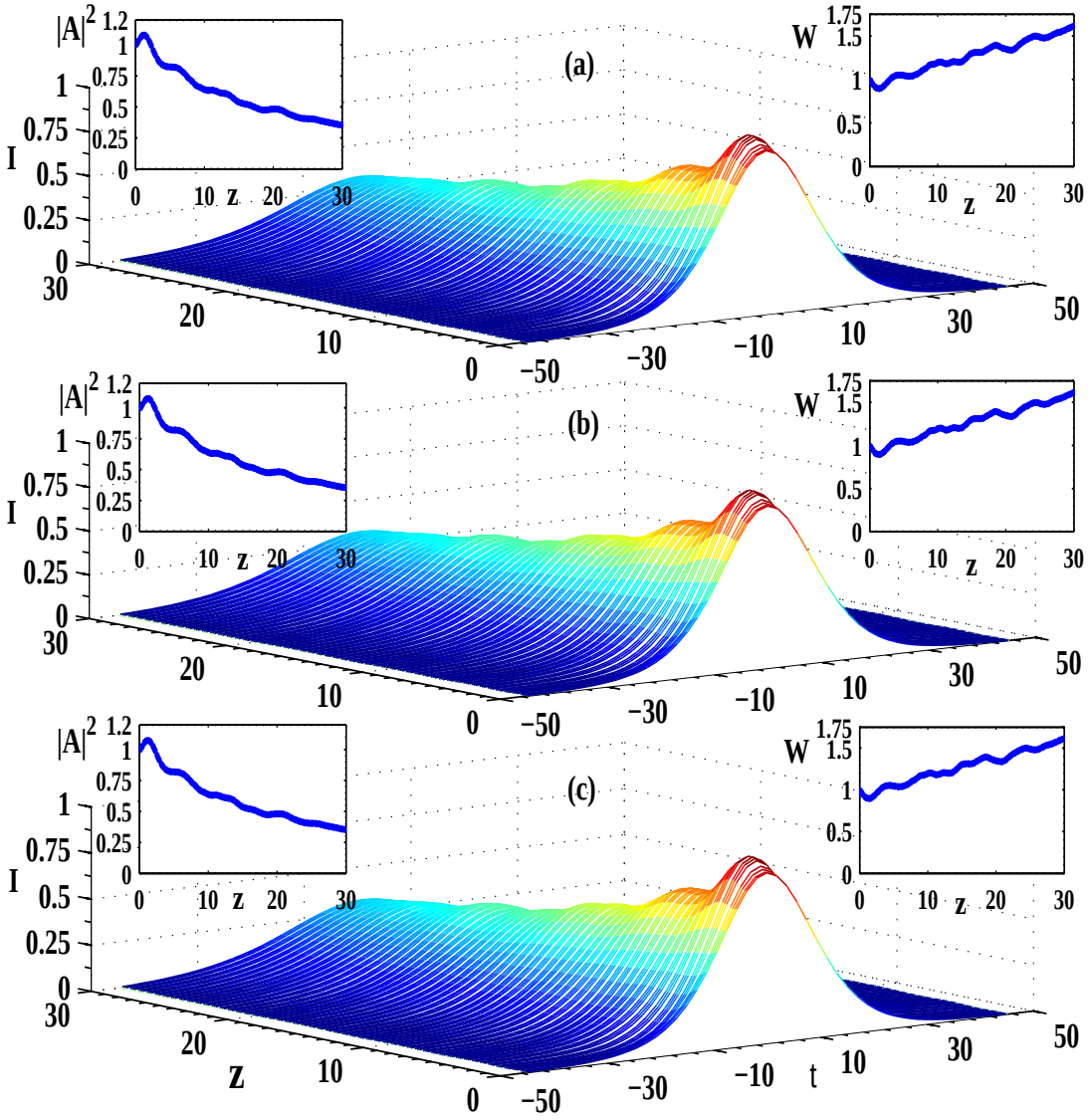

Fig. 3.8: 3D pulse evolution in presence of both TPA and 3PE along the fiber length for (a) γ = -0.001, (b)γ = -0.05, (c) γ = -0.1 respectively. Left hand side insets show the variation of peak intensity and right hand side insets show the variation of normalized pulse width with propagation along the fiber. Here, $K = 0.01$, $d = 0.05$ but ν = -0.01.

plying right amount of gain in the system. This can be done by a suitable choice of Δg ($= g_0 - \alpha$), where $g_0 > \alpha$. If g_0 is not sufficiently larger than α an additional gain might be introduced in the system. An effective and suitable gain is must and we refer that by Δg. In this section, we search for the desired gain and demonstrate the evolution of solitonic pulse. Since these solitons originate in dissipative media they

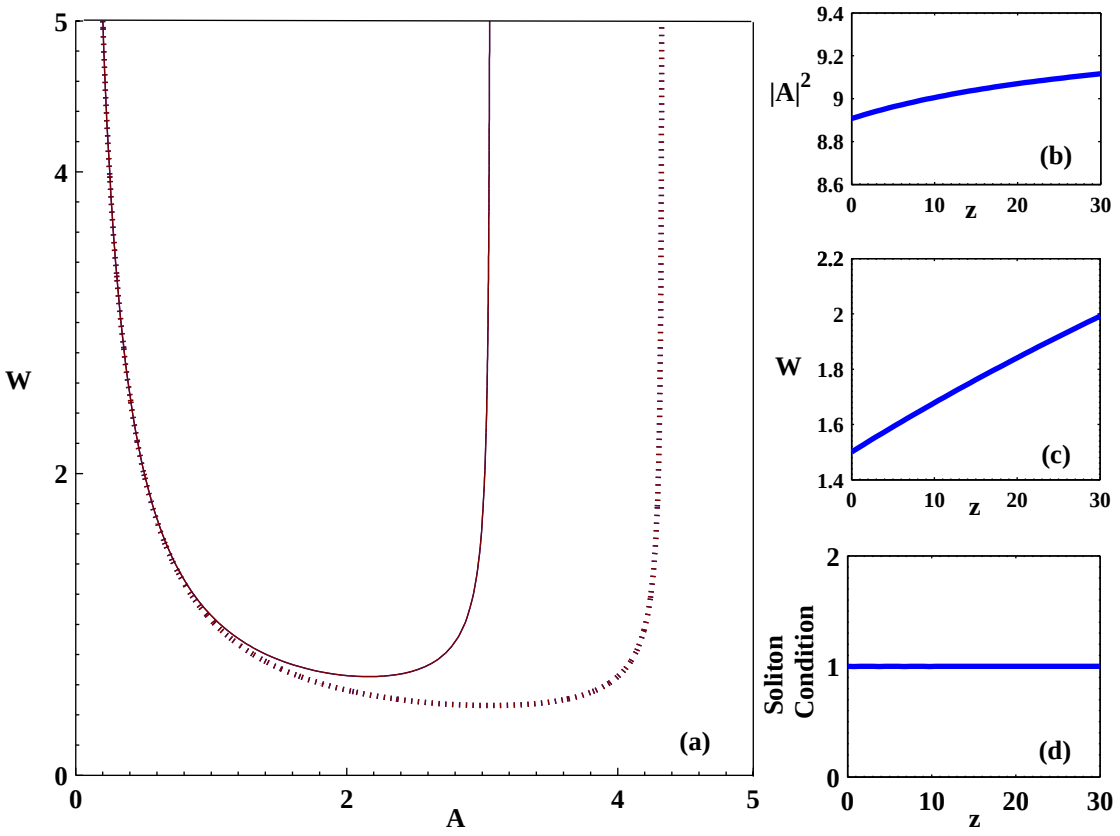

Fig. 3.9: (a) Bistability curve corresponding to Eqn. 3.14. Solid line is for γ = -0.1 and dashed line for γ = -0.05. (b) and (c) show the peak intensity and width respectively whereas (d) depicts the soliton condition, which is conserved.

can be considered as dissipative soliton. Such dissipative solitons might be bistable due to the quintic term in the fundamental soliton condition given by Eqn. 3.14. Figure 3.9 (a)plots the bistability curves for γ = -0.1 and γ = -0.05. All the points on the curves satisfy soliton condition. Figure 3.9 (d) shows the analytically obtained soliton condition with one such point, while Figs. 3.9 (b) and (c) show the peak intensity and pulse width variation. We found from Figure 3.9 (a) that solitons of same width but of two different amplitudes can arise and leads to bistability. One such bistable soliton corresponding to Figure 3.9 (a) is shown in Figs.3.10 (a)-(c) and (e)-(g) analytically. Corresponding numerically obtained bistable soliton is presented in Figs.3.10 (d) and (h) and their insets. We now find the dissipative soliton for all three cases of multipho-

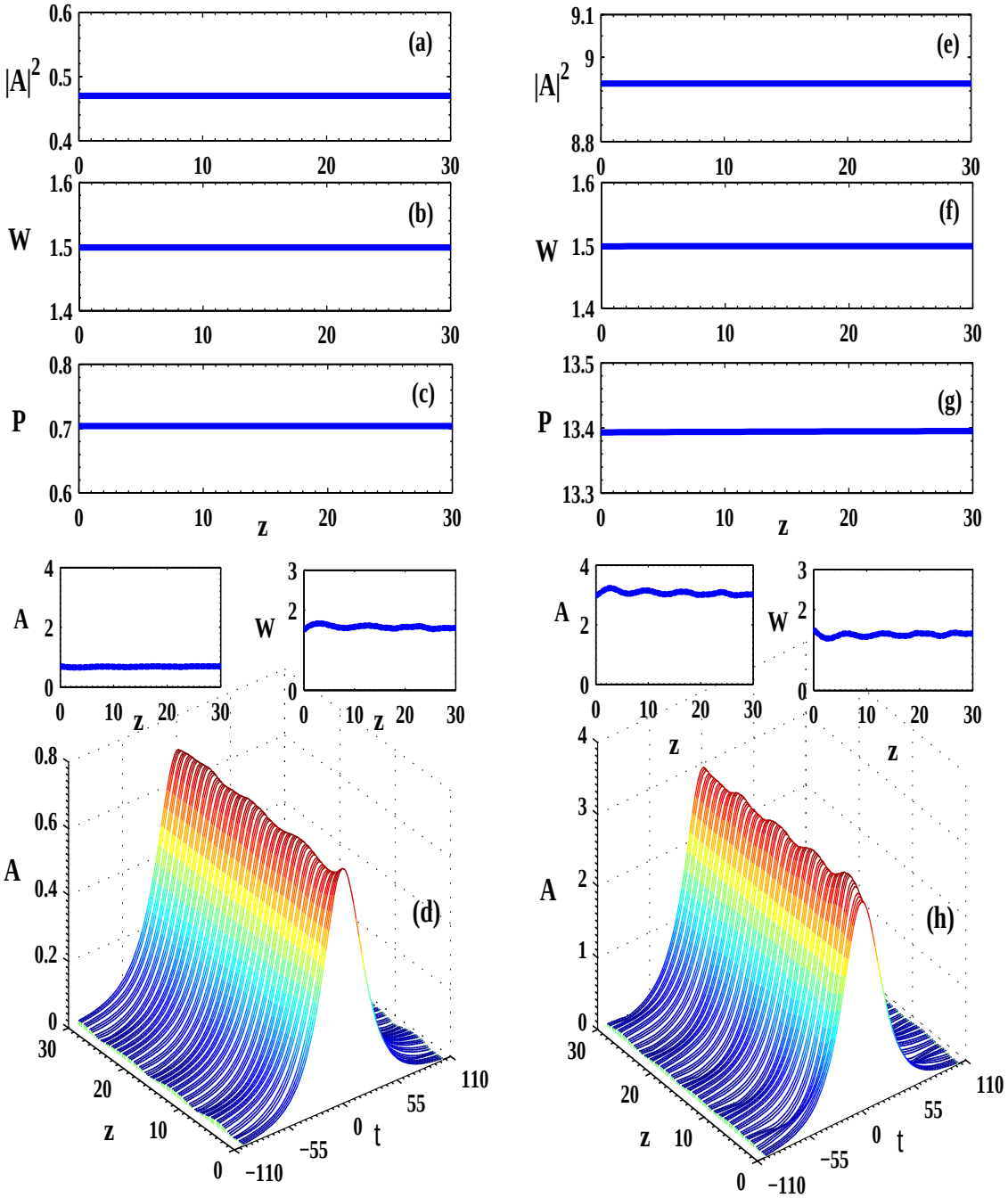

Fig. 3.10: Bistable dissipative solitons of low and high amplitude corresponding to bistability curve and obtained by injecting proper gain into the system. (a), (b), (c) show analytical evolution, whereas, (d) show numerical evolution for low amplitude soliton. Similar evolution for high amplitude soliton is shown analytically in (e), (f), (g) and numerically in (h).

ton absorption with gain dispersion and cubic-quintic nonlinearity. For TPA case, a normalized Δg of 0.805×10^{-6} leads to constant peak intensity, width and integrated

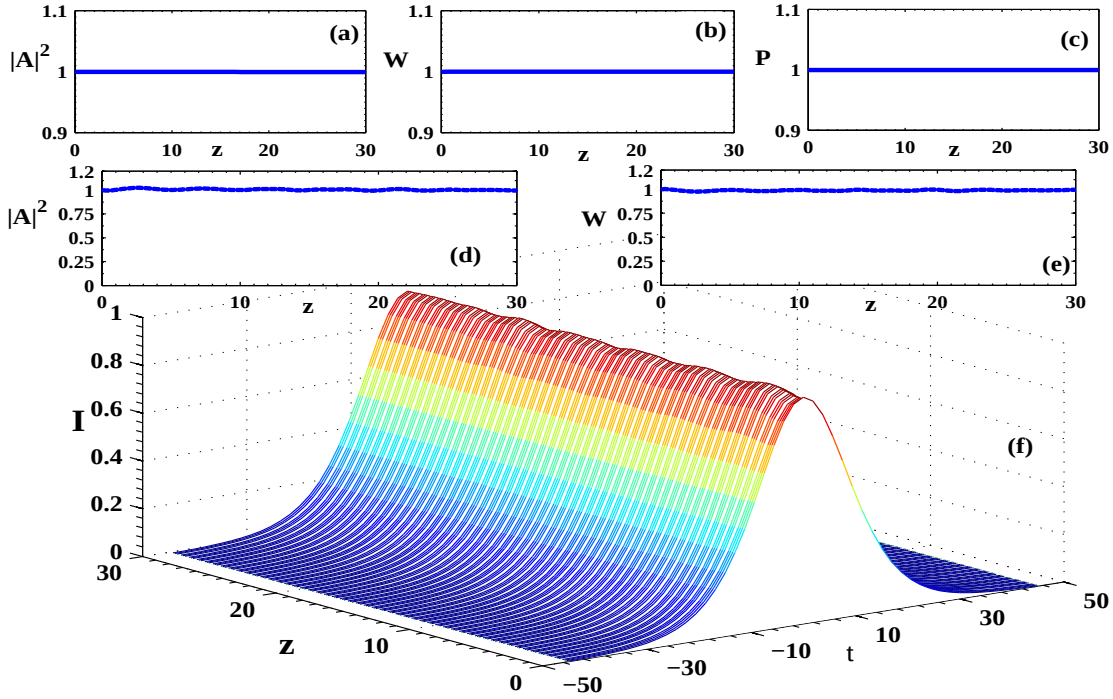

Fig. 3.11: Evolution of dissipative soliton under effect of TPA. The parameters taken are γ = -0.001, d = 0.05 and K = 0.01.

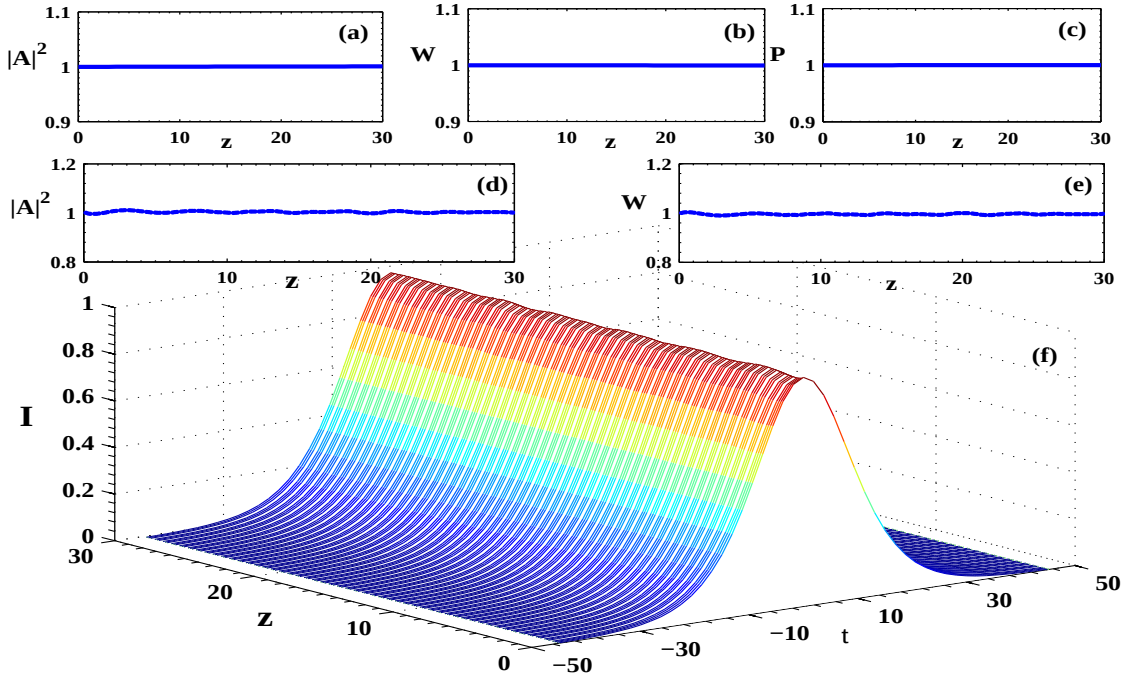

Fig. 3.12: Evolution of dissipative soliton in presence of 3PA. Here, γ = -0.001, d = 0.05 and ν = 0.01.

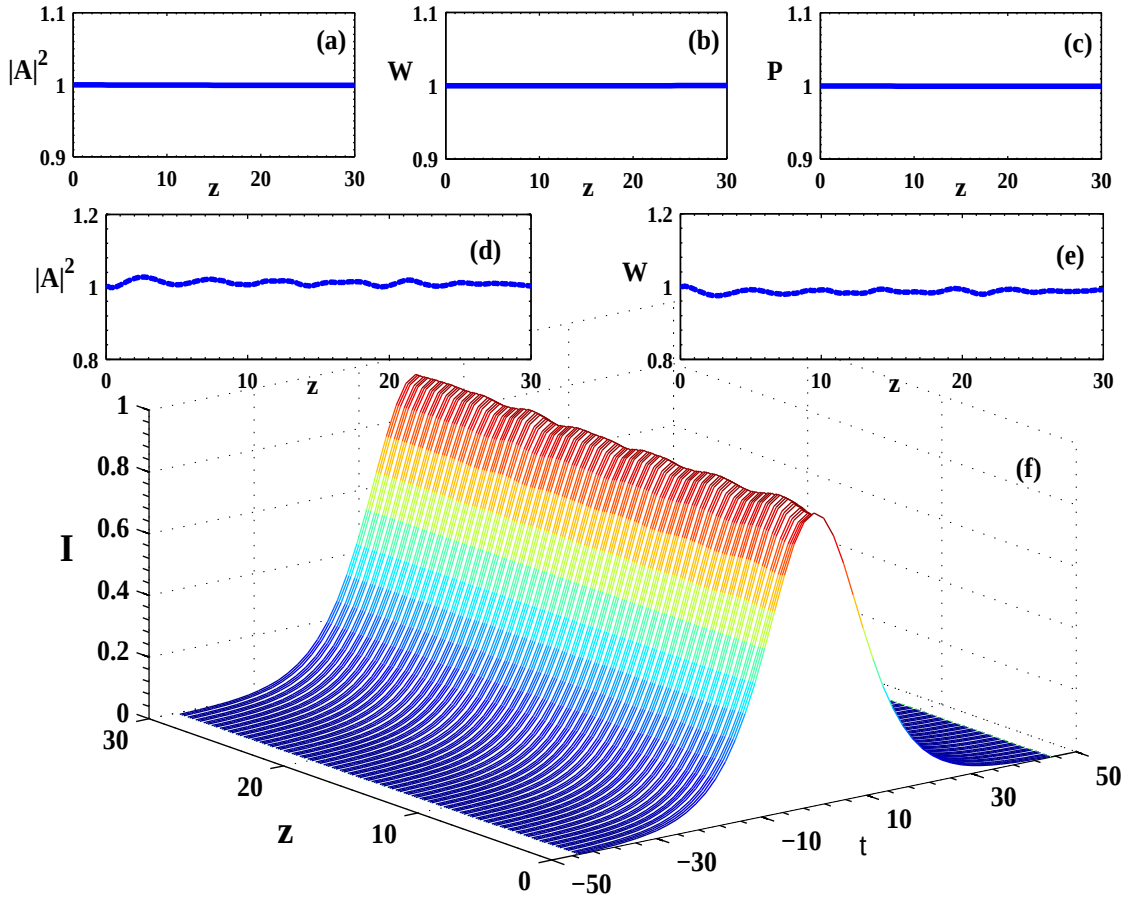

Fig. 3.13: Evolution of dissipative soliton under combined effect of TPA and 3PA. The parameters are γ = -0.001, d = 0.05, ν = 0.01 and K = 0.01.

intensity as described in Figs. 3.11 (a), (b) and (c) respectively using the analytical method. Their corresponding numerical curves are presented in Figs. 3.11 (d), (e) and (f) respectively. Other than the slight fluctuation due to quintic terms, the numerical results also show self-similar propagation of the pulse. This shows the generation of dissipative soliton. Similar evolution of dissipative soliton is shown for 3PA in Fig. 3.12 with a normalized $\Delta g = 0.500 \times 10^{-6}$. When it comes to the combined case of TPA and 3PA normalized Δg of 0.805×10^{-6} leads to the formation of dissipative soliton. The analytical as well as numerical results are presented in Fig. 3.13.

3.5 Effect of Initial Chirp

Till now we considered a pulse or soliton profile with zero initial chirp. Effect of initial chirp on the soliton propagation has been studied by taking ansatz of the form:

$$E(z,t) = Asech\left(\frac{t}{W}\right) exp\left[i\left\{\phi - \frac{c}{2}\frac{t^2}{W^2}\right\}\right] \tag{3.20}$$

where, A denotes complex amplitude, t_0 is temporal width, ϕ denotes phase and c represents chirp. It has been observed that by increasing the value of initial chirp, the oscillations in the pulse increases along with the emergence of more side band oscillations (Fig. 3.13). This is true for both low amplitude (Fig. 3.13 a,c,e) and high amplitude (Fig. 3.13 b,d,f) soliton.

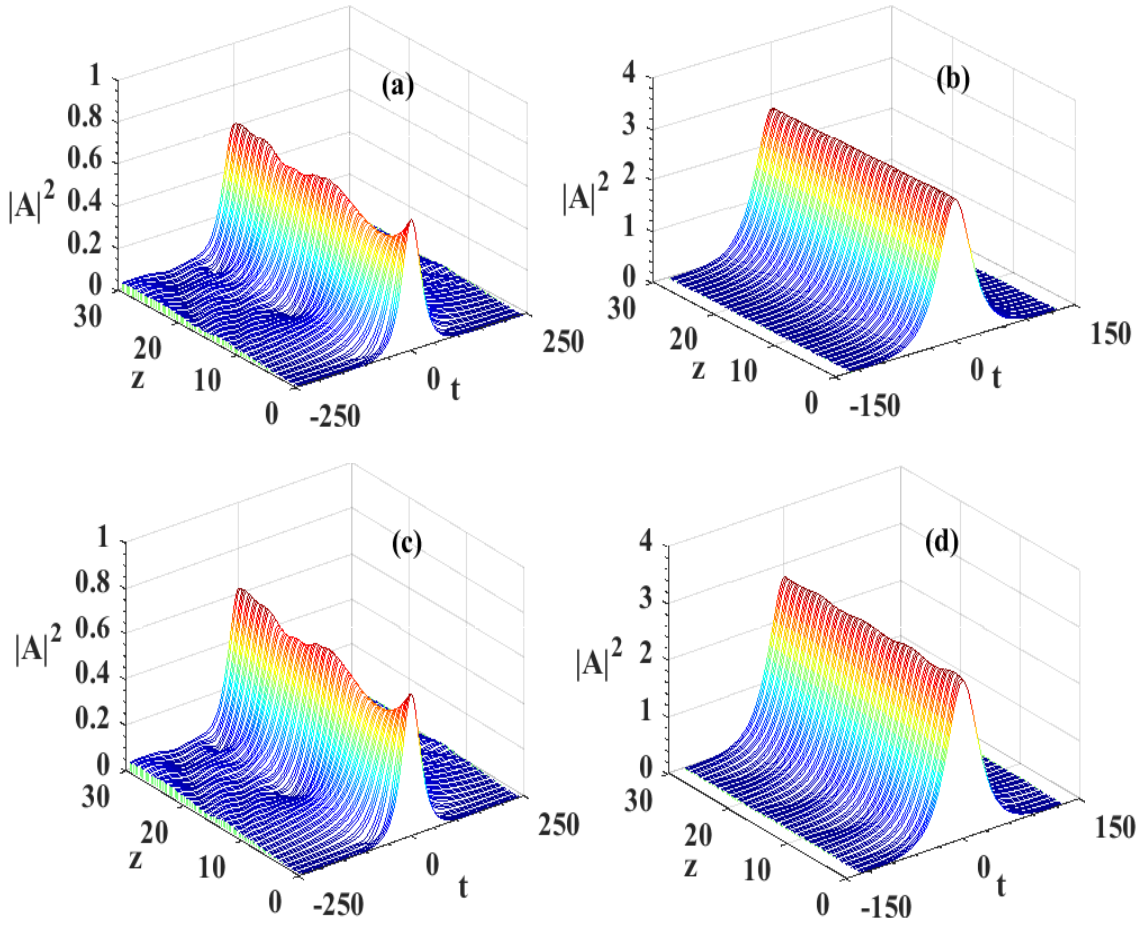

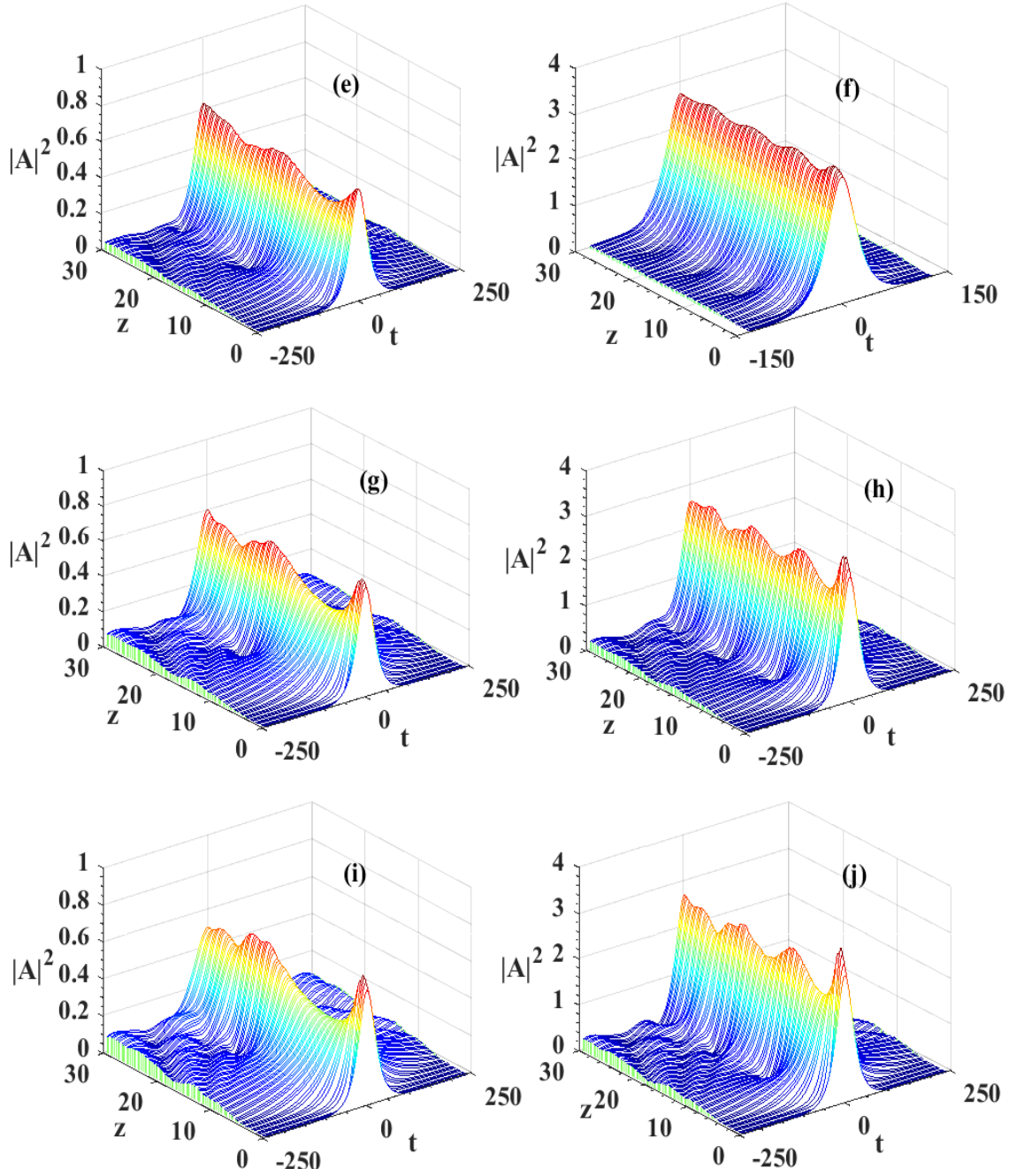

Fig. 3.13: Effect of chirp on (a, c, e) the low amplitude and high amplitude (b, d, f) solitonic pulse by incresing the value of chirp in presence of both TPA and 3PA. The parameters are γ = -0.001, $d = 0.05$, $\nu = 0.01$and $K = 0.01$. For(a) & (b) chirp = 0.01, for(c) & (d) chirp = 0.05, for (e) & (f) chirp =0.1, for(g) & (h) chirp = 0.3 and for(i) and (j) chirp = 0.4.

Also, dissipative soliton have been generated with low and high value of initial chirp with TPA, 3PA and both TPA & 3PA (Fig. 3.14). For high value of initial chirp (0.3),

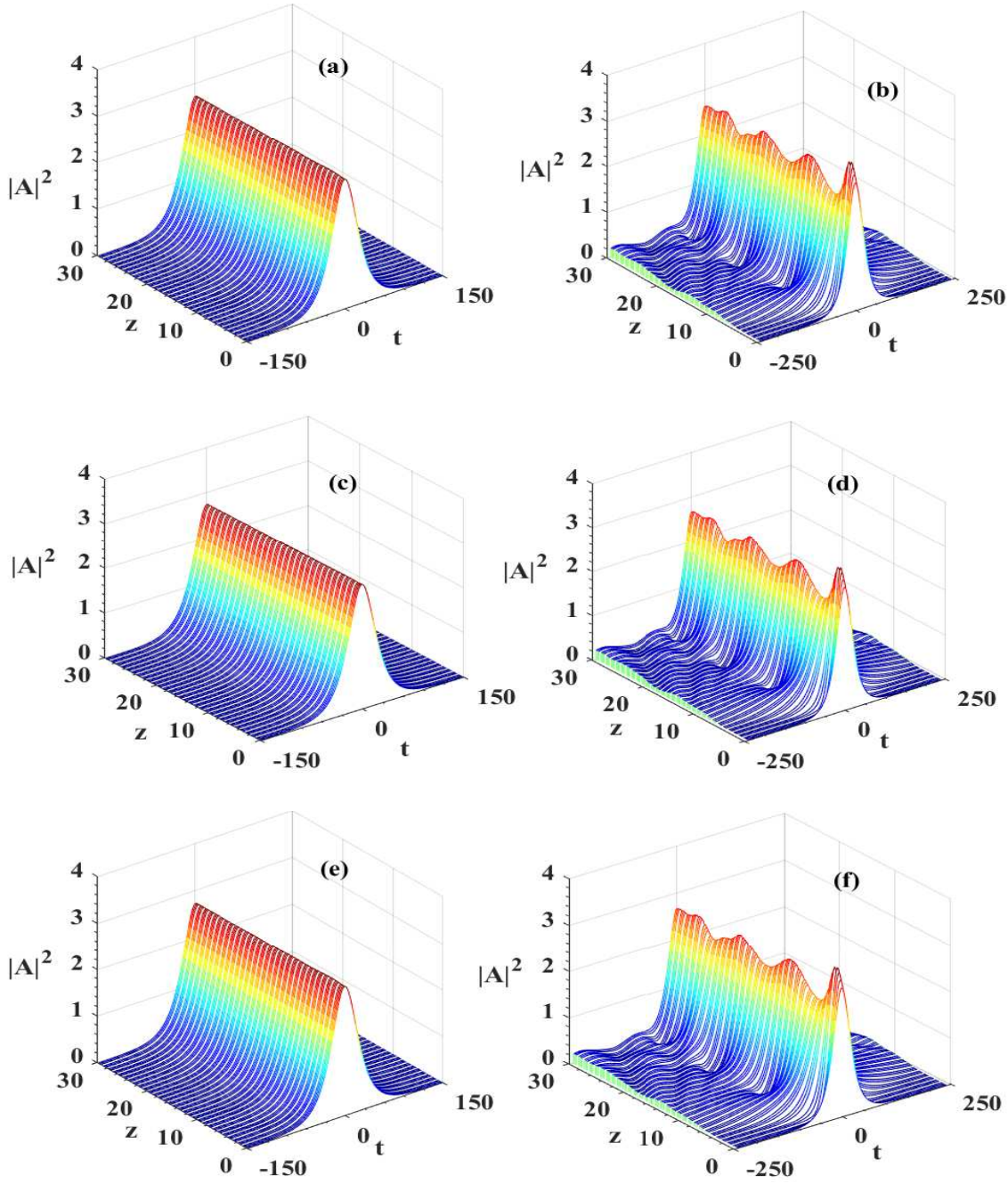

Fig. 3.14: Solitonic pulse propagation in presence of chirp when TPA is present in the system as shown by (a & b), (c & d)when 3PA is present in the system and (e & f)when both TPA and 3PA are present. For left panel (i. e., a, c, e)value of chirp=0.01 and for right panel (i. e., b, d, f) value of chirp C=0.3. Here $K = 0.01$, $\nu = 0.01$, $d = 0.05$ and $\gamma = -0.01$.

the side bands are much more prominent (Fig. 3.14 b,d,f) while for the chirp value (0.01), those are almost absent (Fig. 3.14 a,c,e). Frequency chirp has been witnessed

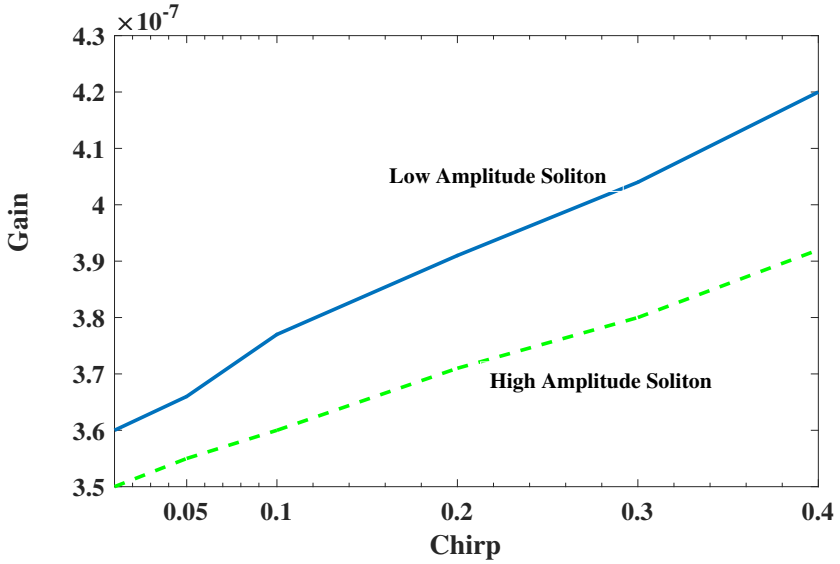

Fig. 3.15: Gain vs initial chirp plot for incresing value of chirp for lower and higher amplitude soliton.

to play a detrimental role on the solitonic propagation as gain required to sustain the soliton during propagation increases with increasing chirp value (Fig. 3.15). In case of bistable solitons, more gain is required for lower amplitude soliton than the higher amplitude soliton as they are more prone to decay and oscillations as shown in figures.

3.6 Conclusion

We studied the combined dissipative effect of three cases of multiphoton absorption in conjugation with gain dispersion on the pulse propagating in a medium having cubic-quintic nonlinearity. The results are obtained both analytically and numerically. When compared, they come out to be in close proximity with each other. The presence of quintic nonlinearity in the system helps in self-trapping of the pulse. It is found that shifting from TPA to 3PA wavelength is more beneficial as the later has a less detrimental effect on pulse dynamics. A material with negative valued imaginary χ^5 is found to be promising for arresting pulse degradation. Dissipative solitons are obtained by introducing different gains in highly nonlinear fiber with TPA only, 3PA only and

combined case of TPA and 3PA. The dissipative solitons thus obtained are bistable in nature. Effect of initial chirp on the dissipative soliton is studied. The results presented in this chapter have potential applications in fiber laser optical communication systems and devices. Since, at longer 3PA wavelength, the penetration capability into biological cells is greater and damaging effect to the tissues is lesser, the current investigation has potential application in biology and medical science, e.g., bio-imaging and light-activated therapy.

Chapter 4

Dissipative Soliton Fiber Lasers With Random Dispersion, Higher Order Nonlinearity, Multiphoton Absorption And Emission

---

In the previous chapter we investigated dissipative soliton in an ideal fiber that is usually consider for theoretically studies. However, practical fibers and fiber lasers possess several random effects that lead to random dispersion. In this chapter, we introduce this important aspect of a real fiber namely random dispersion in the investigation of the generation and dynamics of optical dissipative soliton in fiber lasers cavity with higher order nonlinearity, multiphoton absorption and emission. The soliton stability is explored and bistability nature of the dissipative solitons is highlighted. Phase mediated soliton switching phenomena and other intriguing dissipative soliton interaction dynamics are portrayed.

4.1 Introduction

Fiber lasers attract increasing growth due to their high output power, compact size, low manufacturing cost, and reliable performance, including robust mode-locking operation [85, 86, 125, 126]. These days, fiber lasers are used in a wide range of applications, from cutting and welding to telecommunications. As a result, the growth rate of

manufacturing fiber lasers (14% in 2014 and 13% in 2015) far outperforms that of solid-state (-3% in 2014 and 2015) and carbon-dioxide lasers (2% in 2014 and -1% in 2015) [127]. Initially, fiber lasers were inferior to solid-state counterparts in some performance parameters (such as the pulse power, duration etc.). But improvement of the design has made fiber lasers strong competitors of their solid-state counterparts.

Laser cavities are dissipative in nature. Thus, the operation of fiber lasers can be efficiently modelled in terms of dissipative solitons (DSs), which are stable localized modes formed in nonlinear dispersive media featuring interplay of gain and loss. DSs need continuous supply of energy for their existence as they are formed in lossy medium [1, 2, 128, 129]. DSs are formed as the result of two way equilibrium. One is the equilibrium between group-velocity dispersion, GVD (or diffraction) and nonlinear self-focusing, as in any soliton-bearing system, including conservative ones. The other condition is the balance between gain and loss in the system, which is a requirement specific for dissipative systems. In contrast to conservative [12] and PT-symmetric [130, 131] models, in which solitons exist in continuous families, parameters of DSs, such as their width, amplitude, velocity, etc., are uniquely selected by the two balances, and do not depend on initial conditions. It is in agreement with the fact that the stable DS is an attractor in the dynamics of the dissipative system [132]. These two balance conditions hold in fiber lasers operating in the DS regime.

The passive [48, 50] and active [133] mode-locking operational stability regimes of fiber lasers helps to make them compact sturdy devices operating in the alignment-free mode. Passive mode-locked fiber lasers are also popular as sources of ultra-short pulses [134]. The inclusion of a saturable absorber (SA) into the fiber-laser circuit helps to achieve the passive mode-locking. In particular, a semiconductor saturable absorber mirrors (SESAM) may operate as an SA [85, 86]. Recently, carbon nanotubes and graphene were also used as SAs [125, 126]. Besides that, artificial SA can be realized by employing a variety of other techniques, such the use of nonlinear couplers,

second-harmonic-generating elements, and nonlinear polarization rotation [135–137]. In addition to commonly used single-wavelength fiber lasers [134,138], multi-wavelength operation has been reported too [139]. Another variety, viz., fiber disk lasers are getting quick acceptance due to their customized applications [140].

Interaction of two DSs in a fiber laser may lead to the formation of a stable bound state with the group velocity different from that of a single soliton [141–146]. Further, collisions between bunched complexes of two or several DSs and a free one may lead to the absorption of the incident free soliton by the bound state [147, 148].

A new kind of high-energy femtosecond modes based on the spectral filtering of highly chirped pulses have been observed in an Ytterbium-doped fiber laser in the all-normal-GVD configuration [149]. Similar settings have been used to generate DSs in normal-GVD fiber lasers [40, 87, 150], in which the DS energy strongly increases, while the pulse becomes highly chirped (unchirped bright solitons cannot exist under the normal GVD), and its spectrum attains an approximately rectangular shape with two or three local maxima [151].

An all-normal-GVD Erbium-doped fiber laser produces a high-energy flat-top DS, thus demonstrating the dissipative-soliton-resonance (DSR) effect, which infers that the DS may achieve indefinitely high values, at certain values of the system parameter. Although DSR usually occurs in the normal-GVD region in fiber lasers, but it can be shifted to the anomalous-GVD region by changing parameters of the governing equation, which is the complex Ginzburg-Landau equation (CGLE) in most cases [3, 152, 153]. This has been established experimentally in an anomalous-GVD Erbium-doped fiber laser. Generally, the anomalous GVD gives rise to the modulational instability, which may break the high-energy soliton into multiple lower-energy ones. Formation of rectangular DSs takes place as the result of DSR whose energy can be enhanced to a much higher level in comparison with conventional DSs [154, 155]. Formation and evolution of DSs in anomalous-GVD fiber lasers has been reported too.

In particular, a high-energy DS at 2 μm has been observed in the case of anomalous-GVD [156].

Optical materials may feature saturable nonlinearity, which is often approximated by the cubic-quintic (CQ) form, i.e., a combination of self-focusing cubic and self-defocusing quintic terms, which correspond to real parts of the cubic (χ^3) and quintic (χ^5) susceptibilities. On the other hand, imaginary parts of χ^3 and χ^5 represent the two-photon absorption (TPA) and three-photon absorption (3PA) effects, respectively. These higher order nonlinear effects may play an important role in fiber-laser cavities.

Theoretical models mostly refer to an ideal fiber, which has a constant core diameter with fixed material parameters and doping density. However, real fibers may feature various imperfections, including shape variations, inhomogeneities of the refractive index, fluctuation in the dopant concentration, and effects of bending and ellipticity due to external stress. Random fluctuations in the fiber's core diameter and other imperfections give rise to random variations of the GVD. Even weak GVD fluctuations produce significant cumulative effects in the course of long transmission in fiber systems. The influence of the random GVD becomes more prominent for shorter pulses, especially for femtosecond ones, being the major cause of bit-pattern destruction in ultra-short pulses [110, 157–159]. Moreover, there are random fiber lasers (with the randomness provided by disordered distribution of doping nanoparticles) which operate in a specific diffusive regime, and provide for very high efficiency [46, 160, 161].

Although DSs were vastly studied considering a single above-mentioned aspect, as well as combination of two or three of them (e.g., SA, TPA, gain dispersion, etc.), the analysis still needs to be done for a full set of the higher order-nonlinear effects, as well as including randomness emulating the situation in realistic fiber-laser systems. For example, effects of the TPA and gain dispersion on the pulse propagation have been studied [162, 163], whereas formation of solitons in the presence of random GVD and multi-photon absorption has not been considered in detail. In the present work,

we address the propagation of pulses and subsequent formation of DSs in a fiber laser under effects of the random GVD, CQ nonlinearities, and multiphoton absorption (i.e., TPA and 3PA). We also include the gain dispersion, as it plays a prominent role for ultra-short pulses propagating through an active gain medium. Due to the presence of the CQ nonlinearity, the solitons are expected to be bistable. An appropriate model of such dissipative systems is provided by the CGLE with CQ terms.

The chapter is organized as follows. The model is introduced in Section 2. It is considered by means of the variational approximation (VA) in an analytical form, to derive pulse-evolution equations. In Section 3, the generation of DSs in the fiber-laser model is addressed. In particular, approximate VA results are compared with numerical ones. Interactions of the DSs in the fiber laser are considered in Section 4, which is followed by a conclusion in Section 5.

4.2 The Model

The propagation of ultra-short pulses in a lossy dispersive fiber with the CQ nonlinearity, gain dispersion, TPA, 3PA, and randomly varying GVD is governed by the following version of the CGLE [141, 147, 149]:

$$i\frac{\partial E}{\partial z}+\frac{D(z)}{2}\frac{\partial^2 E}{\partial t^2}+\mid E\mid^2 E-\gamma\mid E\mid^4 E=\frac{i}{2}(g_o-\alpha)E+\frac{id}{2}\frac{\partial^2 E}{\partial t^2}-iK\mid E\mid^2 E-i\nu\mid E\mid^4 E \tag{4.1}$$

Here E, z, and t are the amplitude of the electromagnetic wave, propagation distance, and retarded time, respectively. GVD coefficient D(z) in Eqn. 4.1 includes random variations added to the constant GVD. The third and fourth terms represent cubic and quintic nonlinearities, respectively. The original cubic and quintic nonlinear coefficients are $n_2=\frac{3Re(\chi^{(3)})}{8n_0}$ and $n_4=\frac{5Re(\chi^{(5)})}{16n_0}$, where n_0 is the linear refractive index. Equation 4.1 is scaled so as to make the effective cubic coefficient equal to 1, while

γ is respective quintic coefficient, proportional to $\frac{n_4}{n_2}$. As we choose the self-focusing cubic and defocusing quintic nonlinearities, which provides for the stabilization of solitons [99, 164], γ is positive. If the pulse's temporal width is larger than the intra-band relaxation time, the gain spectrum, $g(\omega)$ can be expanded in the Taylor series about the carrier frequency ω_0. This leads to the first two terms on the right-hand side of Eqn. 4.1, where g_o and d are the gain saturation and gain dispersion coefficients, respectively, while α stands for the dimensionless loss coefficient. The imaginary part of $\chi^{(3)}$ gives rise to the TPA coefficient, $\alpha_2 = \frac{3\omega Im(\chi^{(3)})}{2{n_0}^2 c^2 \epsilon_0}$, where ϵ_0 is the vacuum permittivity [165]. Likewise, the imaginary part of the fifth-order susceptibility ($\chi^{(5)}$) gives rise to the 3PA coefficient,$\alpha_3 = \frac{5\omega Im(\chi^{(5)})}{2{n_0}^3 c^3 {\epsilon_0}^2}$. In Eqn. 4.1, α_2 and α_3 are scaled to be to K and ν.

It is usually expected that higher-order effects in fiber lasers are represented by the higher-order GVD and Raman scattering. Here, we consider the setting in which both these effects are absent. Indeed, in mode-locked fiber lasers, the higher-order dispersion can be compensated [166, 167] using segments of specialty fibers (e.g., photonic crystal fibers, or multimode ones in which a higher-order mode is used), or with the help of chirped fiber Bragg gratings, as well as bulk components, such as pairs of diffraction gratings. The Raman scattering, whose effect on high-power may be detrimental, can be suppressed too, using special fiber designs [168], or long-period gratings [169], or chirped-pulse amplification, or, also, hollow-core photonic-crystal fibers filled by an inert gas [43, 170].

To consider the governing equation (4.1) in an analytical form, we use the VA in conjugation with the Rayleighs dissipation function (RDF), which has been widely used to describe the nonlinear pulse propagation in dissipative optical fibers [101, 112]. In the framework of this method, the CGLE is separated into conservative and dissipative parts, which correspond to the left- and right-hand sides of Eqn. (4.1), respectively.

The Lagrangian density for the conservative part is

$$L = \frac{i}{2}(EE_z^* - E^*E_z) + \frac{D}{2} \mid E_t \mid^2 - \frac{1}{2} \mid E \mid^4 + \frac{\gamma}{3} \mid E \mid^6 \tag{4.2}$$

The RDF density, which takes care of the dissipative terms, can be constructed as

$$\begin{aligned} R &= -\frac{i}{2}(g_o - \alpha)(EE_z^* - E^*E_z) + \frac{id}{2}(E_{tt}^*E_z - E_{tt}E_z^*) + iK \mid E \mid^2 (EE_z^* - E^*E_z) \\ &+ i\nu \mid E \mid^4 (EE_z^* - E^*E_z) \end{aligned} \tag{4.3}$$

We adopt the usual sech ansatz for a bright soliton of Eqn.4.1:

$$E(z,t) = A(z)sech\left(\frac{t}{W(z)}\right)\exp\left(i\phi(z)\right) \tag{4.4}$$

where $A(z)$, $W(z)$ and $\phi(z)$ represent the complex amplitude, temporal pulse width and phase, respectively. The total Lagrangian and RDF can be found by inserting ansatz (4) in Eqns.(3.2) and (3.3):

$\mathcal{L} = \int_{-\infty}^{\infty} Ldt$, and $\mathcal{R} = \int_{-\infty}^{\infty} Rdt$. The calculation yields

$$\begin{aligned} \mathcal{L} &= i(AA_z^* - A^*A_z)W(z) + 2W(z) \mid A(z) \mid^2 \frac{\partial\phi(z)}{\partial z} + \frac{D}{3}\frac{\mid A(z) \mid^2}{W(z)} - \frac{2}{3} \mid A(z) \mid^4 W(z) \\ &+ \frac{16}{45}\gamma \mid A(z) \mid^6 W(z) \end{aligned} \tag{4.5}$$

$$\begin{aligned} \mathcal{R} &= -(g_o - \alpha)W(z)\left[2 \mid A(z) \mid^2 \frac{\partial\phi(z)}{\partial z} + i(AA_z^* - A^*A_z)\right] \\ &+ \frac{id}{3W(z)}\left[(AA_z^* - A^*A_z) - 2i \mid A(z) \mid^2 \frac{\partial\phi(z)}{\partial z}\right] \\ &+ \frac{4i}{3}KW(z) \mid A(z) \mid^2 (AA_z^* - A^*A_z) + \frac{8}{3}KW(z) \mid A(z) \mid^4 \frac{\partial\phi(z)}{\partial z} \\ &+ \frac{32}{15}\nu W(z) \mid A(z) \mid^6 \frac{\partial\phi(z)}{\partial z} + \frac{16i}{15}\nu W(z) \mid A(z) \mid^4 (AA_z^* - A^*A_z) \end{aligned} \tag{4.6}$$

Using the Euler-Lagrange equations,

$$\frac{d}{dt}\left(\frac{\partial\mathcal{L}}{\partial\dot{q}_j}\right) - \frac{\partial\mathcal{L}}{\partial q_j} + \frac{\partial\mathcal{R}}{\partial\dot{q}_j} = 0 \tag{4.7}$$

where, $\dot{q}_j = \frac{dq_j}{dt}$, q_j being parameters $A(z)$, $A^*(z)$, $W(z)$ and $\phi(z)$, the following four

equations are obtained:

$$\begin{aligned} -i\frac{d}{dz}\left(W(z)A^*(z)\right) &= iW(z)A_z^*(z) + 2W(z)A^*(z)\frac{\partial\phi(z)}{\partial z} + \frac{D}{3}\frac{A^*(z)}{W(z)} \\ &- \frac{4}{3} \mid A(z) \mid^2 A^*(z)W(z) + \frac{id}{3}\frac{A^*(z)}{W(z)} \\ &+ \frac{4i}{3}K \mid A(z) \mid^2 A^*(z)W(z) + \frac{16}{15}\gamma \mid A(z) \mid^4 A^*(z)W(z) \\ &+ \frac{16}{15}i\nu \mid A(z) \mid^4 A^*(z)W(z) - iW(z)(g_o - \alpha)A^*(z) \end{aligned} \tag{4.8}$$

$$\begin{aligned} i\frac{d}{dz}\left(W(z)A(z)\right) &= -iW(z)A_z(z) + 2W(z)A(z)\frac{\partial\phi(z)}{\partial z} + \frac{D}{3}\frac{A(z)}{W(z)} \\ &- \frac{4}{3} \mid A(z) \mid^2 A(z)W(z) - \frac{id}{3}\frac{A(z)}{W(z)} \\ &- \frac{4i}{3}K \mid A(z) \mid^2 A(z)W(z) + \frac{16}{15}\gamma \mid A(z) \mid^4 A(z)W(z) \\ &- \frac{16}{15}i\nu \mid A(z) \mid^4 A(z)W(z) + iW(z)(g_o - \alpha)A(z) \end{aligned} \tag{4.9}$$

$$i(AA_z^* - A^*A_z) = -2 \mid A(z) \mid^2 \frac{\partial\phi(z)}{\partial z} + \frac{D}{3}\frac{\mid A(z) \mid^2}{W^2(z)} + \frac{2}{3} \mid A(z) \mid^4 - \frac{16}{45}\gamma \mid A(z) \mid^6 \tag{4.10}$$

$$\begin{aligned} 2W(z)\left[A(z)\frac{\partial A^*(z)}{\partial z} + \frac{\partial A(z)}{\partial z}A^*(z)\right] & \\ + 2 \mid A(z) \mid^2 \frac{\partial W}{\partial z} & \\ + \frac{2d \mid A(z) \mid^2}{3W(z)} + \frac{8K}{3} \mid A(z) \mid^4 W(z) & \\ + \frac{32\nu}{15} \mid A(z) \mid^6 W(z) - 2(g_o - \alpha) \mid A(z) \mid^2 W(z) & \\ = 0 & \end{aligned} \tag{4.11}$$

Further manipulations with the equations yield balance relations for the pulse propagation.

Multiplying Eqn. (4.8) and Eqn. (4.9) by $A(z)$ and $A^*(z)$, respectively, and subsequent subtraction yields

$$\frac{d}{dz}\left[2 \mid A(z) \mid^2 W(z)\right] = -\frac{2d \mid A(z) \mid^2}{3W(z)} - \frac{8}{3}KW(z) \mid A(z) \mid^4 - \frac{32}{15}\nu W(z) \mid A(z) \mid^6 + 2W(z)(g_o - \alpha) \mid A(z) \mid^2 \quad (4.12)$$

The integrated intensity of the pulse is $\int_{-\infty}^{\infty} \mid E(z,t) \mid^2 = 2 \mid A(z) \mid^2 W(z)$. Therefore, Eqn. (4.12) describes the variation of pulse's energy in the course of the propagation.

Further, multiplying Eqn. (4.8) and (4.9) by $A(z)$ and $A^*(z)$, respectively, and adding the results, one obtains

$$i(AA_z^* - A^*A_z) = -2 \mid A(z) \mid^2 \frac{\partial\phi(z)}{\partial z} - \frac{D}{3}\frac{\mid A(z) \mid^2}{W^2(z)} + \frac{4}{3} \mid A(z) \mid^4 - \frac{16}{15}\gamma \mid A(z) \mid^6 \quad (4.13)$$

Comparing Eqn. 4.10 and Eqn. 4.13 we get,

$$\frac{\mid A(z) \mid^2 W^2(z)}{D(z)} - \frac{16\gamma \mid A(z) \mid^4 W^2(z)}{15D(z)} = 1 \quad (4.14)$$

Equation (4.14) is the fundamental constraint for pulse propagation which holds throughout the propagation. Notably, no contribution from the dissipative part appears in Eqn. (4.14). To have a solution obeying this condition, one should ensure the gain-loss balance.

Equations (4.12) and (4.14) give rise to the evolution equations for the pulse's amplitude, $A(z)$ and width, $W(z)$:

$$\frac{dW(z)}{dz} = \frac{\left[\begin{array}{r} \frac{-d}{3sW}\left(1-\sqrt{M}\right) - \frac{2KW}{3s^2}\left(1-\sqrt{M}\right)^2 - \frac{4\nu W}{15s^3}\left(1-\sqrt{M}\right)^3 \\ - \frac{2}{W\sqrt{M}}\frac{dD}{dz} + W(g_o-\alpha)\frac{1}{s}\left(1-\sqrt{M}\right) \end{array}\right]}{\left[\frac{-4D}{W^2\sqrt{M}} + \frac{1}{s}\left(1-\sqrt{M}\right)\right]} \quad (4.15)$$

$$\frac{dA(z)}{dz} = \frac{\left[\begin{array}{l} \left[\frac{1}{2AW^2-4sW^2A^3}\right]\frac{dD}{dz} - A(1-sA^2) \\ \quad \left[\begin{array}{r} \frac{-d}{3sW}\left(1-\sqrt{M}\right) - \frac{2KW}{3s^2}\left(1-\sqrt{M}\right)^2 - \frac{4\nu W}{15s^3}\left(1-\sqrt{M}\right)^3 \\ - \frac{2}{W\sqrt{M}}\frac{dD}{dz} + W(g_o-\alpha)\frac{1}{s}\left(1-\sqrt{M}\right) \end{array}\right] \end{array}\right]}{W(1-2sA^2)\left[\frac{-4D}{W^2\sqrt{M}} + \frac{1}{s}\left(1-\sqrt{M}\right)\right]} \quad (4.16)$$

where $M = \frac{1-4sD}{W^2}$ and s = $\frac{16\gamma}{15}$.

4.3 The Dissipative Pulse Dynamics and Generation of Dissipative Solitons

The evolution of the pulse's parameters is predicted by solving Eqns. (4.15) and (4.16). Subsequently DSs can be generated in the approximate form, using these solutions for a suitable set of parameters. The investigation is done under two the conditions of (i) the balance between the nondispersive gain and linear loss, $g_o = \alpha$ or (ii) in the absence of the balance:$g_o \neq \alpha$.

4.3.1 Case (I): $g_o = \alpha$ (The Nondispersive-Gain-Linear-Loss Balance)

To examine the influence of the nonlinear losses (i.e., TPA and 3PA) and the gain dispersion, we adopt condition $g_o = \alpha$, to eliminate the linear gain and loss in the system. Overall, the system still remains dissipative under the effect of the TPA, 3PA and gain-dispersion terms. The GVD coefficient, $D(z)$, comprises a constant part (scaled to be 1) plus a randomly varying part (ϵ), with mean value 0.03. The effect of the finite gain bandwidth must be taken into account because the femtosecond-pulses' spectra are very wide [112]. The gain dispersion in conjugation with the GVD significantly affects the pulse dynamics and energy profile.

Variational results shows that the gain dispersion reduces its intensity (Fig. 4.1 (a))

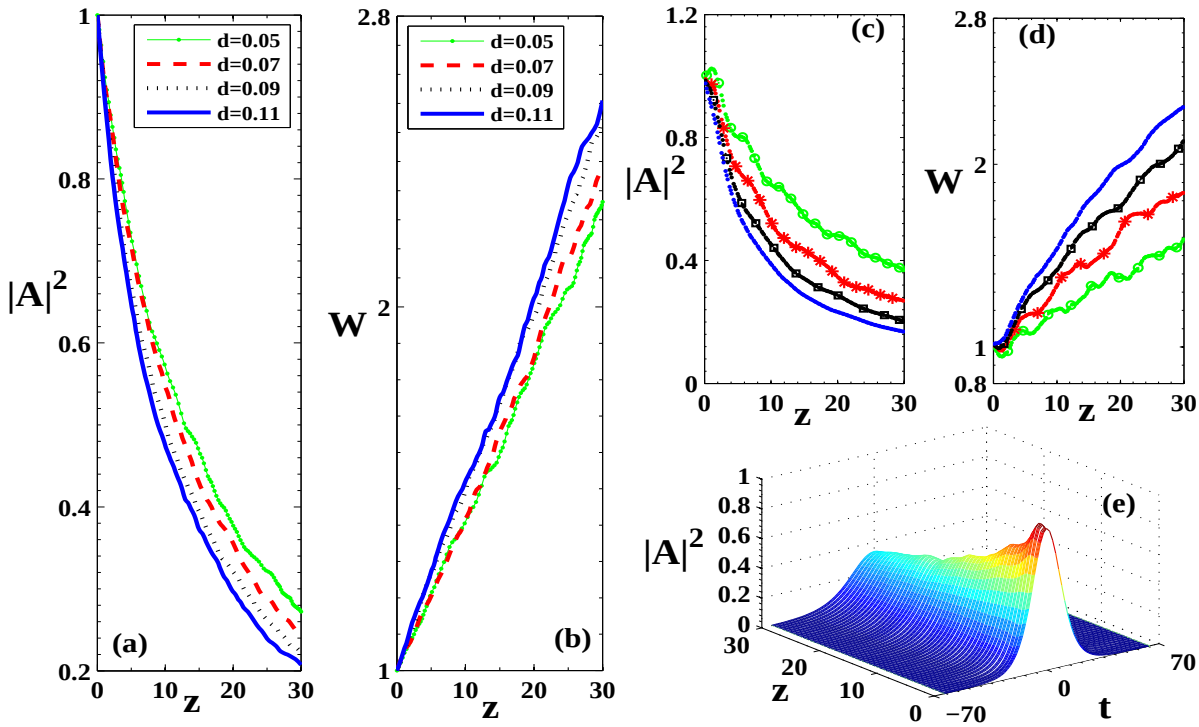

Fig. 4.1: Pulse degradation under the combined effect of the TPA, 3PA, gain dispersion, and random GVD, while the nondispersive gain is in balance with the linear loss. (a) The decay of pulse's intensity, and (b) the increase of its width for different values of gain dispersion d, as produced by the solution of variational equations (4.15) and (4.16) Here, $K = 0.01$, $\nu = 0.01$, $\gamma = 0.1$. Counterparts of these results, as obtained from direct simulations of Eqn. (4.1) with $d = 0.05$ (green line with circles), $d = 0.07$ (red line with stars) $d = 0.09$ (black line with squares) $d = 0.11$ (blue line) are displayed in panels (c) and (d), respectively. (e) The numerically generated 3D profile of the dissipative-pulse's evolution for $d = 0.05$.

and makes it broader (Fig. 4.1 (b)), causing degradation of the pulse quality. The verification of the variational results is provided by direct simulations of Eqn. (4.1), using the split-step Fourier method, see Figs. 4.1 (c-e). Here we set the integration step size equal to $10^(-3)$. The propagation length is taken to be tantamount to 30 soliton periods.

The systematic pulse decay, observed in Fig. 4.1 (c), and its broadening, as seen in Fig. 4.1 (d), are close to the averaged VA-predicted counterparts. The fluctuations in the VA curves and ones generated by the full simulations are different, representing an

effect of the random part of the GVD. Being the third-order nonlinear-loss phenomenon, the TPA has a quadratic dependence on the amplitude of the electromagnetic wave. Generally, it limits the efficiency of optical switching and causes reshaping and broadening of solitons, as well as splitting of higher-order ones into constituents fundamental pulses [101]. In the general case, the number of the emerging solitons depends on the gain and length of the fiber amplifier, if it is present in the system [100, 102]. The TPA coefficient is estimated as $6.2 \times 10^{15} mW^{-1}$ in As_2S_3-based glass at 1.55μm [121]. The 3PA leads to a higher degree of confinement, as it is proportional to the fourth power of the field amplitude, and has potential applications to wavelength shifting, pulse reshaping, and stabilization in narrow-pulse fiber communication systems [109]. In As_2S_3-based glass, the 3PA coefficient is $2.0 \times 10^{-27} m^3 W{-}2$ at the wavelength of 1.55μm [106]. Recently, both saturable absorption and TPA of few-layer molybdenum diselenide ($MoSe_2$) have been observed at 1.56 μm wavelength, and subsequently used in an all-fiber Erbium-doped mode-locked ultrafast fiber laser [171].

Currently, much attention is drawn to mid-infrared (IR) wavelengths (¿ 3000 nm), and the operation of fiber lasers based on materials which are appropriate in this range, such as chalcogenide glasses. With this in mind, throughout this work we adopt physical parameters relevant to the mid-IR wavelengths, where the higher-order nonlinear effects are prominent [172]. Actually, all analysis throughout this chapter is performed for parameters corresponding to wavelength 3500 nm propagating in chalcogenide fibers.

The nonlinear absorption in the fiber reduces the pulse's intensity. It can also represent injection of electron-hole pairs, leading to the free-carrier absorption and dispersion. TPA and 3PA individually have detrimental effect on the pulse propagation, the decay rate caused by 3PA being smaller than its TPA-induced counterpart. Actually, the TPA is more prominent at shorter wavelengths, while 3PA is dominant at longer wavelengths, both effects being essential in the intermediate region [121].

The pulse's dynamics is more interesting in the presence of a negative imaginary

part of the $\chi^{(5)}$ coefficient, i.e., a negative 3PA coefficient, which implies the quintic gain, rather than loss. The resulting amplification effect is sometimes called the three-photon emission (3PE) [25]. In particular, the action of the polarization-correlated 3PE leads to formation of a positively charged triexciton (a bound state of three electron-hole pairs) in a self-assembled GaAs quantum dot [123].

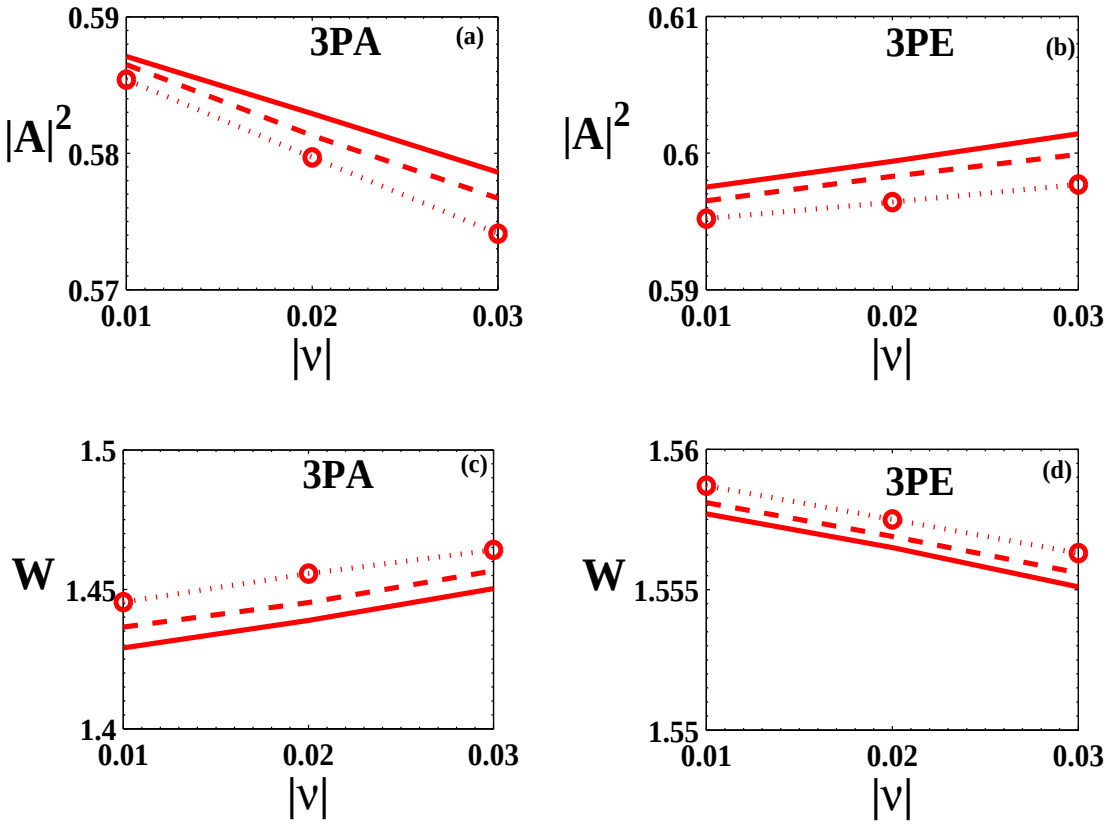

Fig. 4.2: Variation of (a) the normalized pulse's intensity and (c) its width with the increase of | | in the cases of the 3PA. (b) and (d) are the same for 3PE. In all the panels, solid lines correspond to $\gamma = 0.03$, while dashed and dotted lines correspond to $\gamma = 0.05$ and 0.1 respectively. Other parameters are $K = 0$, and $d = 0.05$.

In semiconductor devices, the cubic gain, i.e., two-photon emission, was observed in optically pumped GaAs and in current-driven GAInP/AlGaInP quantum wells [124]. However, experimental realization of the 3PE still has to be elaborated. Our VA results

show that, with the increase of | |, while the 3PA leads to the decay of the pulse's intensity (Fig. 4.2 (a)) and its broadening (Fig. 4.2 (b)), 3PE naturally causes the opposite, i.e., growth of the intensity and decrease of the pulse's width. We stress that the 3PE does not lead to blow-up of the pulses, as the 3PE coefficient considered here is small enough.

4.3.2 Case (II): $g_o > \alpha$ (The Nondispersive Gain Greater than the Linear Loss)

The pulse degradation discussed above can be arrested, and a DS can be built, by applying proper gain to the system, which makes $\Delta g \equiv g_o - \alpha > 0$ in Eqn. (4.1). Strictly speaking, this condition, i.e., the presence of the excess linear gain, makes the zero background unstable around any soliton. Nevertheless, it is shown below that the background instability may be avoided, in a properly chosen setting (in particular, limiting the excess gain to sufficiently small values, $\Delta g \sim 10^{-5}$, see below). This may be explained by the fact the small disturbances are set in motion by the GVD, which then adds effective loss due to the gain dispersion, and, eventually, the disturbances hit edges of the integration domain, or the DS; in the latter case, the nonlinear dissipation can help to suppress them. Furthermore, the presence of CQ terms in the system suggests (see, in particular, Eqn. (4.14) that DSs can be made bistable. Figure 4.3 (a) shows the bistability: for a fixed pulse's width (e.g.,$W = 1.25$), two amplitudes ($A = 0.853$ and $A = 2.947$) are obtained from the curve corresponding to $\gamma = 0.1$. This means that a 12 ps pulse can generate dissipative solitons of power $87mW$ and $750mW$.

Direct numerical simulations reveal that the smaller-amplitude DS is stable for $\Delta g = 4.35 \times 10^{-6}$, see Fig. 4.3 (b)(i), while the larger-amplitude one eventually blows up, in Fig. 4.3 (b)(ii), at the same gain. However, the latter DS may be made quasi-stable by choosing suitable loss, namely, $\Delta g = -1.69 \times 10^{-5}$, see Fig. Fig. 4.3 (b)(iii).

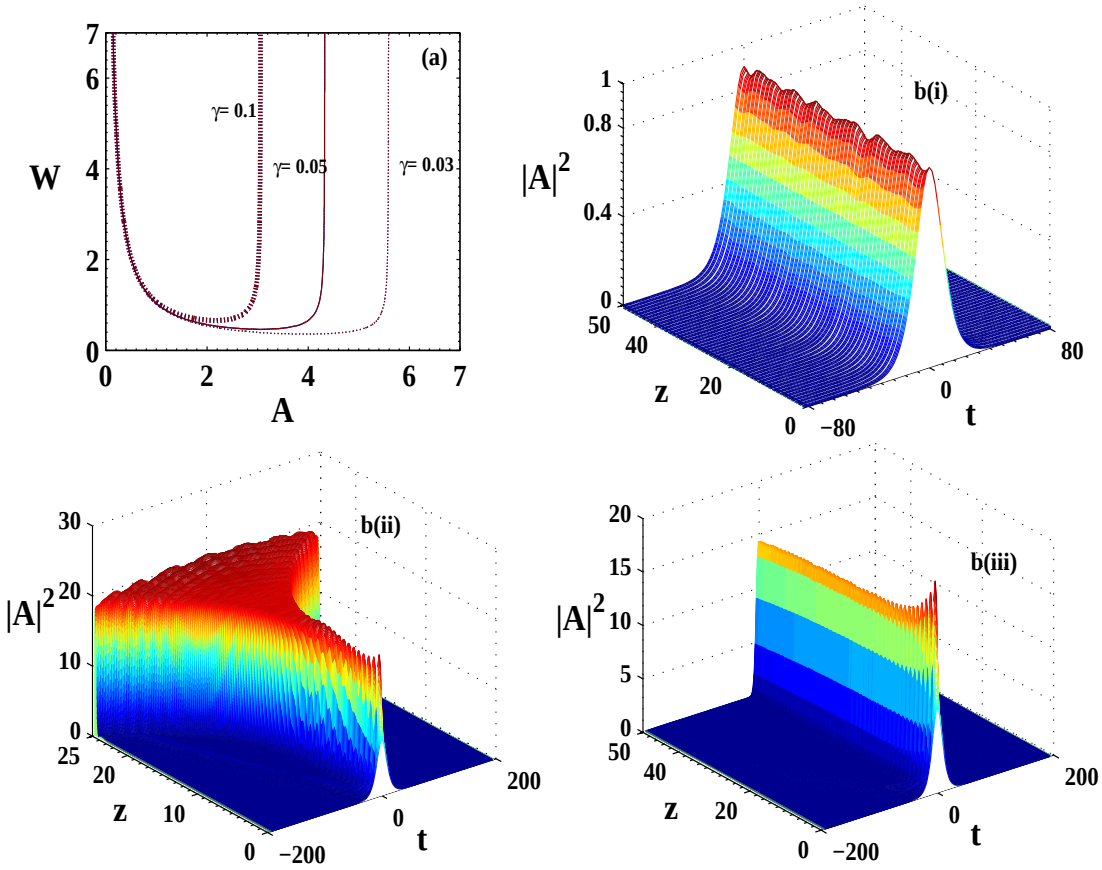

Fig. 4.3: (a) The bistability curve corresponding to Eqn. (4.14) for $\gamma = 0.1$, 0.05 and 0.03. (b) Numerically generated pulse evolution pertaining to the same width ($W = 1.25$) but different amplitudes selected from (a) for $\gamma = 0.1$. In panel (b), (i) displays the evolution of a stable DS corresponding to the smaller amplitude ($A = 0.853$) for excess gain $\Delta g = 4.35 \times 10^{-6}$, while (ii) shows the blowup of an unstable DS with the larger amplitude ($A = 2.947$) and the same excess gain. In addition, panel (iii) displays quasi-stabilization of the higher-amplitude DS with $A = 2.947$, in the presence of a very weak effective loss, viz., $\Delta g = -1.69 \times 10^{-5}$. In panels (b), the parameters are $K = 0.01$, $\nu = 0.01$.

Here, $\gamma = 0.1$, $W = 1.25$ and $A = 0.853$ or 2.947 are chosen for the explicit presentation of the results. Similar results are obtained by choosing other sets of values of γ, W and A from the bistability curves in Fig. 4.3 (a).

It is known that solitons in complex models may feature internal modes, which manifest themselves as persistent oscillations of the soliton's shape [173]. In our system, small-amplitude shape oscillations are observed in stable solitons with the lower

amplitude, see Fig. 4.3 (b)(i). We now proceed to the analysis of the DS evolution in the presence of the TPA and 3PA/3PE terms. In the presence of the TPA, small excess gain, $\Delta g = 4.23 \times 10^{-6}$, results in a slightly fluctuating but generally steady peak intensity and pulse's width, as shown in Fig. 4.4.

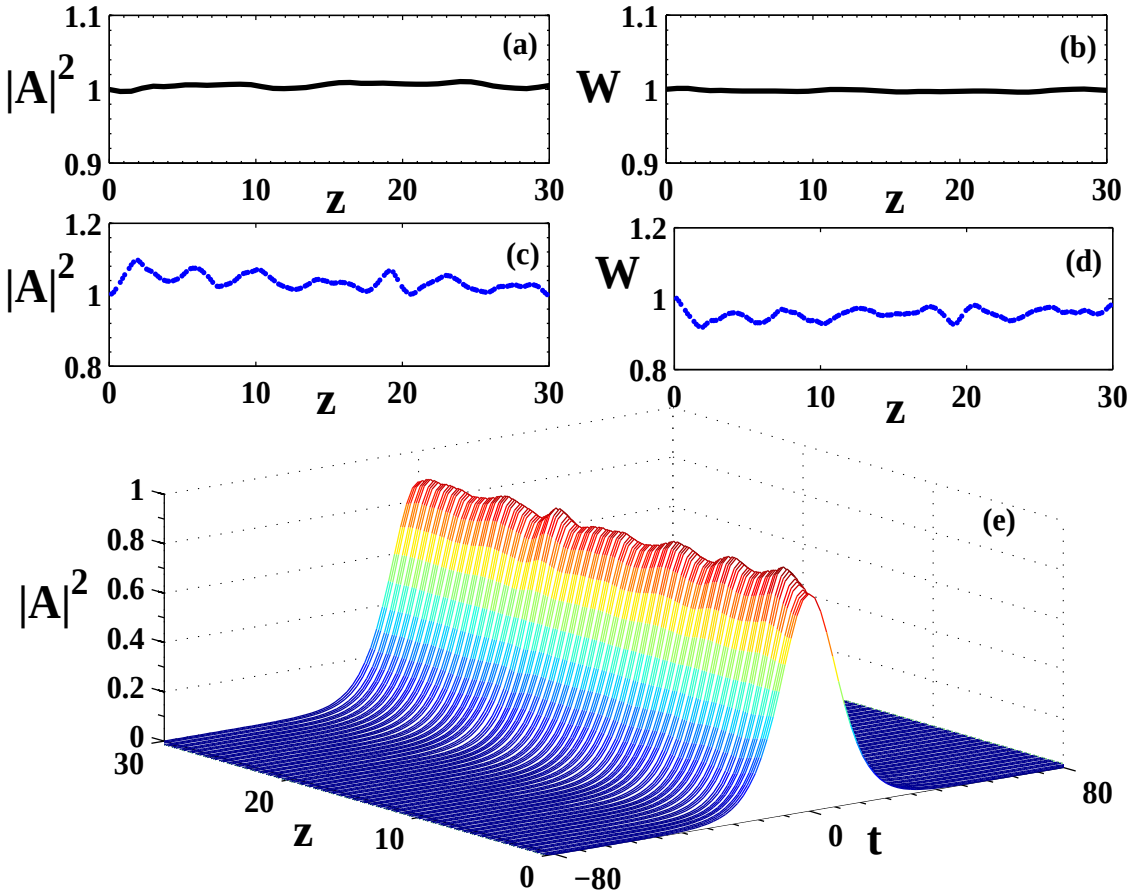

Fig. 4.4: Evolution of the DS in the presence of the TPA effect, while the 3PA term is absent. The corresponding variation of the soliton's intensity and width, as predicted by the VA, are shown in (a) and (b), respectively. Panels (c) and (d) display the same, but as obtained from direct simulations. The 3D plot of the numerically simulated evolution of the DS is displayed in (e). In all panels, $\gamma = 0.1$, $d = 0.05$ and $K = 0.01$, $\nu = 0$. Here the excess gain is $\Delta g = 4.23 \times 10^{-6}$.

The fluctuations are more prominent in the full simulations, but mean values of the peak intensity and width almost exactly match their numerically computed counterparts ($\langle A^2 \rangle_{num} = 1.0537$ and $\langle W \rangle_{num} = 0.9727$, respectively). Further, the evo-

lution of the DS under the action of the 3PA is shown in Fig. 4.5 with excess gain $\Delta g = 4.10 \times 10^{-6}$, which is somewhat less than that required to compensate the nonlinear loss in the case of the TPA. Mean values of the simulated peak intensity and width are $\langle A^2 \rangle_{num} = 1.0247$ and $\langle W \rangle_{num} = 0.9825$, that are close to variationally obtained values. Naturally, a stronger excess gain is required (actually, it is $\Delta g = 4.35 \times 10^{-6}$ to form the DS in the presence of both the TPA and 3PA, see Fig. 4.6. In this case, mean values of the simulated peak intensity and width are $\langle A^2 \rangle_{num} = 1.0298$ and $\langle W \rangle_{num} = 0.9825$, respectively.

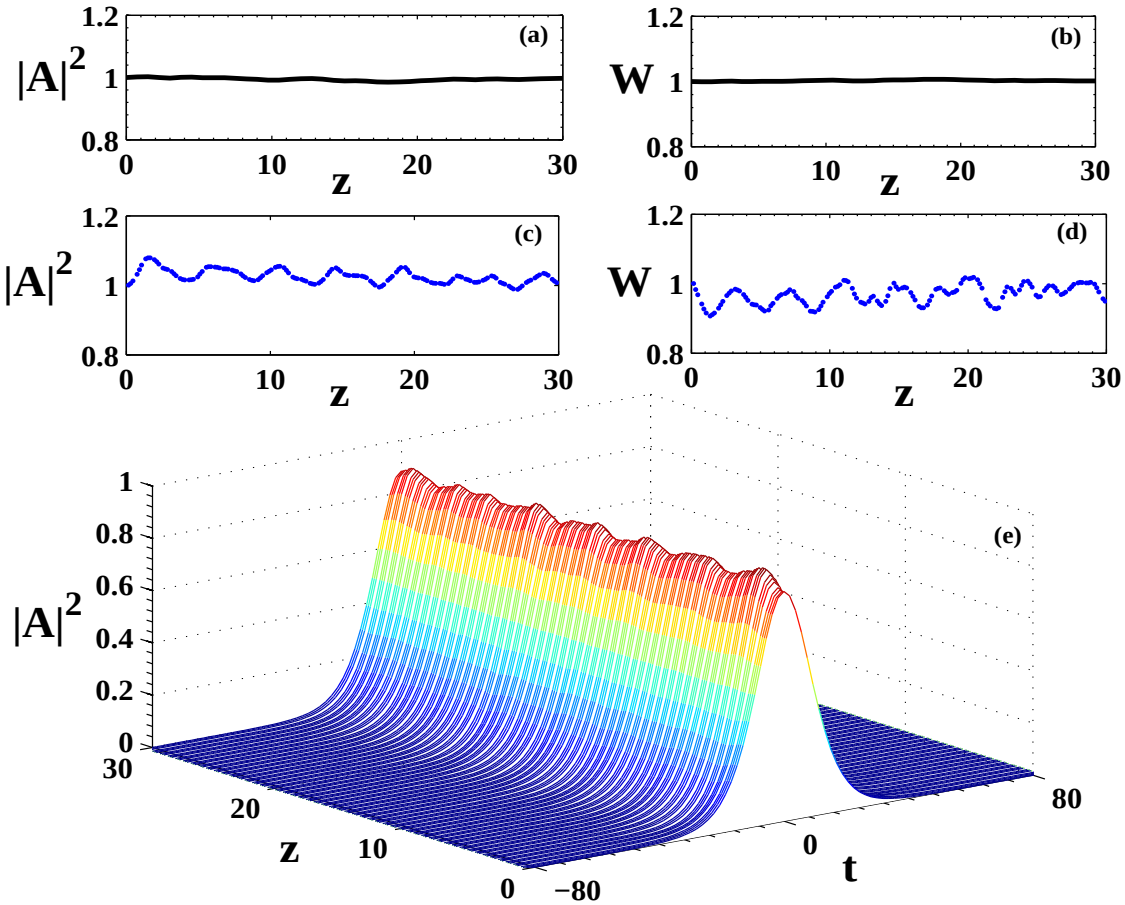

Fig. 4.5: Same as in Fig. 4.4, but for the case of the evolution of the DS under the action of the 3PA, in the absence of the TPA. Here, $\gamma = 0.1$, $K = 0$, $d = 0.05$ and $\nu = 0.01$. Here excess gain $\Delta g = 4.10 \times 10^{-6}$.

Thus, we conclude that the VA-predicted results generally match findings produced by the direct simulations in Figs. 4.4 - 4.6, although the numerical results show more

prominent oscillations in the pulse's peak intensity and width. Nevertheless, the mean values of the numerically obtained peak intensity and width are almost exactly fitted by the VA-predicted counterparts.

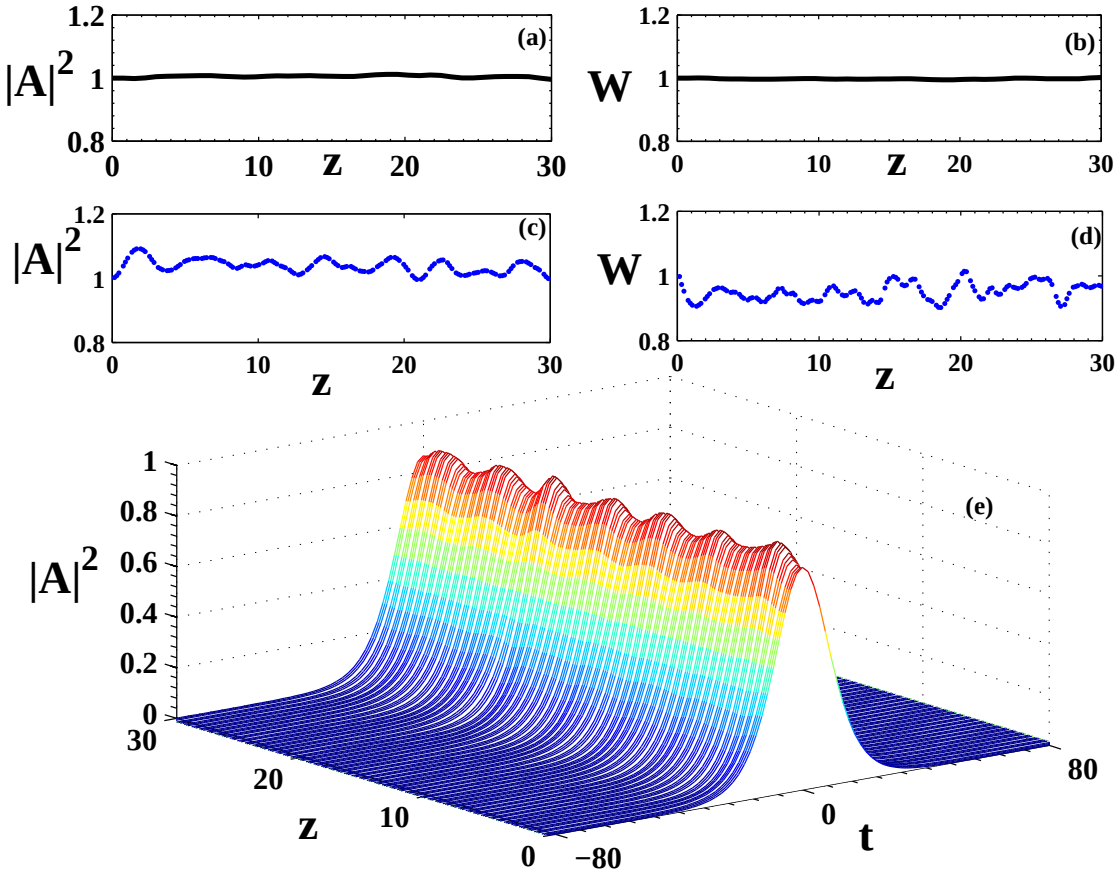

Fig. 4.6: Same as in Figs. 4.4 and 4.5, but in the case of the evolution of the DS under the combined action of the TPA and 3PA terms. In all panels, $\gamma = 0.1$, $K = 0.01$, $d = 0.05$ and $\nu = 0.01$. Here excess the gain is $\Delta g = 4.35 \times 10^{-6}$.

Now, it is relevant to consider the 3PE as an alternate source of gain. Instead of the TPA-3PA combination considered above, the TPA-3PE one requires a smaller excess gain, $\Delta g = 4.15 \times 10^{-6}$ to form a DS, see Fig. 4.7. Thus, 3PE may indeed be harnessed as an alternative gain mechanism, provided that it is small enough to avoid the onset of the blowup. In that case, the use of the 3PE is actually a stabilizing factor, as it allows one to use a smaller linear excess gain, and thus improve the stability of the zero background. In the parameter region investigated here, the blowup is absent indeed for

the DSs belonging to the left branch of the bistability curve in Fig. 4.3 (a), while the solitons with the larger amplitude, belonging to the right branch, eventually do blow up.

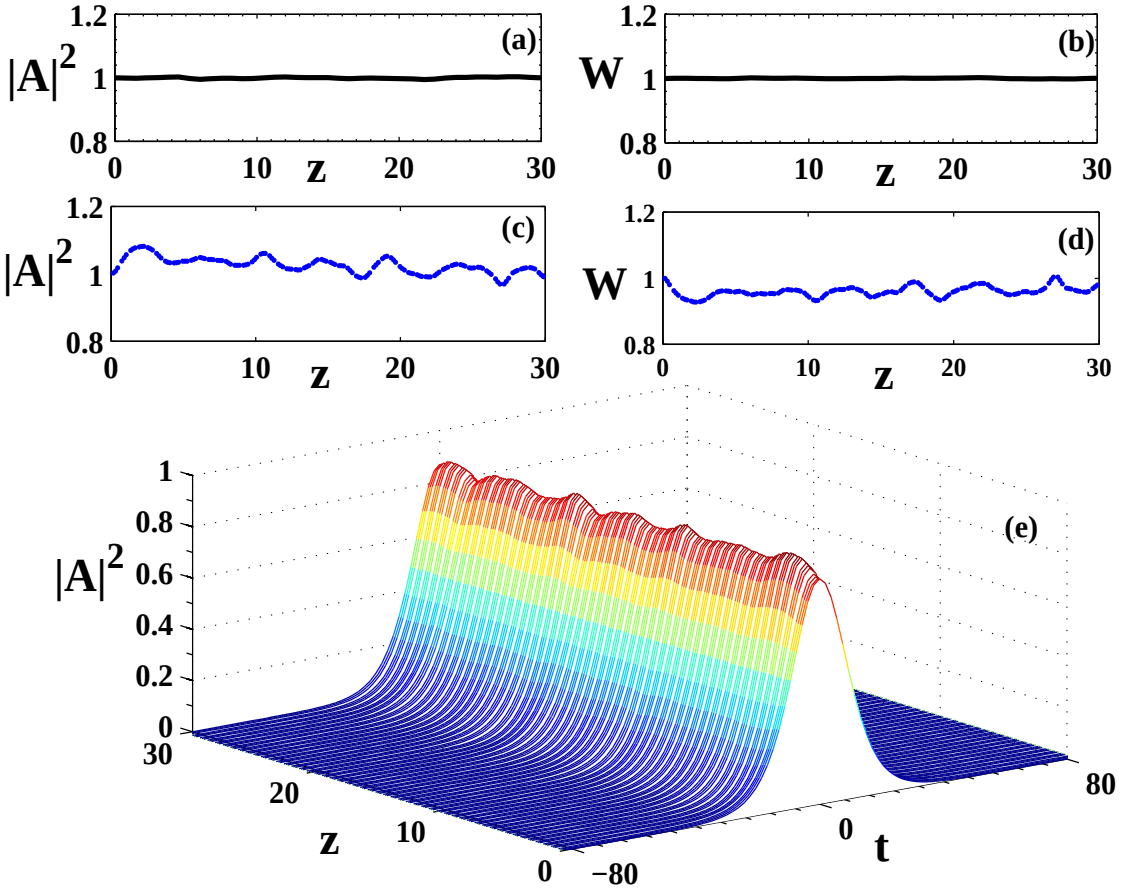

Fig. 4.7: Same as in Figs. 4.4 and 4.5, but for the evolution of the DS under the combined action of the TPA and 3PE terms. Here, $\gamma = 0.1$, $K = 0.01$, $d = 0.05$ and $\nu = -0.01$, while the excess gain is $\Delta g = 4.35 \times 10^{-6}$.

In this connection, it is relevant to mention that stable states supported by the unsaturated gain (i.e., the higher-order amplification not capped by attenuation of a still higher degree) were previously found in some other models [174, 175]. A generic feature of such models is the existence of an unstable solution with a larger amplitude, which plays the role of a separatrix, i.e., a boundary between initial states which are attracted to a stable smaller-amplitude solution, and those which undergo the blowup. In the present case, the DSs belonging to the right branch of the curve in Fig. 4.3 (a)

plays this role.

Although the analysis presented in this section includes the random GVD, it is easy to check that this ingredient of the model is not responsible for the stability of the DSs, as they remain equally stable or unstable when solely the constant GVD is kept. On the other hand, the analysis of the system including this practically important term is relevant, as it additionally attests to the stability of the DSs in the presence of the random perturbations, see Figs. 4.3 - 4.7.

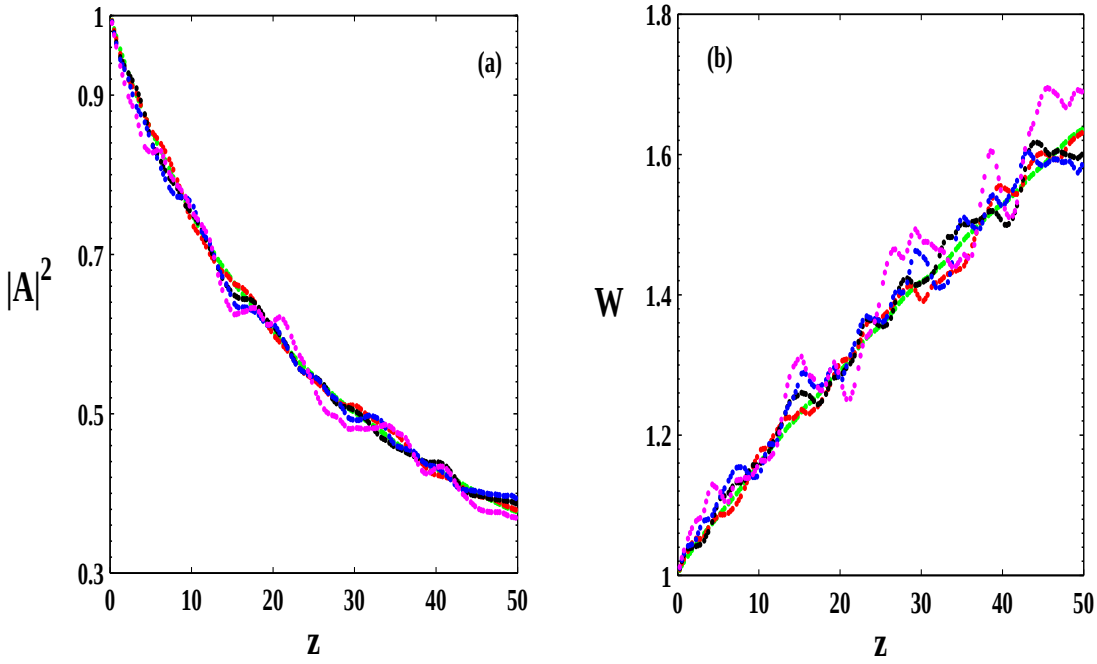

Fig. 4.8: (a) The pulse's intensity and (b) width for different relative magnitudes of the random part of the dispersion in comparison with its constant part, as obtained from direct simulations of Eq. (1). Color dots correspond to the following magnitudes: 0% (green), 3% (red), 5% (black), 7% (blue), and 9% (magenta). Here, $\gamma = 0.1$, $K = 0.01$, $d = 0.05$ and $\nu = 0.01$.

It is essential to take into account effects of random GVD on the soliton propagation. As the randomness enhances the bit-error-rate, its effect is obviously detrimental for the propagation of ultra-short pulses. Randomness of the GVD may be, in principle, both temporal and spatial. Possible temporal variation of the GVD being, in any case,

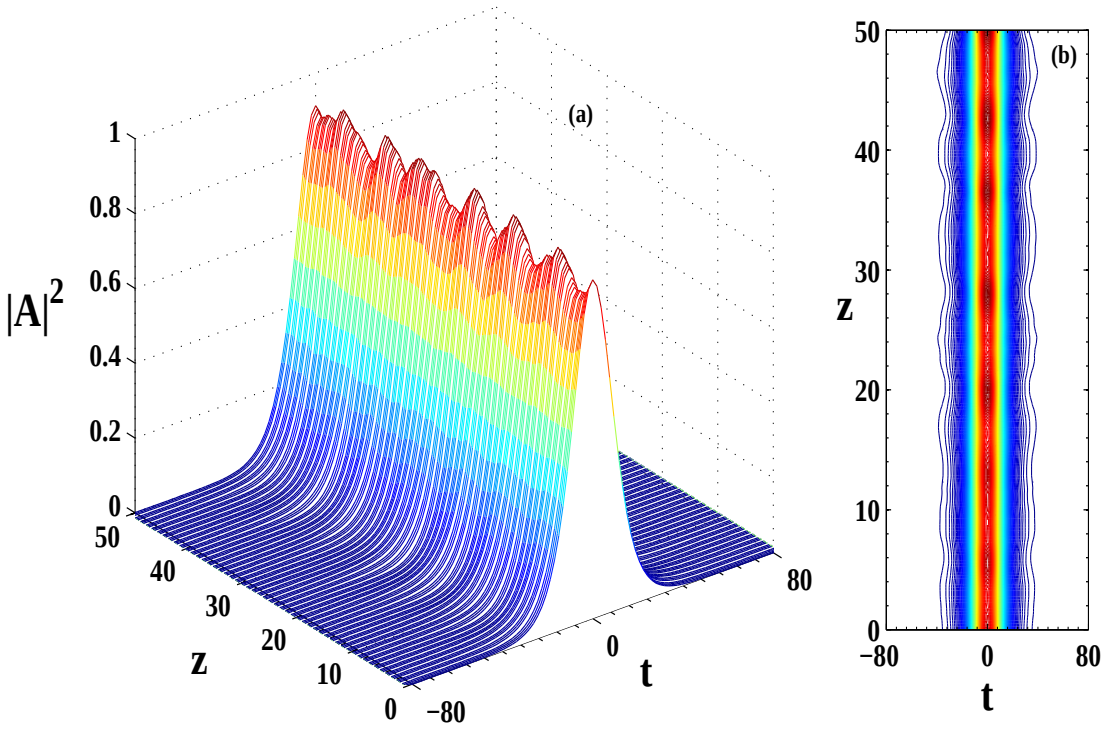

Fig. 4.9: (a) The propagation of a robust soliton in the presence of the random dispersion at the 7% level, with respect to its constant part. (b) The corresponding contour plot. Here $\gamma = 0.1$, $K = 0.01$, $d = 0.05$ and $\nu = 0.01$, and the excess gain is $\Delta g = 4.34 \times 10^{-6}$.

much slower than the high-speed soliton pulse propagation, we here consider only the spatial randomness of the GVD, considering the local dispersion coefficient as a sum of a constant part and a randomly varying one (ϵ). Typically, the mean value of ϵ is zero. To get an idea of robustness of the DS in the presence of the random inhomogeneity of the GVD, in Fig. 4.8 we display the pulse propagation for different magnitudes of the random GVD. Naturally, fluctuations of the pulse's intensity and width increase with the growth of the magnitude of the randomness. In the subsequent analysis, we fix the random-variation magnitude to be 3% of the constant part of the GVD coefficient. In this case, the analysis readily produces stable DSs, which are virtually identical to those displayed in Figs. 4.3 (b),(d), and 4.4 - 4.7. In particular, the randomness at the 7% level still admits quite robust propagation of the pulse, as clearly seen in Fig. 4.9.

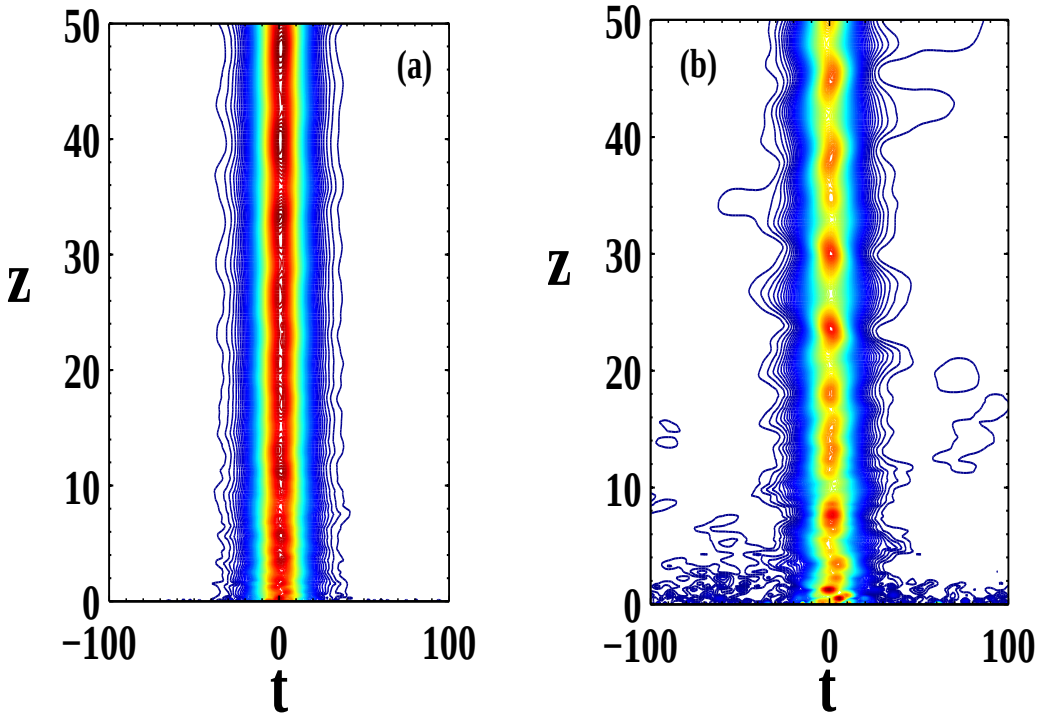

Fig. 4.10: Comparison of the evolution of the DS in the presence of an initial random noise at the 5% level (a), and 15% (b). Here $\gamma = 0.1$, $K = 0.01$, $d = 0.05$ and $\nu = 0.01$.

Along with the study of the effect of the random variation of the GVD coefficient along the fiber, it is necessary to address stability of the DSs against initial injunction of a random noise, a well-known source of which is the amplified spontaneous emission. Results of typical simulations of the noise-affected propagation of the DS are displayed in Fig. 4.10, which clearly demonstrate that the propagation remains robust even in the presence of a strong noise.

4.4 Interactions of Dissipative Solitons in the Fiber Laser

One of the basic features of solitons in (nearly) integrable systems is that they preserve their identity upon collisions. Shifts produced by collisions open a possibility for "steering light by light" [99]. In this section, we study interactions between the DSs, which were constructed above, in two different ways: first, the interaction between

in-phase solitons with different initial separations, and then the interaction between solitons with a constant initial separation but different relative phases, $\Delta\phi$. We have studied the interaction between two high-amplitude solitons (Fig. 4.11) as well as two low-amplitude ones (Fig. 4.12), originally separated by some distance (temporal delay).

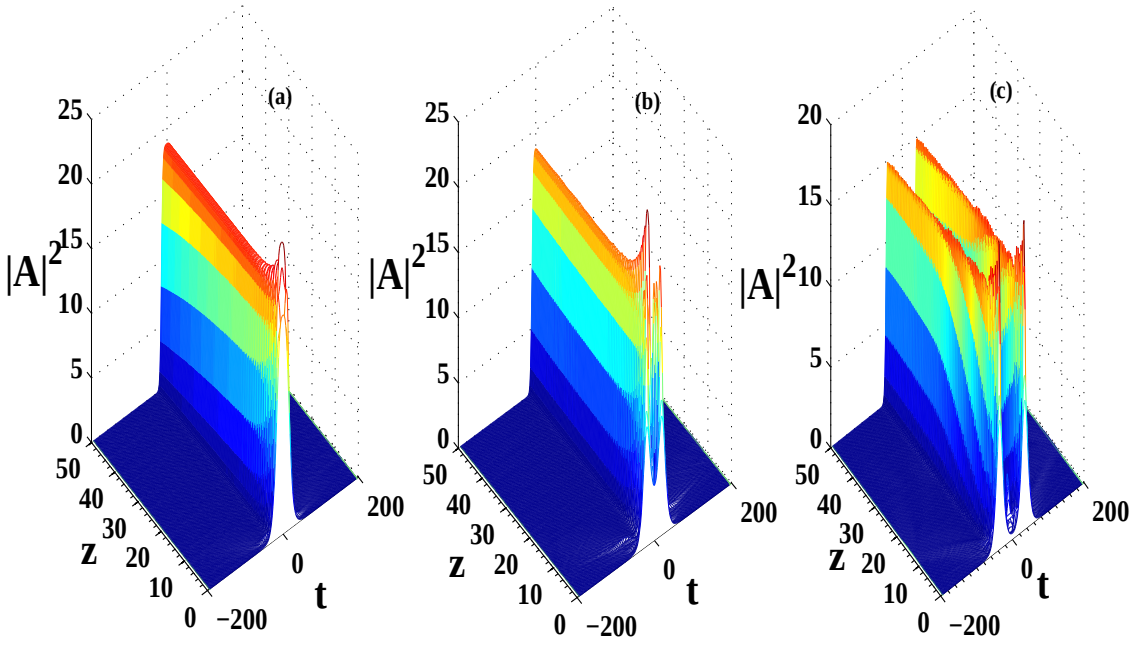

Fig. 4.11: Interactions between two in-phase high-amplitude ($A = 2.947$) DSs for different initial temporal separations (T_g) between them: (a) $T_g = 10$, (b) $T_g = 20$, (c) $T_g = 35$. Other parameters are $\gamma = 0.1$, $d = 0.05$, $K = 0.01$ and $\nu = 0.01$. The linear loss for (a) $\Delta g = -3.80 \times 10^{-5}$ (b) $\Delta g = -3.80 \times 10^{-5}$ and for (c) $\Delta g = -1.7255 \times 10^{-5}$.

Initially, the DS pairs are taken to be in-phase, with zero relative velocity between them. The large-amplitude solitons eventually blow up. A suitable loss Δg is applied to make them quasi-stable. The ensuing interaction dynamics significantly depends on the initial separation. At smaller separations, the DSs exhibit periodic collision and eventually merge into a single DS (breather), that maintains periodic oscillation of its amplitude and width in the course of subsequent propagation. With the increase of

the initial separation, the interaction becomes weaker, and ceases at the separation of $T_g \geq 50$.

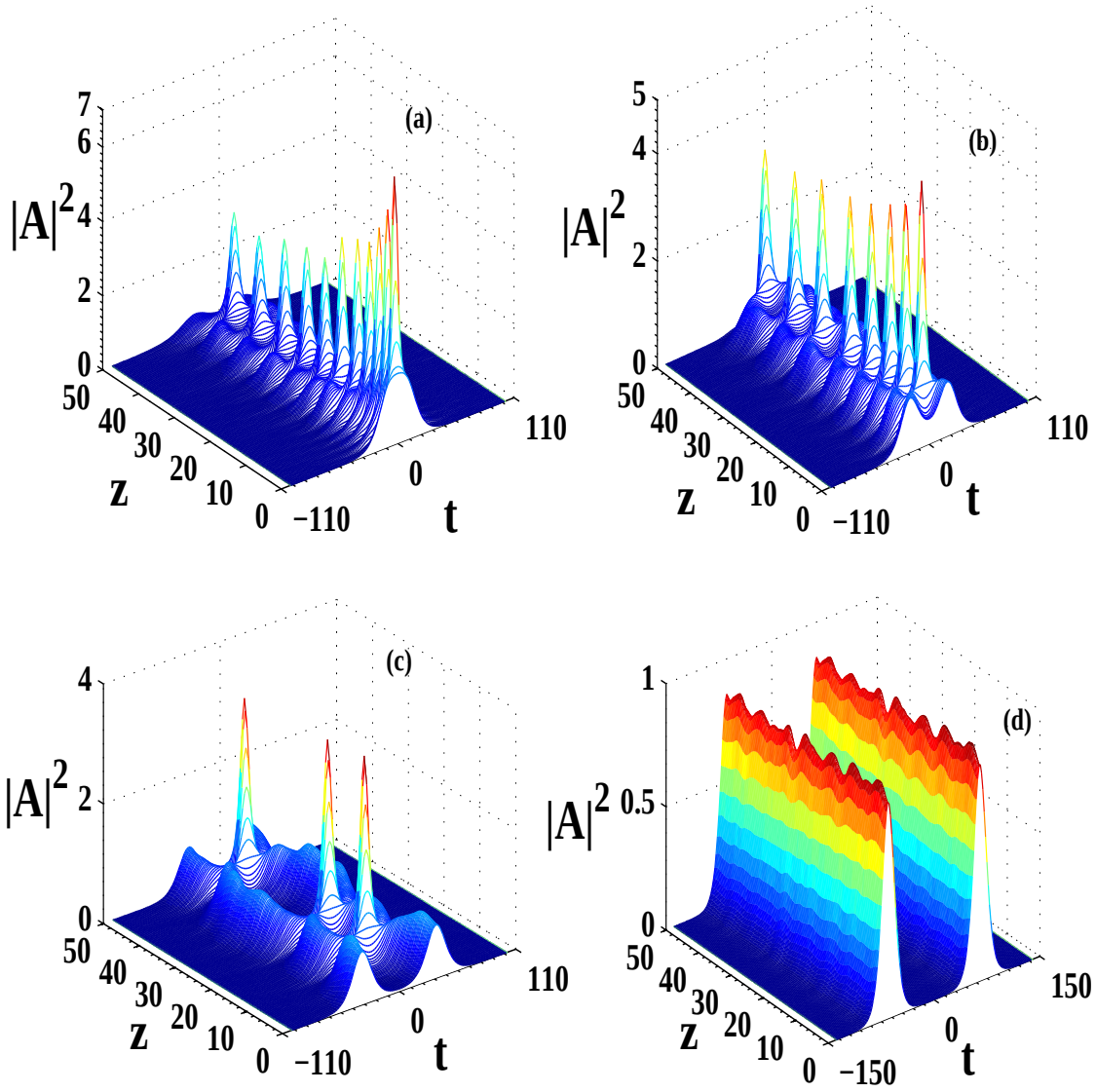

Fig. 4.12: Interactions between two in-phase low-amplitude ($A = 0.853$) DSs for different initial separations (T_g) between them. (a) $T_g = 10$, (b) $T_g = 20$, (c) $T_g = 35$, and (d) $T_g = 65$. The corresponding top views are displayed in panels are (e), (f), (g) and (h), respectively. Other parameters are $\gamma = 0.1$, $d = 0.05$, $K = 0.01$ and $\nu = 0.01$. The excess linear gain is $\Delta g = 4.35 \times 10^{-6}$.

The interaction of small-amplitude DSs shows a different behavior. Instead of merging, they continue to coalesce and split periodically, thus exhibiting very robust breather-like propagation. The frequency of the periodic collisions decreases with the

increase of the initial separation T_g up to 65, beyond which the interaction ceases.

More interesting phenomenology was observed, varying relative phase $\Delta\phi$ between two interacting solitons with a constant initial separation. Figure 4.13 portrays such interaction for initial separation $T_g = 10$. In particular, for small $\Delta\phi = \pi/10$, one of the two interacting pulses quickly vanishes, transferring its energy to the other, which features deceleration in the course of subsequent propagation. At larger $\Delta\phi$, the energy transfer takes place quicker, and the deceleration decreases. At $\Delta\phi = \pi/2$, the two solitons undergo very fast merger, without any deceleration.

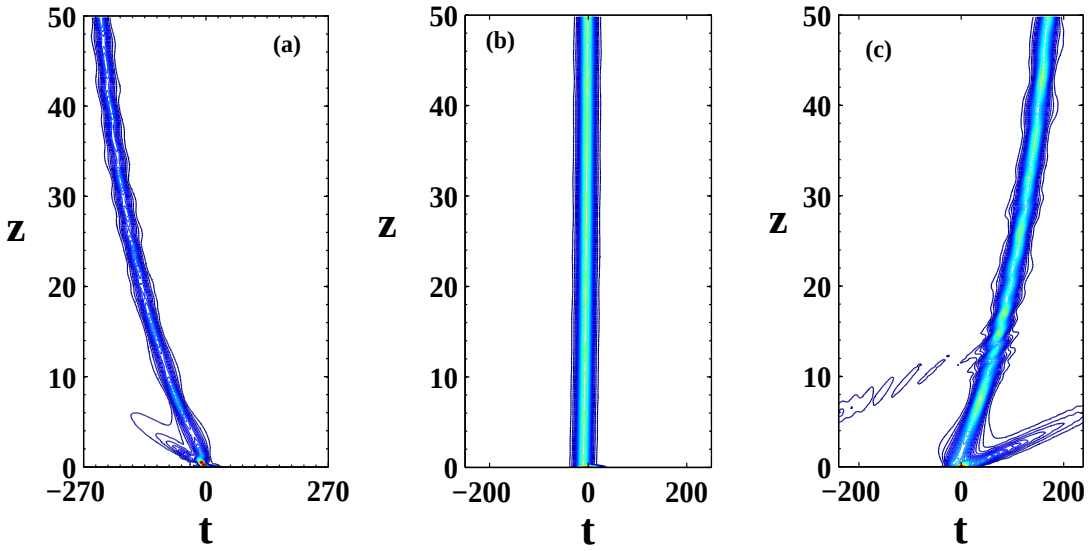

Fig. 4.13: Relative-phase-controlled switching, featured by the interaction of two DSs at different relative phases but with a fixed initial separation $T_g = 10$. The phase difference is $\Delta\phi = \pi/10$ in (a),$\pi/2$ in (b), and π in (c). Other parameters are $\gamma = 0.001$, $K = 0.01$, $\nu = 0.01$, $d = 0.01$. Here the excess linear gain is $\Delta g = 4.32 \times 10^{-6}$.

Further increase of the relative phase gives rise to emission of radiation from one pulse and eventual transformation of the pair into a single pulse, which accelerates (on the contrary to the deceleration observed at $\Delta\phi < \pi/2$). The acceleration increases with the increasing of $\Delta\phi$ up to π. Figure 4.14 shows the temporal shift of the pulse as a function of $\Delta\phi$ at a fixed normalized propagation distance, $z = 30$, for initial

separation $T_g = 10$.

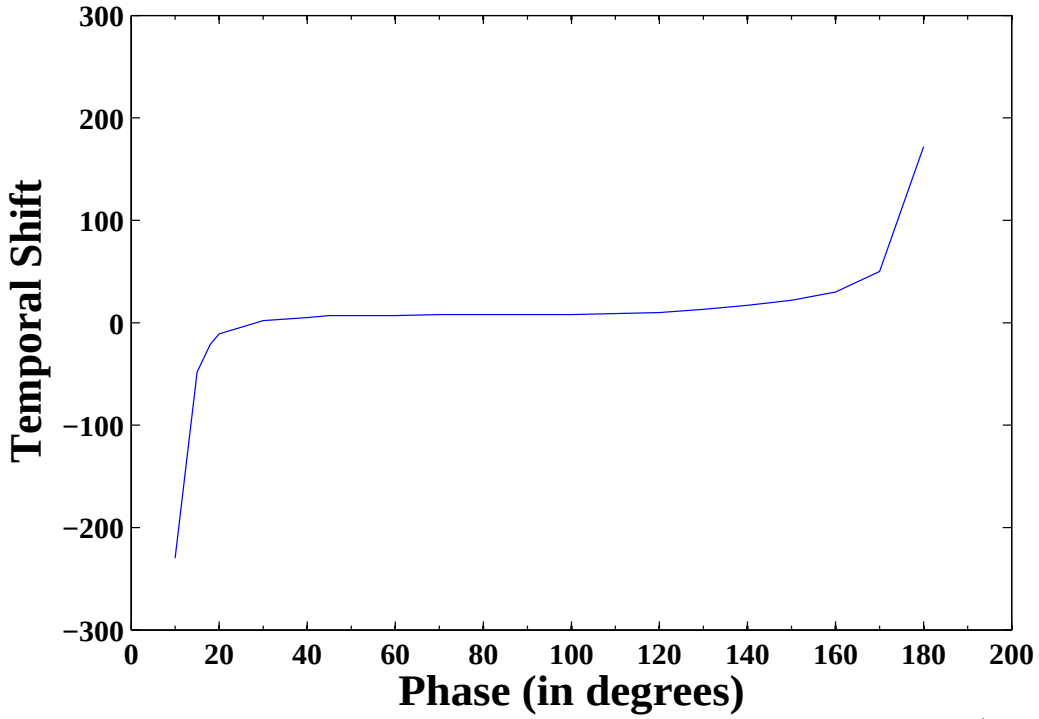

Fig. 4.14: Temporal shift of the single DS emerging from the original pair (with initial $T_g = 10$) versus the phase shift between the initial DSs. Other parameters are $\gamma = 0.001$, $K = 0.01$, $\nu = 0.01$, $d = 0.05$.

The switching from the deceleration to acceleration stage occurs much faster at smaller T_g. For example, at $T_g = 10$ the temporal-shift rate is $2.36/degree$ is observed, while at $T_g = 1$ it is $3.32/degree$.

4.5 Conclusion

We have studied the pulse propagation in the realistic model of fiber laser cavities under the action of the randomly varying GVD, loss, multiphoton absorption or emission (nonlinear gain), higher-order nonlinearity, and gain dispersion. We have found conditions for the stable operation of the laser in the dissipative-soliton regime. A nontrivial feature is the stability of the zero background around the solitons, in spite of the presence of the linear gain; an explanation of this feature was given. DSs were

obtained in an approximate form by means of the variational approximation and direct simulations, with a conclusion that the quasi-analytical results produced by the VA are in reasonable agreement with the numerical findings. An essential result, produced by both methods, is that the nonlinear amplification, provided by the 3PE (three-photon emission, i.e., the quintic gain) provides for an efficient alternative gain mechanism for the stable DSs, provided that it is not too strong, to avoid the onset of the blowup. Another noteworthy fact is that the DSs remain stable under the action of the perturbation in the form of the random GVD as well as noise. The DSs are bistable, with two different pulses, low- and high-amplitude ones, found for a given width. In the presence of the nonlinear gain, the low-amplitude DS is stable, while its high-amplitude counterpart is subject to the blowup instability. Interactions between the DSs lead to fusion of high-amplitude solitons into breathers, and periodic merger-splitting sequences for low-amplitude ones. One important result is obtained in form of relative phase controlled switching. The results reported in the chapter suggest new experiments for DSs in fiber lasers.

Chapter 5

Dispersion-Managed Dissipative Soliton in Fiber Laser Cavity: Generation and Interaction

---

In preceding two chapters we presented the generation and dynamics of dissipative soliton in semiconductor doped fiber laser cavities. In this chapter we introduce yet another important technique of soliton generation; the dispersion-management. We present generation and interaction dynamics of dispersion-managed dissipative soliton (DMDS) in a doped fiber laser cavity with cubic-quintic nonlinearity, multiphoton absorption and gain dispersion. Dispersion management technique uses a dispersion map comprising an anomalous and then a normal dispersion fiber segment. Each of the anomalous and normal fiber segments of the dispersion map is having some random dispersion fluctuation, alike a practical fiber. Role of gain dispersion, higher order nonlinearity and randomness on generation of DMDS is demonstrated. Role of temporal separation as well as phase difference between the interacting DMDSs and switching phenomena have been studied.

5.1 Introduction

In recent years, fiber laser has emerged as one of the most competent member of the industrial and medical laser families. It is compact in size but can yield high output

power. Also it is of lower cost but produces high quality beam. The structure of fiber laser are simple but output is robust [87, 88, 176, 177].Since, generated within the optical fiber itself, fiber laser naturally finds its compatibility in fiber optic communication and data processing. Moreover, it simplifies those operations manifold. The electrical-to-optical efficiency is very high; typically of the order of 50% in practical application. The same is above 70% in laboratory situation. Also, the optical-to-optical conversion efficiency can be achieved as high as 70% [178, 179]. A fiber laser basically consists of a semiconductor doped fiber having mirrors (generally fiber Bragg grating) at the two ends to build the cavity structure. Generally, doping is done by rare earth elements, popularly, Erbium, ytterbium. The fiber cavity can be end-pumped by one or more lasers. Typically diode or other fiber laser is used for this. Also it can be side-pumped by many lasers. A large variety of core structure, dopants and overall configuration enables fiber laser for multipurpose applications and consequently pulls down the monopoly of non-fiber lasers. The output quality and overall performance of a conventional fiber laser can be made significantly improved by enabling it to emit soliton pulses. Such a soliton fiber laser can be achieved by several self-started, passive mode-locking techniques [86, 147, 180, 181], often based on artificial saturable absorber (ASA). Mode-locking is a technique in which all oscillating modes of a laser are made to maintain equal frequency spacing with a fixed phase relationship with one another. Mode-locking is achieved by incorporating saturable absorber into the laser resonator in passive mode-locked technique whereas in active mode-locking it is attained by periodic modulation of resonator losses by using acousto-optic or electro-optic modulator etc. [182]. Owing to its easier implementation and comprehensiveness nonlinear polarization rotation (NPR) [183] is frequently preferred as ASA. NPR is a nonlinear variation in the polarization state of optical pulse while propagating through not polarization maintaining fiber. Otherwise, nonlinear loop mirror (NOLM) can be used [184]. The presence of polarization dependent component in NPR-cavity always produces a

scalar soliton [185]. To generate a vector soliton the polarization dependency should be removed as much as possible. In this context semiconductor saturable absorber mirror (SESAM) [186, 187] and now popular carbon nanotubes (CNT) are extensively used for the mode-locking [125]. In addition, a variety of two-dimensional optical materials, namely, graphene, molybdenum disulfide (MoS_2) and tungsten diselenide (WSe_2) are also being used. Owing to their faster recovery time, higher absorption power and higher saturation fluency they are replacing SESAM gradually [126, 188, 189]. Other than adopting mode-locking technique, the performance of the soliton fiber laser can be remarkably improved by using the technique of dispersion management [190–192]. The concept of dispersion management (DM) has become an attractive technology for long-haul, high speed soliton based optical communication systems [83, 84, 193, 194] since early 1990s. In DM system, the group velocity dispersion (GVD) of fiber varies alternatively between the anomalous and normal dispersion [195]. This leads to the net average GVD to be positive, negative or even zero. Insightful reviews on DM soliton highlighting the techniques as well as current and future applications are available in [89, 196, 197]. Stabilizing the soliton is always an important issue. The condition for stationary pulse propagation in strong dispersion-managed system can be obtained analytically [198]. The jitter suppression factor can be enhanced in lossy system by properly choosing the segment length ratio. Jitter suppression enhances due to dispersion compensation period rather than the ratio of the dispersion [199]. Inclusion of DM technique in fiber laser cavity, drastically reduces the detrimental effect of amplified spontaneous emission on the phase noise, side by side, greatly extends the power range of generation of uninterrupted single pulse [200]. Using variational approach, a theoretical study of timing jitter and stability of actively mode-locked DM fiber ring laser shows that for strong dispersion management, the timing jitter becomes smaller [90]. The location of the filter, amplifier and modulator in the cavity also significantly control the magnitude of timing and energy jitter. A bound state of DM solitons at near zero

net cavity GVD in a passively mode-locked erbium-doped fiber ring laser have been obtained [59]. Passively mode locked, polarization maintaining, figure eight erbium doped fiber laser with a DM cavity has been used to generate the extremely robust soliton pulses [201]. Anti-symmetric DM solitons have been observed in a Yb-doped fiber laser by using a strong dispersion map. These can be considered as a tightly bound soliton pair with a phase difference of π between the component solitons [177]. Dependence of laser performance on the output coupling ratio and net cavity dispersion has been observed experimentally in a passively mode-locked, ultrashort-pulse, Er-doped fiber laser using a polyimide film containing dispersed single-wall carbon nanotubes (SWNTs) [202].

One of the basic thrust areas of soliton research is the dissipative soliton (DS), the perception of which immensely improves the theoretical prediction on the performance of soliton fiber laser. In one hand the DS mode-locking enhances (even doubles) the pulse energy, on the other hand, acknowledges the dissipative nature of a practical fiber. In practical fiber cavities, so in a DM cavity, there will be linear as well as may be nonlinear losses [6, 12]. Therefore, to keep the soliton 'alive' we must introduce an appropriate gain in the cavity. The structure thus formed is called dissipative soliton as it is formed by a gain-loss balance in addition to the essential GVD and nonlinear self-focusing equilibrium [1,40]. The operation of DMDS soliton fiber laser has been reported at $2\mu m$ fiber laser [62]. Both stretched pulse type and positively chirped pulse type DMDS are demonstrated in mode locked lasers [203]. By using a strong DM cavity, a harmonically mode-locked Er-fiber soliton lasers has been fabricated [200]. Generation of a stable DM soliton is possible even in the presence of detrimental effects like self-phase modulation as well as stimulated Raman scattering [204]. Gain-guided soliton operation of DM fiber laser have been observed both numerically and experimentally [58]. The generation of dissipative vector solitons in large net normal dispersion cavity has been studied [205]. Despite the large frequency chirp of the dis-

sipative soliton formed in the cavity, the polarization rotating and polarization locked dissipative vector soliton have been observed to be stable.

Soliton fiber laser has been widely investigated, but some of its relevant issues have gone unaddressed. Particularly, the role of random dispersion and multiphoton absorption/emission has not been addressed explicitly. In theoretical modelling, mostly ideal fibers having constant core diameter and constant doping densities are used. In contrary, in real fibers, there are various kinds of imperfections such as shape variations, fluctuations in the dopant concentration, inhomogeneities of the refractive index and effect of bending and ellipticity due to external stress [153, 154]. These imperfections are random in nature and manifest themselves through random dispersion. The influence of random GVD is inherent even in a sophisticated fiber laser cavity [155, 156]. Propagation of optical pulse in a random dispersion-managed fiber system has been rarely studied [206]. Another issue arises due to one of the main attribute of fiber laser cavity, i.e., generation of ultrashort pulses. These ultrashort pulses have high peak power. In fibers, Kerr/cubic nonlinearity is the dominating nonlinearity. But in many fibers even at moderate power, the fifth order nonlinear effect become relevant [207–210]. Although, the quintic nonlinearity is very minute with respect to cubic nonlinearity, its commutative effect is significant. Also, the combined presence of self-focusing cubic (which corresponds to real part of cubic susceptibility χ^3) and self-defocusing quintic nonlinearity (corresponding to real part of χ^5) leads to the very interesting pulse feature and dynamics. The imaginary parts of χ^3 and χ^5 give rise to two-photon absorption (TPA) and three-photon absorption (3PA) effects respectively in the fiber cavity [25, 211]. Besides, multiphoton absorption, the effect of finite gain bandwidth become important for femto-second and few pico-second pulses. Wide spectrum of the ultrashort pulses leads to the dispersion in gain, which when couples with the GVD, modifies the pulse dynamics and energy profile significantly [112].

Therefore, in the current communication we investigate the role of random dis-

persion, gain dispersion and multiphoton absorption in generation and dynamics of DMDS. A lossy DM fiber with cubic-quintic nonlinearity can be modelled using the following complex cubic-quintic Ginzburg-Landau equation (CQGLE),

$$i\frac{\partial E}{\partial z}+\frac{D(z)}{2}\frac{\partial^2 E}{\partial t^2}+\mid E\mid^2 E-\gamma\mid E\mid^4 E=\frac{i}{2}(g_o-\alpha)E+\frac{id}{2}\frac{\partial^2 E}{\partial t^2}-iK\mid E\mid^2 E-i\nu\mid E\mid^4 E. \tag{5.1}$$

Here, E is the normalized field inside the cavity, z is the normalized length of propagation, and t is retarded time. $D(z)$ represents the dispersion map that comprises alternate anomalous and normal dispersion. A randomly varying dispersion is added to each of anomalous and normal dispersion each fiber segment of the map. The third and fourth terms represent contribution of cubic and quintic nonlinearities respectively. If the intra-band relaxation time is smaller than its temporal width, the gain spectrum, $g(\omega)$ can be expanded in the Taylor series about the carrier frequency ω_0. The first two terms of the expansion lead to gain saturation and gain dispersion. g_o and d are the gain saturation and the gain dispersion coefficients, respectively, while dimensionless coefficient α estimates the linear loss. The net gain, Δg is given by, $\Delta g = (g_0 - \alpha)$. The third and fourth terms on the right are due to TPA and 3PA respectively. K denotes the TPA coefficient and ν represents the 3PA coefficient. K and ν are connected to $\chi^(2)$ and $\chi^(3)$ via the relation $\alpha_2 = \frac{3\omega Im(\chi^{(3)})}{2{n_0}^2 c^2 \epsilon_0}$ and $\alpha_3 = \frac{5\omega Im(\chi^{(5)})}{2{n_0}^3 c^3 {\epsilon_0}^2}$ respectively. Such systems are generally solved through numerical approach. However, Variational method based analytical approach, even though an approximate, is useful in getting a deep understanding of the system. We use the variational method in conjugation with Rayleigh's dissipative function (RDF) to solve the governing CQGLE. The main advantage of this method is that it gives explicit evolution of individual system parameters. The evolution equation may further be used for stability analysis for the system. We consider the sech ansatz of the following form:

$$E(z,t) = A(z)sech\left(\frac{t}{W(z)}\right)\exp\left(i\phi(z)\right), \tag{5.2}$$

where, $A(z)$, $W(z)$ and $\phi(z)$ represent the complex amplitude, temporal pulse width and phase, respectively. Following the standard procedure of variational method we obtain Lagrangian density and RDF density. Subsequently, using Euler-Lagrange equation for different system parameters the fundamental soliton condition is obtained as,

$$\frac{\mid A(z) \mid^2 W^2(z)}{D(z)} - \frac{16\gamma \mid A(z) \mid^4 W^2(z)}{15D(z)} = 1 \tag{5.3}$$

However, 'soliton condition' is a debatable concept for dissipative systems. Since the dissipative systems involves exchange of particle and/or energy with the surrounding the energy will not be a constant. Eqn. (5.3) does not contain any gain or loss term. Thus to make Eqn. (5.3) as soliton condition we need to balance the system loss with the applied gain, which we will take care of while doing numerical experiments. Eqn.(5.3), further gives rise to evolution equations of amplitude $A(z)$ and width $W(z)$ of the pulse:

$$\frac{dW(z)}{dz} = \frac{\left[\begin{array}{r} \frac{-d}{3sW}\left(1-\sqrt{M}\right) - \frac{2KW}{3s^2}\left(1-\sqrt{M}\right)^2 - \frac{4\nu W}{15s^3}\left(1-\sqrt{M}\right)^3 \\ - \frac{2}{W\sqrt{M}}\frac{dD}{dz} + W(g_o-\alpha)\frac{1}{s}\left(1-\sqrt{M}\right) \end{array}\right]}{\left[\frac{-4D}{W^2\sqrt{M}} + \frac{1}{s}\left(1-\sqrt{M}\right)\right]}, \tag{5.4}$$

$$\frac{dA(z)}{dz} = \frac{\left[\begin{array}{l} \left[\frac{1}{2AW^2-4sW^2A^3}\right]\frac{dD}{dz} - A(1-sA^2) \\ \quad \left[\begin{array}{r} \frac{-d}{3sW}\left(1-\sqrt{M}\right) - \frac{2KW}{3s^2}\left(1-\sqrt{M}\right)^2 - \frac{4\nu W}{15s^3}\left(1-\sqrt{M}\right)^3 \\ - \frac{2}{W\sqrt{M}}\frac{dD}{dz} + W(g_o-\alpha)\frac{1}{s}\left(1-\sqrt{M}\right) \end{array}\right] \end{array}\right]}{W(1-2sA^2)\left[\frac{-4D}{W^2\sqrt{M}} + \frac{1}{s}\left(1-\sqrt{M}\right)\right]}. \tag{5.5}$$

Here, $M = \frac{1-4sD}{W^2}$ and s $= \frac{16\gamma}{15}$.

5.2 Generation of DMDS in Random Media

In DM fiber, fiber dispersion is the sum of a locally varying part and an average dispersion $< d >$, is represented mathematically as:

$$d(z) = \begin{cases} d_1 + < d > & if \quad 0 \leq z \leq L/4 \\ d_2 + < d > & if \quad L/4 \leq z \leq 3L/4 \\ d_1 + < d > & if \quad 3L/4 \leq z \leq L \end{cases}$$

where, d_1 and d_2 are normal and anomalous dispersion values of the fiber and L is the total length of the fiber.

DM soliton can be found with a variety of dispersion map, as for example, zero average dispersion (Fig. 5.1 a), normal average dispersion (Fig. 5.1 b), and anomalous average dispersion (Fig. 5.1 c). In all these cases both the anomalous and normal dispersion fiber segments have constant dispersion value. To replicate a real time fiber, a random dispersion is to be added to the dispersion map (Fig. 5.1 d).

Each of the normal and anomalous dispersion fiber segment is added with 3% random dispersion on the top of the constant dispersion value. This eventually leads to an average random anomalous dispersion. In view of the low order defects of modern fiber, 3% random dispersion seems to be optimum. We now use these dispersion maps to generate DMDS. Generally, getting a DMDS is easier with the average anomalous dispersion map (Fig. 5.2 c). However, the same parametric values of DMDS system lead to blow up with zero average dispersion (Fig. 5.2 a) and normal average dispersion (Fig. 5.2 b) map. It may be noted that these two types of dispersion map can give rise to DMDS only with some special set of parameters. Even with the randomness in the dispersion map, the formation of DMDS is observed (Fig. 5.2 d), indeed, by the virtue of tuning the gain. The influence of randomness is noticeable and lies within the limit of tolerance for practical applications.

The randomness of the dispersion in fiber may be of different nature:: (i) uniformly distributed random values of dispersion (UDR), (ii) uniformly distributed inte-

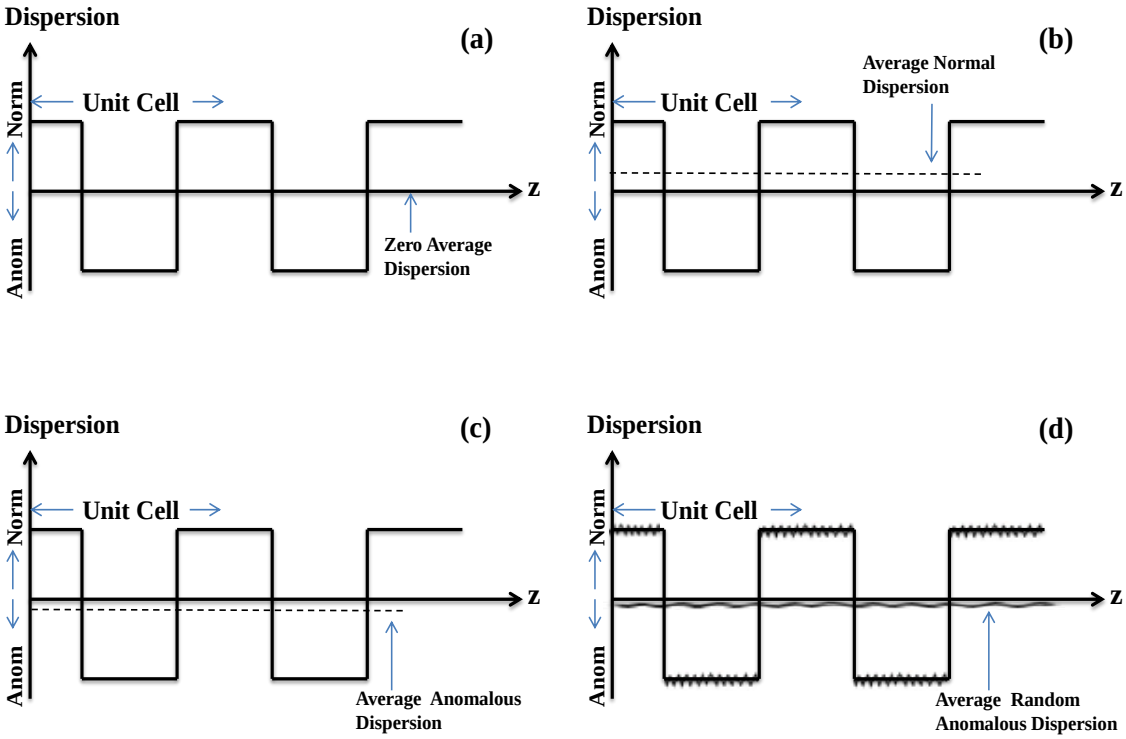

Fig. 5.1: Different types of symmetric two-stage dispersion map (a) zero average dispersion (b) average normal dispersion (c) average anomalous dispersion (d) average random anomalous dispersion.

ger random values of dispersion (UDRI) and (iii) randomly distributed random values of dispersion (RDR). A stable DMDS can be found for all these types of dispersion-randomness (Fig. 5.3 (a, b, c)). The typical breathing (expansion-contraction) rate of the DMDS are different for all these randomness. The breathing rate is highest for RDR, intermediate for UDRI and lowest for UDR case. In the current chapter 'UDR' type random dispersion map is used henceforth. The confinement behaviour of the breathing DMDS can be shown by a (Amplitude-Width) phase plot. DMDSs obtained are confined both in the absence (Fig. 5.4 a) and in presence (Fig. 5.4 b) of random dispersion in the DM map. The nonlinear multiphoton absorption, gain dispersion and quintic nonlinearity play a significant role in estimating the required gain evolution of DMDSs. Using dispersion map (Fig. 5.5 c), we obtain (Fig. 5.5 a). In the random dispersion environment also we got such effects (using Fig. 5.5 d dispersion

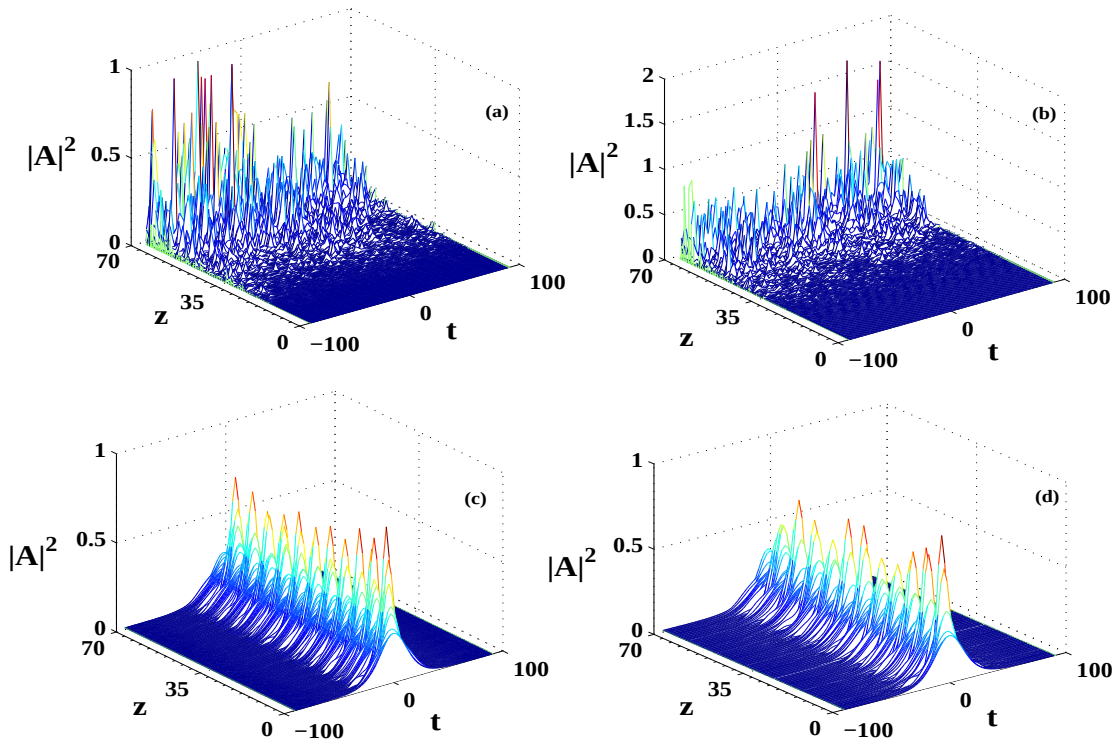

Fig. 5.2: Evolution of pulse under (a) zero average dispersion (b) average normal dispersion (c) average anomalous dispersion (d) average random anomalous dispersion. Here, $K = 0.01$, $\gamma = 0.01$, $\nu = 0.01$ and $d = 0.05$. Here excess gain Δg for (c) 1.35×10^{-6} and for (d) 1.47×10^{-6} respectively. No stable Soliton is available for (a) and (b) for a Δg value ranging from -2.78×10^{-6} to 1.50×10^{-6}.

map) and is portrayed in Fig. 5.5 b. Increase in gain dispersion demands larger net gain to stabilize a DMDS generated both in the non-random (Fig. 5.5 a) and random (Fig. 5.5 b) dispersion maps. For a given value of gain dispersion, the requirement of net gain is maximum for a fiber with TPA and minimum for one with 3PA [25, 211]. Interestingly, a fiber with both TPA and 3PA witnesses the intermediate gain requirement (Fig. 5.5 a). For random dispersion fiber segment map the net gain significantly increases keeping the effect of multiphoton absorption unaltered (Fig. 5.5 b). Likewise, the quintic nonlinearity controls the net gain requirement to stabilize the DMDS both for non-random (Fig. 5.6 a) and random dispersion map (Fig. 5.6 b). An increase in quintic nonlinearity significantly increase the required net gain (Δg). For a given value

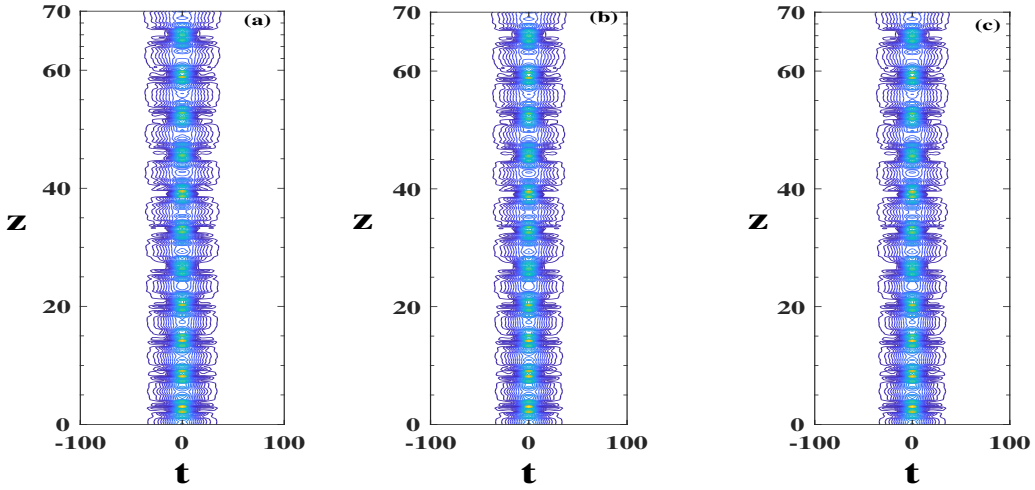

Fig. 5.3: DMDS (Contour plot) for different types of dispersion-randomness (a) UDR (b) UDRI (c) RDR. Here, $K = 0.01$, $\gamma = 0.01$, $\nu = 0.01$ and $d = 0.05$. Here net gain Δg is (a) 1.35×10^{-6}, and for (b) 1.59×10^{-6}, and (c) 1.64×10^{-6}.

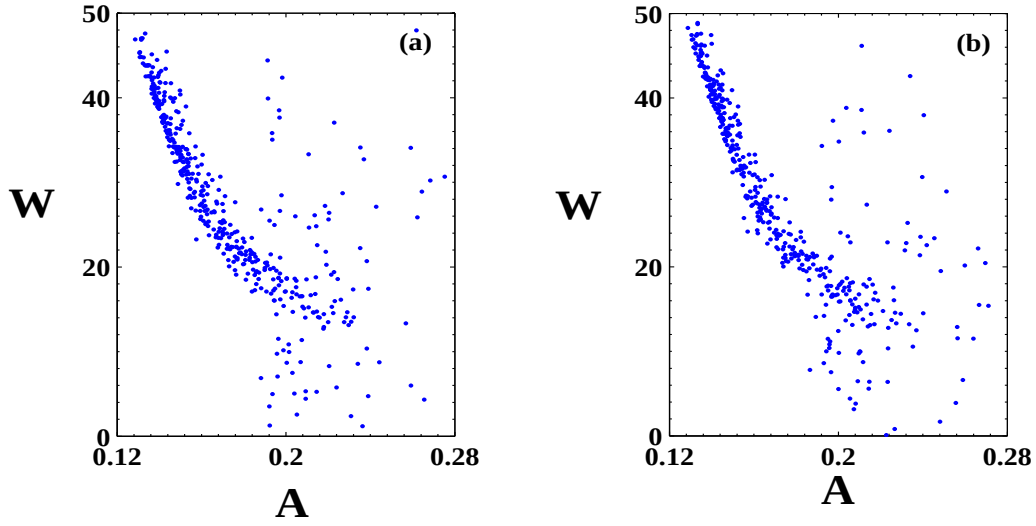

Fig. 5.4: Amplitude-Width (A-W) phase plot for DMDS (a) without Random Dispersion, (b) with Random Dispersion. Other parameters are $K = 0.01$, $\nu = 0.01$, $d = 0.05$ and $\gamma = 0.01$. The excess linear gain is (a) $\Delta g = 1.37 \times 10^{-6}$ and for (b) $\Delta g = 1.45 \times 10^{-6}$ respectively.

of quintic nonlinearity, the required value of Δg is maximum for a fiber in presence of both TPA and 3PA and it is minimum when only 3PA is present in the system. In presence of TPA only the intermediate gain (max Δg) is required for generating

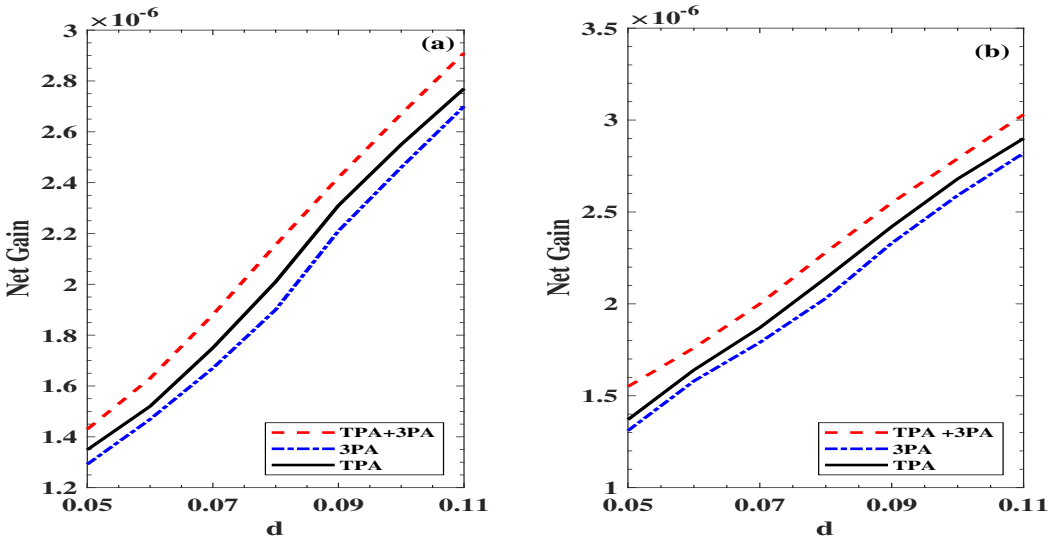

Fig. 5.5: Variation of net gain Δg required to generate DMDS with gain dispersion d under the influence of TPA, 3PA and both TPA and 3PA for (a) dispersion map (Figure 5.1 c) (b) dispersion map (Figure 5.1 d). Here, $K = 0.01$, $\gamma = 0.01$, $\nu = 0.01$.

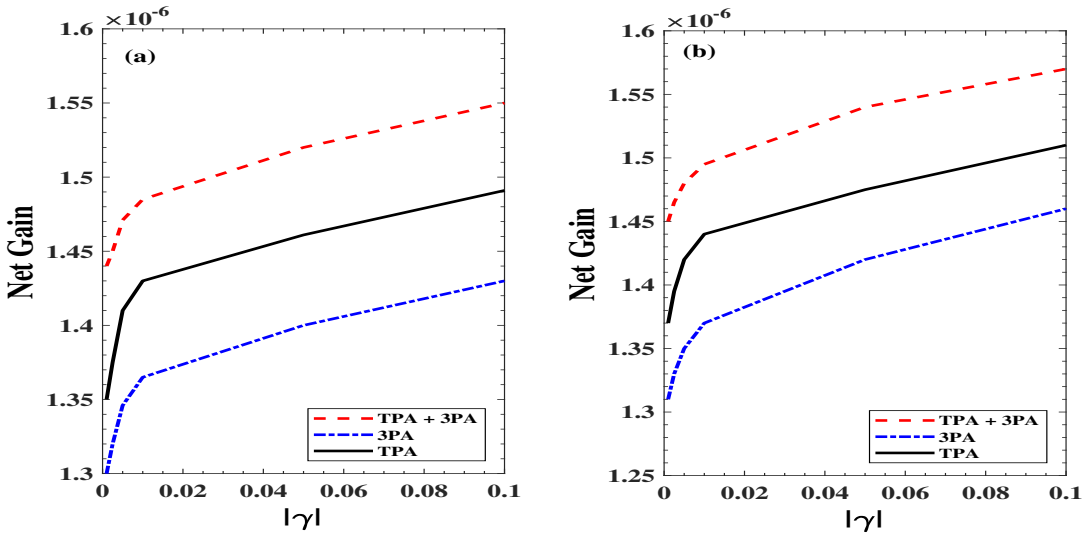

Fig. 5.6: Variation of net gain Δg required to generate DMDS for different value of quintic Nonlinearity under effects of TPA and 3PA for (a) constant dispersion fiber segment (b) random dispersion. Here, $K = 0.01$, $\nu = 0.01$, $d = 0.05$.

DMDS.

For any operation in optical fiber system, whatever good the quality is, presence of some random noise is very usual. DS, and so DMDS formation significantly gets

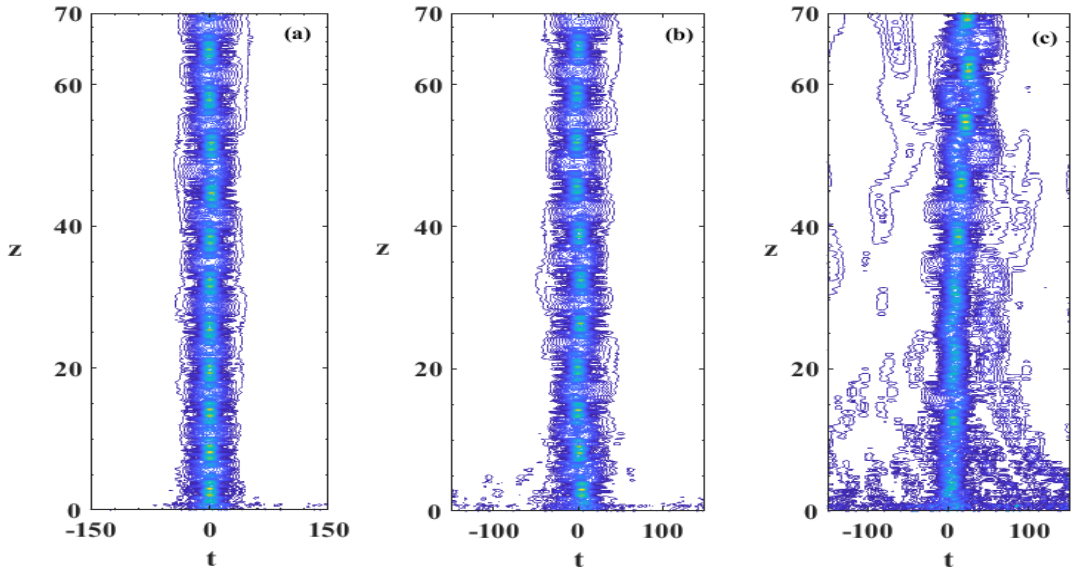

Fig. 5.7: Comparison of the evolution of the DMDS in the presence of an initial random noise at (a) the 3% level (b) 5%. And (c) 9%. Here, $K = 0.01$, $\nu = 0.01$, $d = 0.05$ and $\gamma = 0.01$.

affected by the noise. With lower value of noise, there is no as such change in the DMDS (3% random noise, Fig. 5.7 a). Even with 5% random noise (Fig. 5.7 b) a traceable DMDS is obtained but beyond that(e.g., 9%) it is severely affected (Fig. 5.7 c). Thus below 9% noise tolerance is quite acceptable in view of current available fiber optics laser cavity.

5.3 Interactional Behaviour and Switching

Whether it's a fiber optic communication system (where soliton pulses are to be closely spaced) or a fiber laser, soliton interaction is inevitable. The interactional behaviour not only ensures the particle like behaviour of soliton (which is a fundamental property of it) but also brings out significant information of the system.

Interaction behaviour of DM soliton is equally attracting like its generation. In intra channel collisions, collision-induced frequency shift is noteworthy. For high DM strength, the collision induced position shift becomes significant than frequency shift

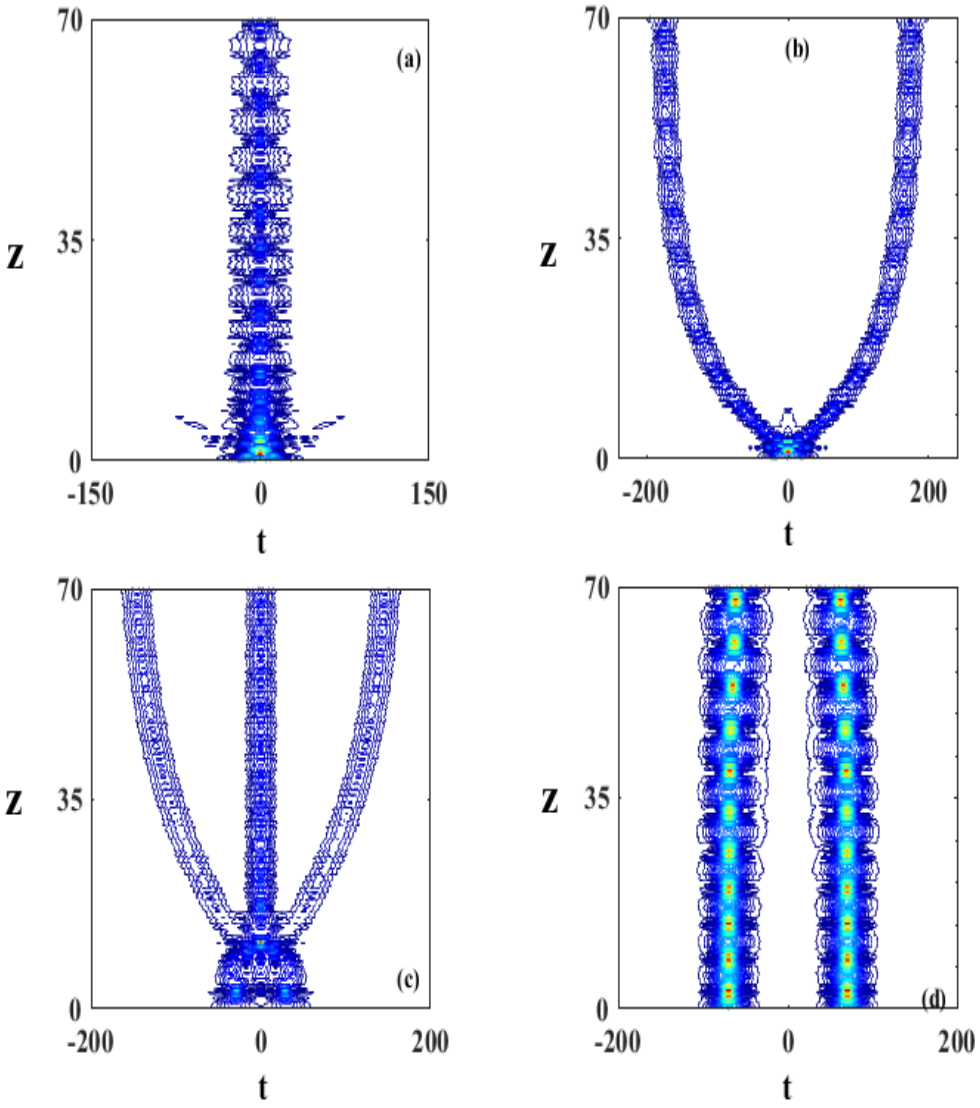

Fig. 5.8: Interactions between two in-phase DMDSs for different initial separations (Tg) between them. (a) $Tg = 5$, (b) $Tg = 13$, (c) $Tg = 32$, and (d) $Tg = 75$. Other parameters are $K = 0.01$, $\nu = 0.01$, $d = 0.05$ and $\gamma = 0.01$. The net gain is $\Delta g = 1.45 \times 10^{-6}$.

produced by the incomplete collision [212]. Both the proximity between the DMDSs and their phase relationship significantly control the interactional behaviour. This behaviour of DM soliton is equally attracting like its generation. In intra channel collisions, collision-induced frequency shift is noteworthy [213]. In the current section interaction behaviour is presented with at least 3% randomness in the system unless mentioned otherwise. The interaction between two in-phase DMDSs may yield

single united DMDS of higher width (Fig. 5.8 a) or two eventually parallel branches (Fig. 5.8 b) or even three branch DMDS (Fig. 5.8 c), depending on their initial separation. However, it cannot be generalized that the number of branches is proportional

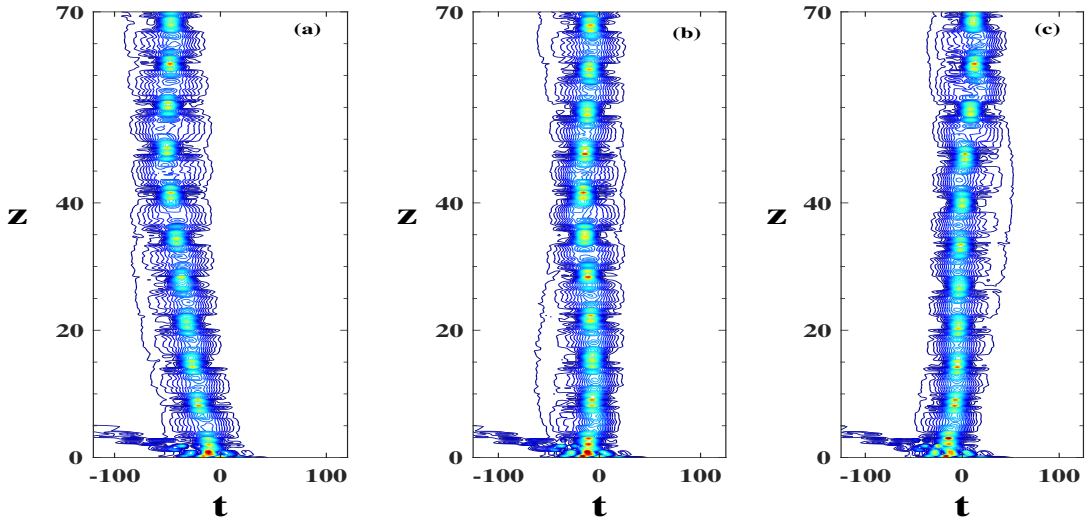

Fig. 5.9: Intensity profiles of two DMDSs when they interact with each other for different temporal separation (Tg) between them: (a) $Tg = 10$, (b) $Tg = 15$, (c) $Tg = 20$. Initial phase difference between the two solitons is $\pi/10$. Other parameters are $K = 0.01$, $\nu = 0.01$, $d = 0.05$ and $\gamma = 0.01$.

to the initial separation.

The threshold initial separation for in-phase interaction is determined as $Tg = 75$ (Fig. 5.8 d). More interesting phenomena are observed by studying the interaction of two DMDSs by changing temporal separation in presence of initial phase difference between them. After collision, the two DMDSs unite together with some initial radiation. For an initial fixed phase difference of $\pi/10$, by changing the temporal separation between them, the soliton switching has been observed. For $T_g = 10$, DMDSs first combine and then shifts towards the left side of the time axis. Thus showing the slowing down of DMDS (Fig. 5.9 a). It shifts toward the fast axis i.e., DMDS speeds up, when the value of T_g is increased, say $T_g = 20$ (Fig. 5.9 c). It propagates without any change in its speed for $Tg = 15$ (Fig. 5.9 b). The switching profile with respect

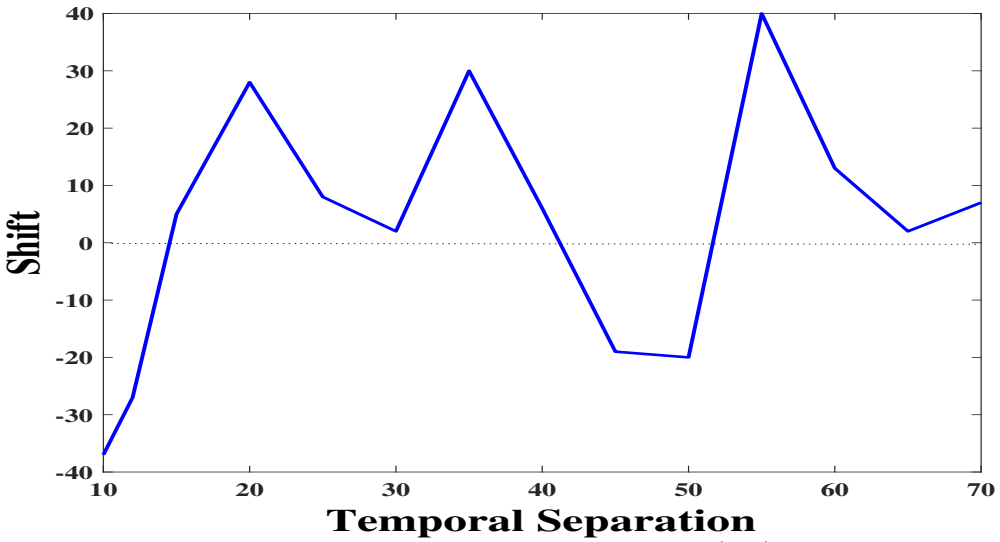

Fig. 5.10: Switching with increasing temporal separation (Tg) between two interacting DMDSs. Here, phase difference between the two DMDS pulses is $\pi/10$. Other parameters are $K = 0.01$, $\nu = 0.01$, $d = 0.05$ and $\gamma = 0.01$.

to increasing temporal separation between the DMDSs is plotted in Fig. 5.10. DMDS shifting from slow to fast and vice versa takes place as temporal separation between the two pulses is changed. Thus, controlling temporal separation between the interacting DMDSs one can switch between the fast and slow velocity domain. Same is also valid for interaction of two DMDS with fixed temporal separation but varying phase difference. For this we keep temporal separation of $Tg = 10$. DMDS decelerates after merging quickly by transferring its energy to the other for $\pi/10$ (Fig. 5.11 a). At a phase difference of $\pi/3$, a very fast merger of two DMDSs takes place, without any deceleration (Fig. 5.11 b). Further increase of phase angles leads to acceleration of solitons (Fig. 5.11 c). The switching profile with respect to increasing phase difference and constant temporal separation between the DMDSs (Fig. 5.12) shows that slow and fast velocity domain is not very periodic. For other temporal separation also phase controlled switching can be done. Comparison between Fig. 5.10 and Fig. 5.12 reveal that the temporal separation controlled switching is more prominent than that of the phase controlled switching.

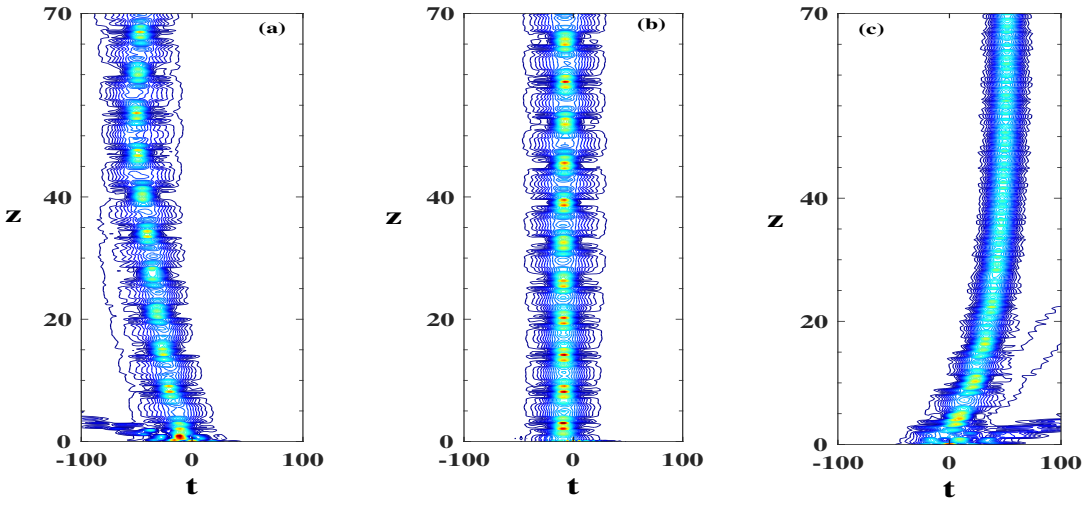

Fig. 5.11: Intensity profiles of two DMDSs when they interact with each other with different phase separation between for fixed temporal separation $Tg = 10$, Initial phase difference between the two solitons is (a) $\pi/10$, (b) $\pi/3$ (c) $2\pi/3$. Other parameters are $K = 0.01$, $\nu = 0.01$, $d = 0.05$ and $\gamma = 0.01$.

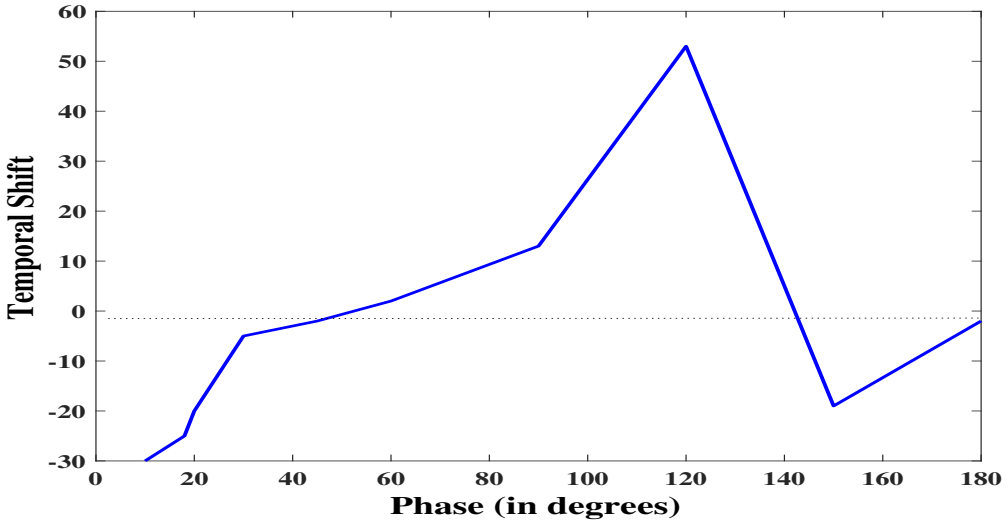

Fig. 5.12: Temporal shift of the single DMDS emerging from the original pair (with initial $Tg = 10$) versus the initial phase difference between the DMDSs. Other parameters are $K = 0.01$, $\nu = 0.01$, $d = 0.05$ and $\gamma = 0.01$.

5.4 Conclusion

In this chapter, we studied the generation of stable DMDSs and their interaction dynamics in doped fiber laser cavity with cubic-quintic nonlinearity, gain dispersion and

multiphoton absorption and dispersion map with random dispersion included. DMDS exhibit breather like characteristics. DMDS thus generated are robust against certain level of noise present in any practical transmission line. The system is studied by analytical (variational method) approach and is supported by direct numerical simulation using split-step Fourier transformation method (SSFT method). The interaction between two DMDSs having same phase may lead to a bound state or branching for a temporal separation below a threshold value. For non-zero phase difference the temporal separation between the interacting DMDSs can control the speed of the bound state soliton and eventually leads to temporal separation controlled all-optical switching. Similarly, phase controlled all-optical switching is demonstrated. Switching observed by tuning temporal separation is found to be more noticeable than phase controlled switching. These findings can be significant in improving the performance of DMDS fiber laser as well as all-optical switching devices, all-optical data processing, all-optical delay lines and optical communication links.

Chapter 6

Dissipative Soliton in Optical Fiber Laser Cavity with Higher Order Dispersive and Nonlinear Effects

---

In this chapter, we investigate the generation, stability and dynamics of dissipative solitons under the effect of third order dispersion and intrapulse Raman scattering in cubic-quintic nonlinear fiber laser with multiphoton absorption and gain dispersion.

6.1 Introduction

In case of the ultrashort pulses or solitons, the multiphoton absorption and gain dispersion are not the only higher order phenomena. Other higher order dispersive and nonlinear phenomena becomes important at this regime. While investigating ultrashort pulses, the higher order effects become relevant in optical fiber [6] as well as fiber laser. The role of higher order effect on the generation, stability and dynamics of soliton become very crucial and therefore proper understanding about these effects in optical fibers is important. Third order dispersion (TOD) is one of the higher order dispersive effects that plays arises in an optical fiber devices with the usage of ultrashort pulses. When ultrashort pulses are used, TOD effect is significant. TOD, being a dispersive effect, has detrimental influence on the pulse and generally causes energy radiation in the system. The stability and interaction dynamics of solitons are

largely influenced by the phase and group velocity between the solitons and radiations due to TOD [214]. Also the collective influence of higher order effects can limit the interaction between the neighbouring solitons [215]. The evolution of the pulse in cubic-quintic nonlinear media in the presence of TOD has been studied [216]. The presence of TOD results in loss of self-similarity and linear chirp characteristics during pulse propagation in dispersion-decreasing fiber with normal group velocity dispersion. However, high-quality compressed pulses can be obtained by using dispersion compensation technique [217]. The influence of higher order effects on the radiation emitted by solitons (i.e. dispersive waves) has been studied [218]. The minimum TOD required for spectral peak appearance of dispersive wave in the output spectrum depends on the soliton order. The stable solitons have been found even in the presence of higher perturbation effect of TOD [219]. But the presence of TOD results in structural changes of the similariton pulse in presence of linear gain [220]. It can drastically also change the phase-sensitive parametric gain in continuous-pumped fiber systems [221]. The investigation of erupting solitons by using CGLE under the higher order effects has been performed. The higher order effects are successfully used to control explosions on both leading and trailing edges of the solitons [222].

The other higher nonlinear effect that can be avoided while investigating inside the fiber of ultrashort pulses. This inter pulse Raman scattering (IRS) results in the self-frequency shift of soliton. The amplification of low frequency components by high frequency components of the pulse itself takes place due to which the shifting of pulse spectrum towards lower, i.e., red frequency side occurs. This shift in frequency enhances with distance and increases significantly for short pulses. It was observed that spectral shifting takes place both in anomalous and normal dispersion regimes and depends on both pulse width and frequency chirp related to the pulse [223]. By adjusting the chirping parameters the propagation of ultrashort pulses in presence of higher order effects described by CGLE can be controlled [224]. The solitonic pulses are

found to be stable under the perturbation [225]. Also in presence of IRS, propagation of stable soliton can be achieved by employing the spectral filtering and nonlinear gain in the system [226]. The pulse propagation in optical fibers in presence of higher order nonlinear terms, linear and nonlinear gain-loss or the pulse evolution in mode-locked fiber lasers is described by using CGLE [1].

In this chapter we have numerically studied the dissipative soliton generation and its stability in fiber laser cavity in the presence of cubic-quintic nonlinearity, third order dispersion, multiphoton absorption and gain dispersion. Such complex systems can be described by using CGLE. The CGLE for our system is given as:

$$\begin{aligned} i\frac{\partial E}{\partial z} + \frac{1}{2}\frac{\partial^2 E}{\partial t^2} - i\frac{\beta}{6}\frac{\partial^3 E}{\partial t^3} + \mid E \mid^2 E + \gamma \mid E \mid^4 E &= \frac{i}{2}(g_o - \alpha)E + \frac{id}{2}\frac{\partial^2 E}{\partial t^2} - iK \mid E \mid^2 E \\ &- i\nu \mid E \mid^4 E + T_R E\frac{\partial \mid E \mid^2}{\partial t^2} \end{aligned} \tag{6.1}$$

where, E is the normalized field inside the cavity, z is the normalized length of propagation, and t is retarded time. The first term in the left hand side of Eqn. (6.1) represents the evolution of the pulse envelope. The second term is the GVD term. The third term on the left is TOD term and β is the corresponding TOD coefficient. The fourth and fifth terms arise due to cubic and quintic nonlinearities respectively. The CQGLE has been normalized in a manner so that coefficient of cubic nonlinearity becomes unity. γ is quintic nonlinearity coefficient normalized with respect to the cubic one. The first term in the right hand side is the gain saturation term, which is meaningful for a pulse of energy comparable to the saturation energy of the amplifier. The second term is the second order gain dispersion term that comes into play when the pulse spectral width and the gain bandwidth are comparable. g_0 and d symbolize the coefficients of gain saturation and gain dispersion respectively. α stands for the dimensionless wave guide loss coefficient, which is inherent. The excess gain is given as $\Delta g = (g_0 - \alpha)$. The third and fourth terms are due to the TPA and 3PA respectively. K denotes the

TPA coefficient, while represents that for 3PA. Since we choose a self-focusing cubic and defocusing quintic nonlinearity, the sign of the cubic nonlinear term in left hand side of Eqn. (6.1) is positive while γ is negative. Sign of both K and ν is positive as they correspond to TPA and 3PA induced losses. The last term corresponds to IRS and T_R is corresponding IRS coefficient.

In order to generate bright soliton in the dissipative nonlinear system, we choose the sech trial wave function for following standard form:

$$E(z,t) = A(z)sech\left(\frac{t}{W(z)}\right)\exp\left(i\phi(z)\right), \tag{6.2}$$

The numerical analysis of the CQGLE is done by using split-step Fourier method (SSFM).

In operator form the governing CQGLE reads as:

$$\frac{\partial E}{\partial z} = \hat{D}E + \hat{N}E, \tag{6.3}$$

where,

$$\hat{D} = \left(\frac{i}{2}\frac{\partial^2}{\partial t^2} + \frac{\beta}{6}\frac{\partial^3}{\partial t^3} + \frac{1}{2}(g_o - \alpha) + \frac{d}{2}\frac{\partial^2}{\partial t^2}\right)E \tag{6.4}$$

and

$$\hat{N} = i\left(\mid E\mid^2 + \gamma \mid E\mid^4 + iK \mid E\mid^2 + i\nu \mid E\mid^4 - T_R\frac{\partial \mid E\mid^2}{\partial t^2}\right)E. \tag{6.5}$$

The dispersion and nonlinear part has been solved following the similar SSFM step adopted in previous chapters. However the IRS part is tricky to solve. The IRS part can be solved by a few ways. We here, consider a method that replace $\frac{\partial|E|^2}{\partial t}$ by ${F_T}^{-1}(-i\omega F_T \mid E\mid^2)$. Here, ω is the frequency in the Fourier domain, F_T and ${F_T}^{-1}$ denotes the Fourier-transform operation and Inverse Fourier-transform operation respectively.

6.2 Effects of TOD

We first investigate the effect of TOD on DS generation keeping IRS =0, in three different conditions of multiphoton absorption (1) TPA (2) 3PA (3) TPA+3PA. In all these cases, however, cubic-quintic nonlinearity and gain dispersion are prsenst.

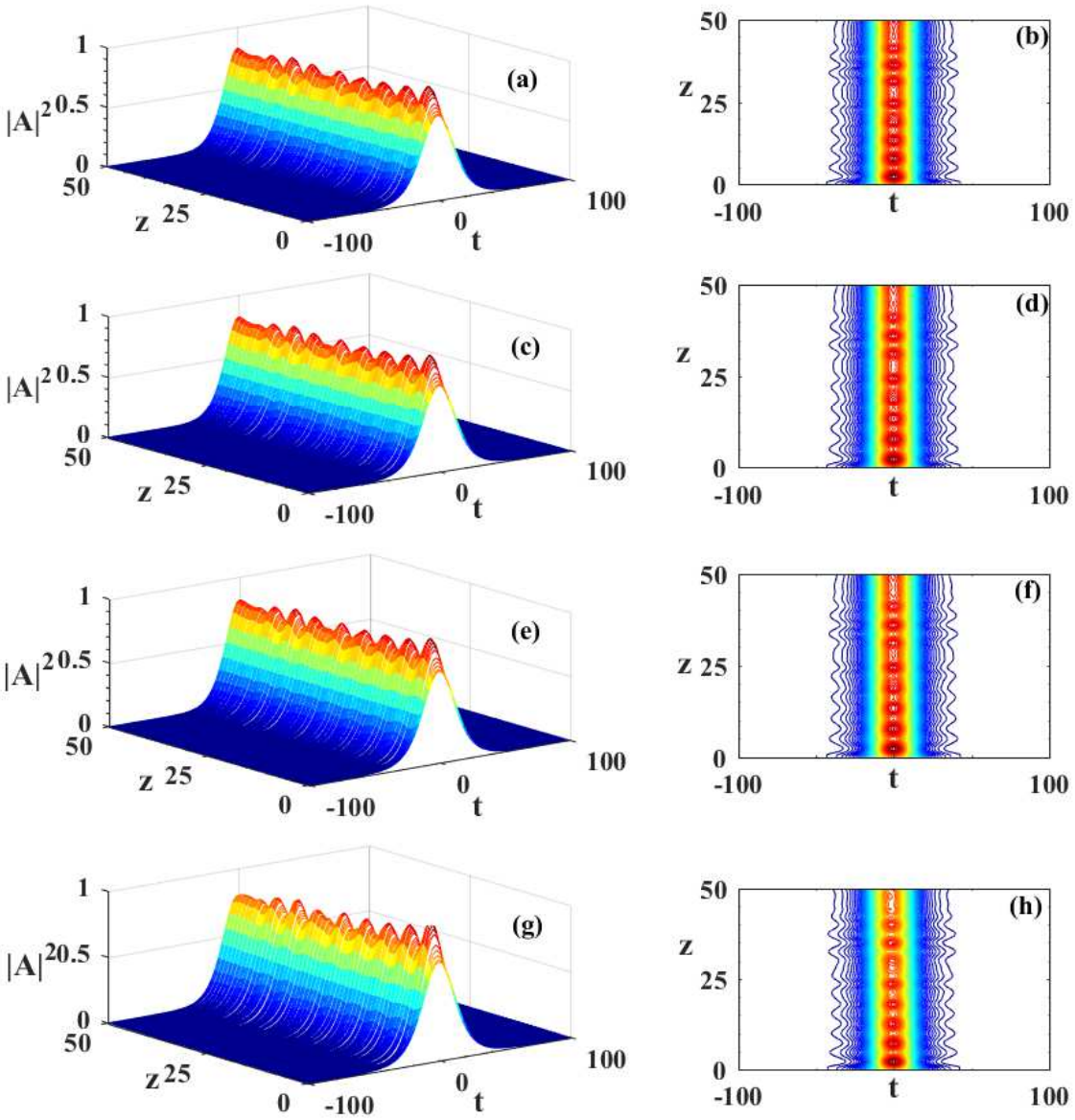

Fig. 6.1: Generation of DS under the effect of TOD, TPA and gain dispersion. The corresponding contour plot are also provided. For (a and b) third order dispersion coeffficient, $\beta = 0.001$, for (c and d) $\beta = 0.005$, for (e and f) $\beta = 0.01$ and for (g and h) $\beta = 0.05$. Other parameters used are $\gamma = -0.01$, $d = 0.05$ and $K = 0.01$. Here $\nu = 0$. Here excess gain, Δg value needed for generation of stable DS is ranging from 5.306×10^{-6} to 5.381×10^{-6}.

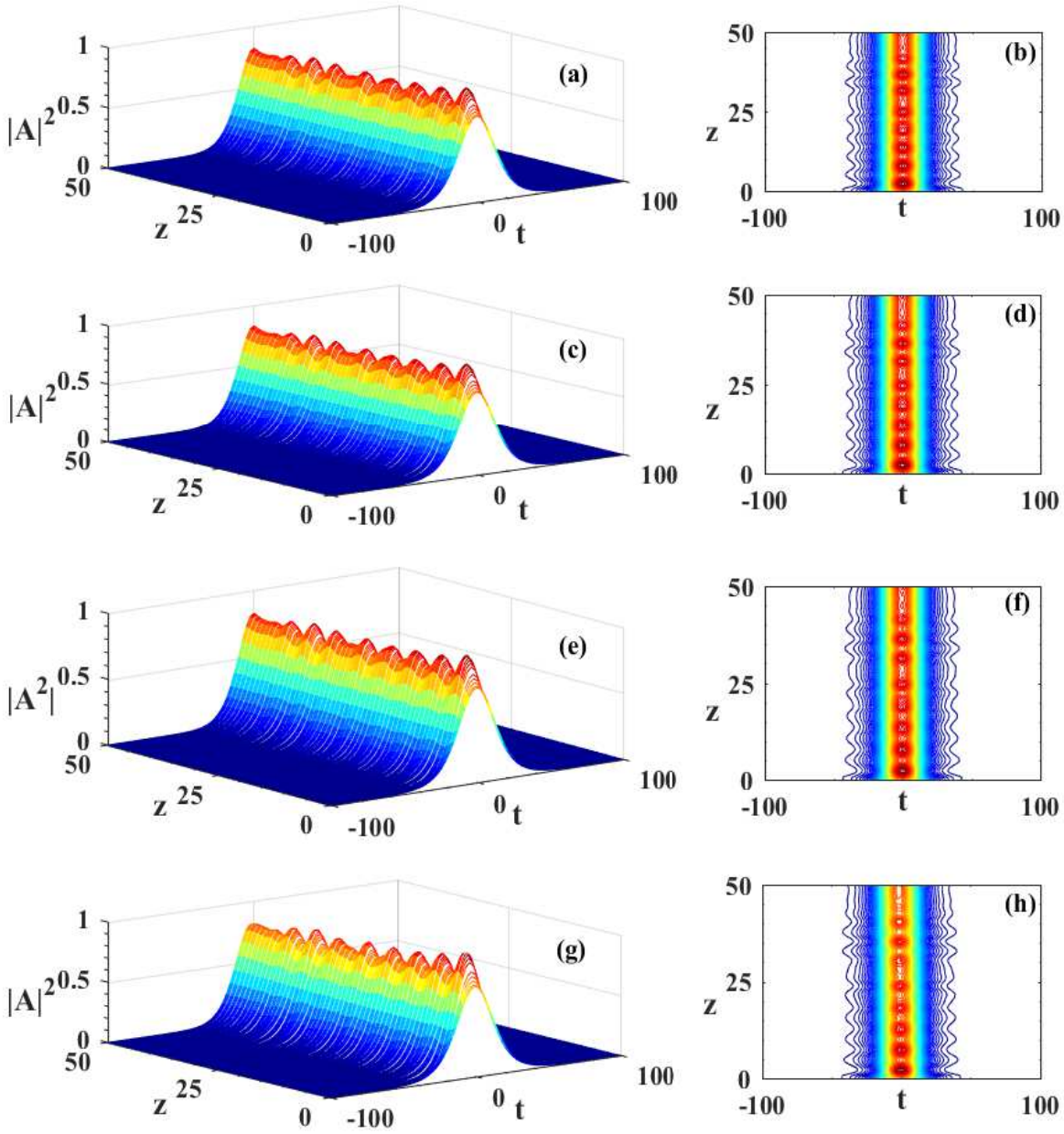

Fig. 6.2: Generation of robust DS under the effect of TOD, 3PA and gain dispersion. The corresponding contour plot are also provided. For (a and b) third order dispersion coeffficient, $\beta = 0.001$, for (c and d) $\beta = 0.005$, for (e and f) $\beta = 0.01$ and for (g and h) $\beta = 0.05$. Other parameters used are $\gamma = -0.01$, $d = 0.05$ and $\nu = 0.01$. Here $K = 0$. Here excess gain, Δg value needed for generation of stable DS is ranging from 5.209×10^{-6} to 5.292×10^{-6}.

Fig. 6.1 portrays DSs for a range of TOD (0.001 to 0.05). All the DSs are stable in nature. Different gains was applied to stabilize these DSs in such highly nonlinear-

dispersive media. Similar stable DSs are obtained for 3PA (Fig. 6.2).

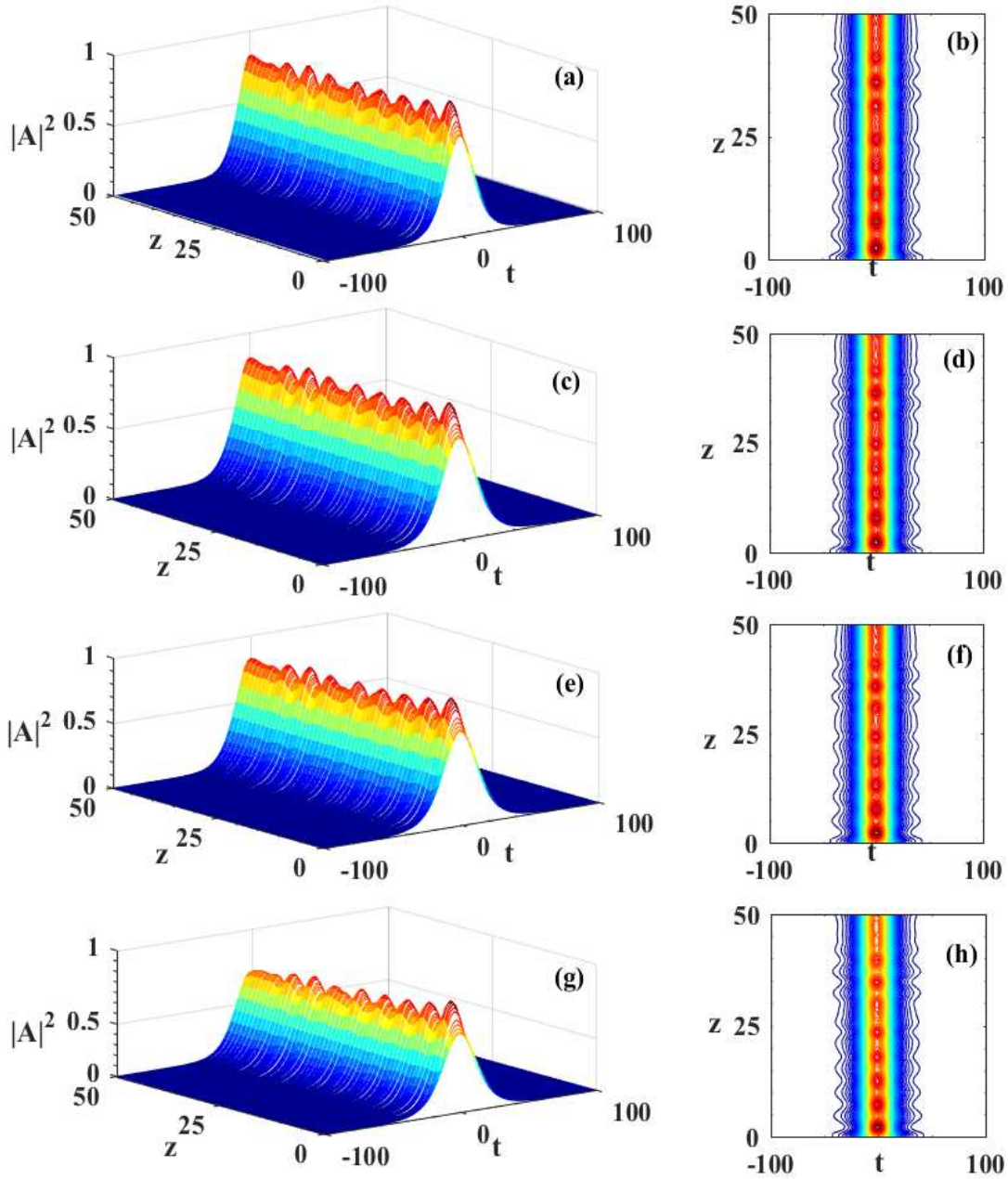

Fig. 6.3: Evolution of robust DS under the effect of TOD, TPA, 3PA and gain dispersion. The corresponding contour plot are also provided. For (a and b) third order dispersion coeffficient, $\beta = 0.001$, for (c and d) $\beta = 0.005$, for (e and f) $\beta = 0.01$ and for (g and h) $\beta = 0.05$. Other parameters used are $\gamma = -0.01$, $d = 0.05$ and $K = 0.01$ and $\nu = 0.01$. Here excess gain, Δg value needed for generation of stable DS is ranging from 5.402×10^{-6} to 5.475×10^{-6}.

While both the multiphoton absorptions are present, one can achieve DSs like those

portrayed in Fig. 6.3. The 3D as well as contour plots of all these Figs. 6.1 to 6.3 assures the stable evolution of DSs in fiber laser cavity. In all these cases, more gain is required

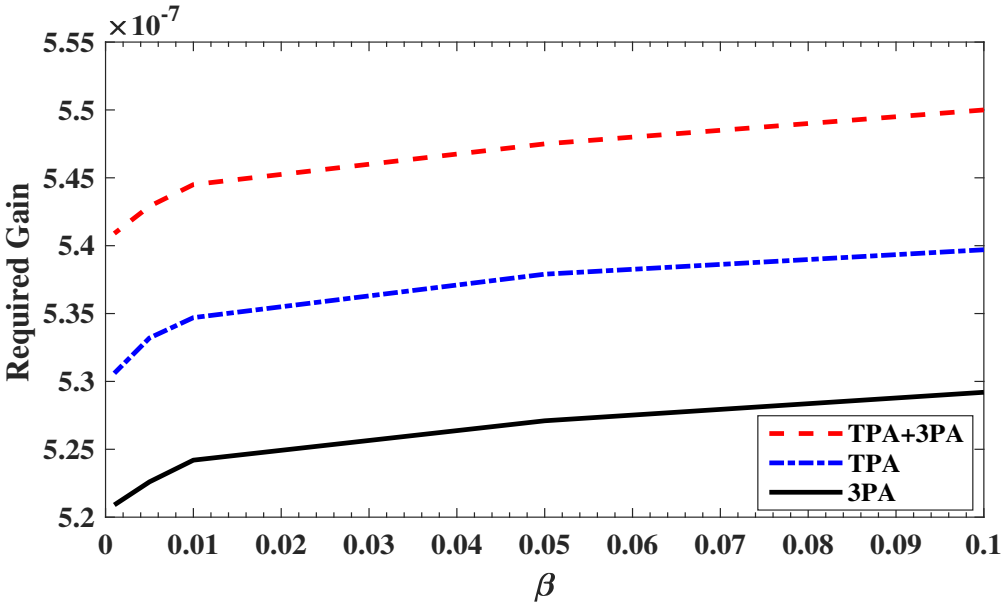

Fig. 6.4: Variation of net gain Δg required to generate DS for different value TOD coefficient β under effects of TPA and 3PA. Here $K = 0.01$, $\nu = 0.01$, $d = 0.05$, $\gamma = -0.01$.

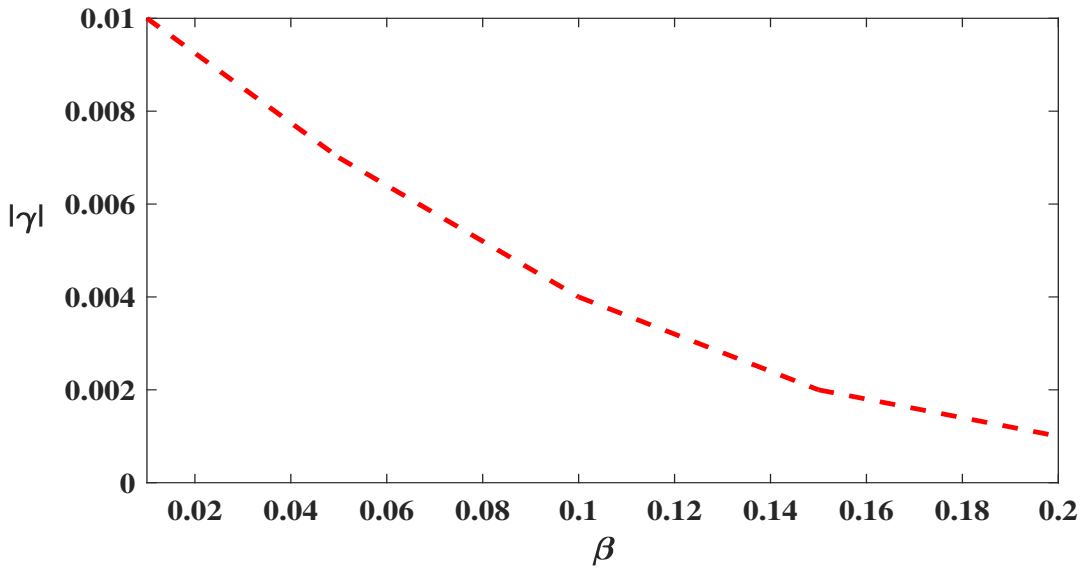

Fig. 6.5: Variation of quintic nonlinearity γ required to generate DS for for different value TOD coefficient β under effects of both TPA and 3PA. Here $K = 0.01$, $\nu = 0.01$, $d = 0.05$.

to stabilize the DSs at higher value of TOD (Fig. 6.4). At a fixed TOD a comparison shows that minimum gain is required for 3PA case, intermediate gain is required for TPA case and obviously presence of both TPA and 3PA demands maximum gain for stabilization.

We also tried to stabilize the DS under TOD effect by controling the quintic nonlinearity. In this case too, stable DSs are achieved (not shown to avoid monotonicity). Figure 6.5 shows how increase in TOD coefficient decreases the required strength of quintic nonlinearity for stabilizing the DSs under the effect of both TPA and 3PA.

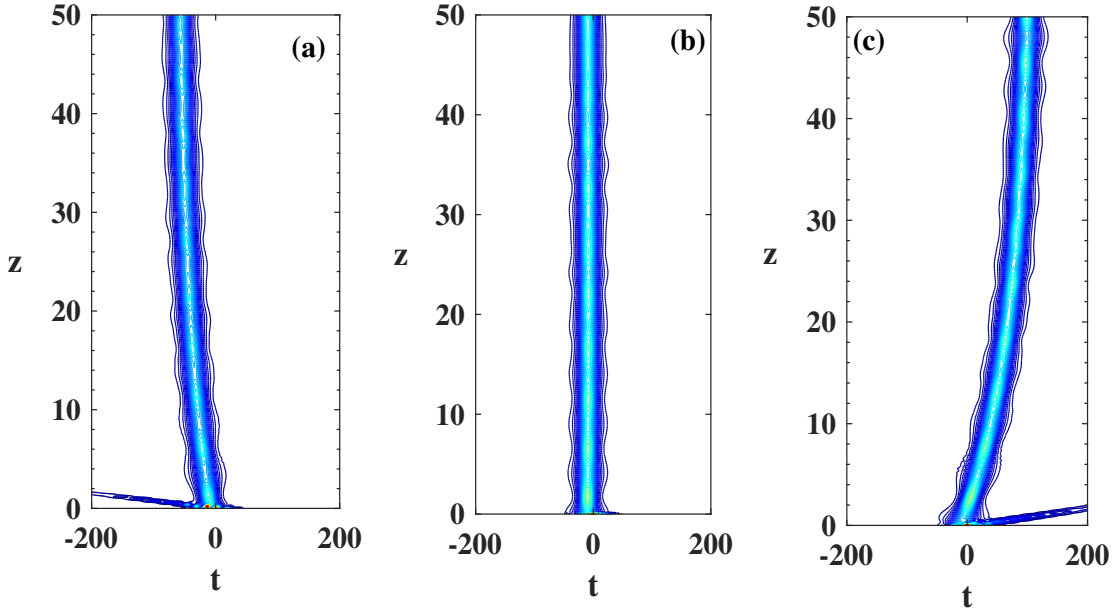

Fig. 6.6: Switching by DSs when they interact with each other with different phase separation between for fixed initial temporal separation $T_g = 10$. Initial phase difference between the two solitons is (a) $\frac{\pi}{12}$ (b)$\frac{\pi}{3}$ (c) $\frac{3\pi}{5}$. Other parameters are $K = 0.01$, $\nu = 0.01$, $d = 0.05$, $\beta = 0.1$ and $\gamma = -0.01$.

Interaction dynamics of DSs generated in the nonlinear dispersive fiber continue to show intriguing interaction dynamics in spite of the presence of TOD effect. We achieved phase controlled switching by the interaction of two DSs having a fixed initial temporal separation (Fig. 6.6). Furthermore, switching can be demonstrated by controlling the initial temporal separation between the two interacting pulses (Fig. 6.7).

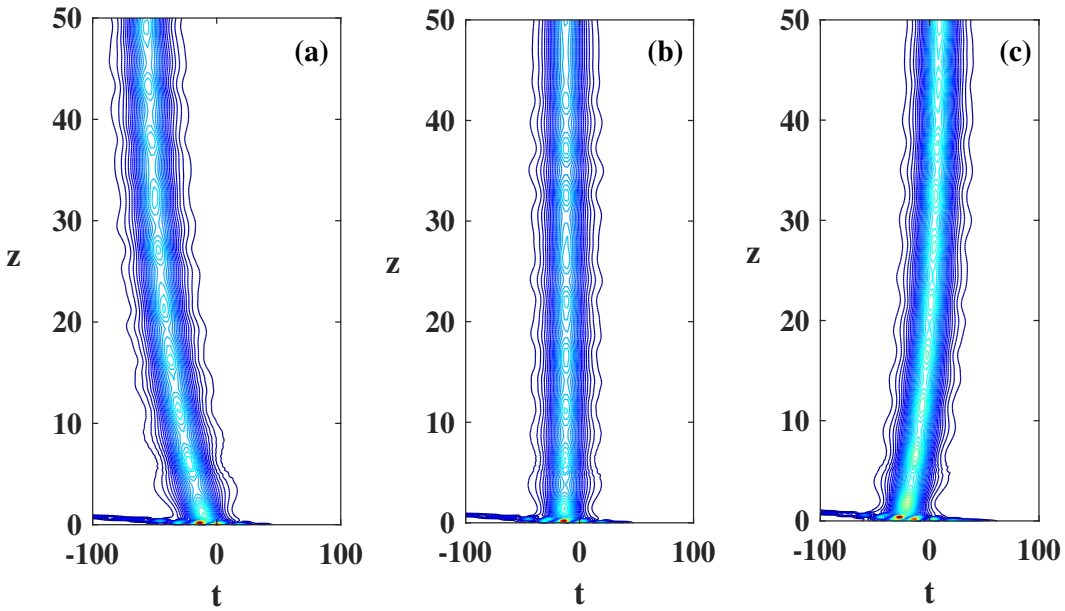

Fig. 6.7: Intensity profiles of two DSs when they interact with each other for different temporal separation (T_g) between them: (a) $T_g = 10$, (b)$T_g = 17$ (c) $T_g = 25$. Initial fixed phase difference between the two solitons is $\frac{\pi}{10}$. Other parameters are $K = 0.01$, $\nu = 0.01$, $d = 0.05$, $\beta = 0.1$ and $\gamma = 0.01$.

6.3 Effect of Intrapulse Raman Scattering (IRS)

The effect of IRS is an important issue for practical operations of fiber laser and fiber based devices. Here we mainly concentrate whether soliton can be achieved under the IRS effect. We found DSs in both the absence and presence of TOD as portrayed in Figs. 6.8 and 6.9 respectively. The characrstic shift in temporal domain of the soliton are very prominent. However, presence of TOD requires more gain for stabilization of the DSs than that required in the absence of TOD. We also obtained stable DSs in absence of 3PA (Fig. 6.10) as well as in absence of TPA (Fig. 6.11).

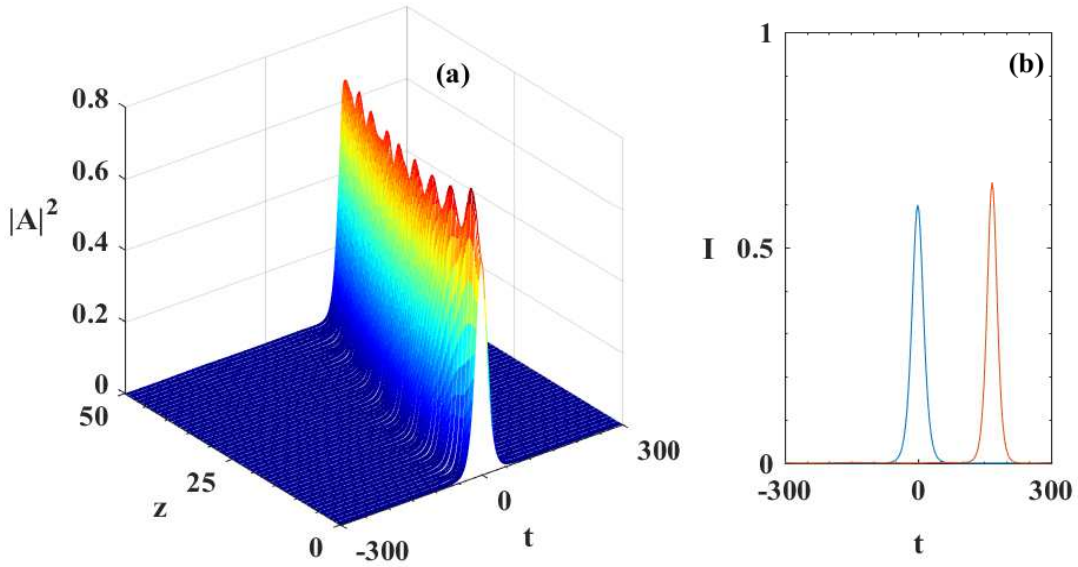

Fig. 6.8: (a) Generation of DS under the effect of TOD, IRS, TPA, 3PA and gain dispersion. (b) The corresponding initial (blue color) and final (blue color) pulse plots are given. Here parameters used are $\gamma = -0.01$, $d = 0.05$, $K = 0.01$, $\nu = 0.01$, $\beta = 0.01$ and $T_R = 0.1$. Here excess gain $\Delta g = 5.860 \times 10^{-6}$.

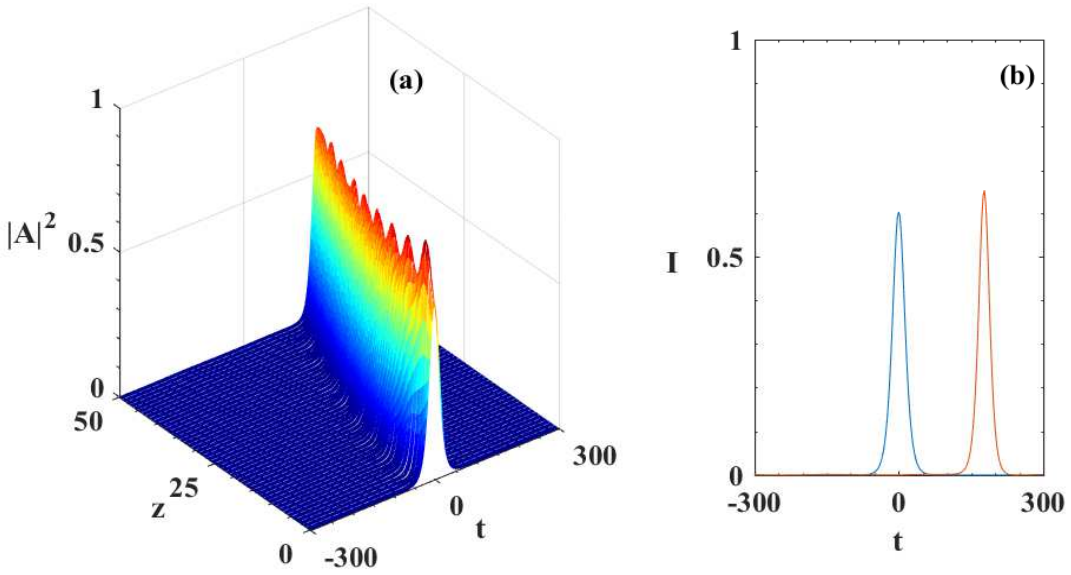

Fig. 6.9: (a) Generation of DS under the effect of IRS, TPA, 3PA and gain dispersion. (b) The corresponding initial (blue color) and final (blue color) pulse plots are given. Here parameters used are $\gamma = -0.01$, $d = 0.05$, $K = 0.01$, $\nu = 0.01$, $T_R = 0.1$ and $\beta = 0$. Here excess gain $\Delta g = 5.751 \times 10^{-6}$.

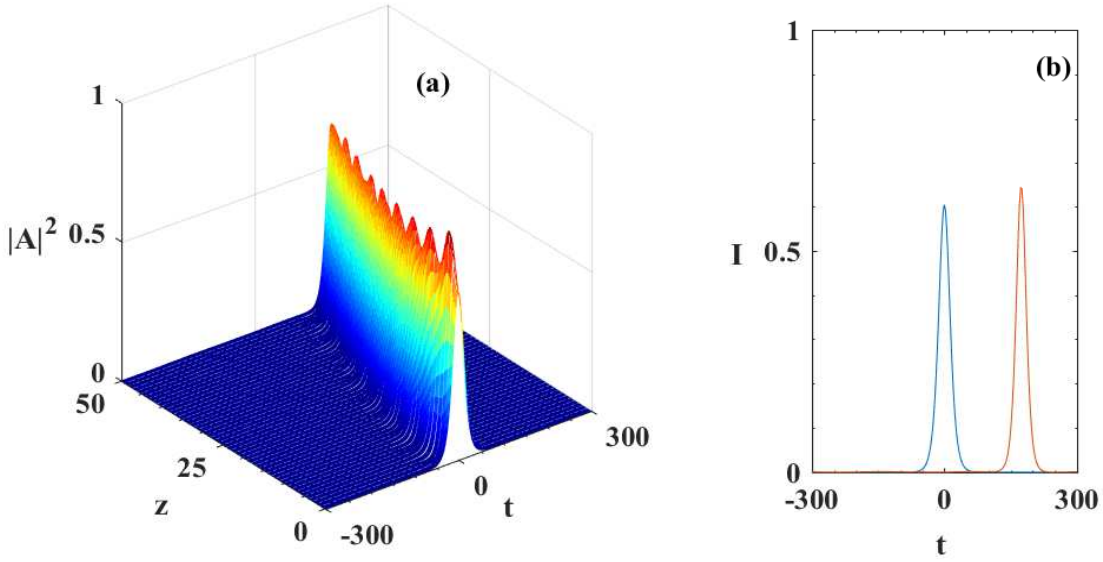

Fig. 6.10: (a)Generation of DS under the effect of TOD, IRS, TPA and gain dispersion. (b) The corresponding initial (blue color) and final (blue color) pulse plots are given. Here parameters used are $\gamma = -0.01$, $d = 0.05$, $K = 0.01$, $\beta = 0.01$, $T_R = 0.1$ and $\nu = 0$. Here excess gain $\Delta g = 5.692 \times 10^{-6}$.

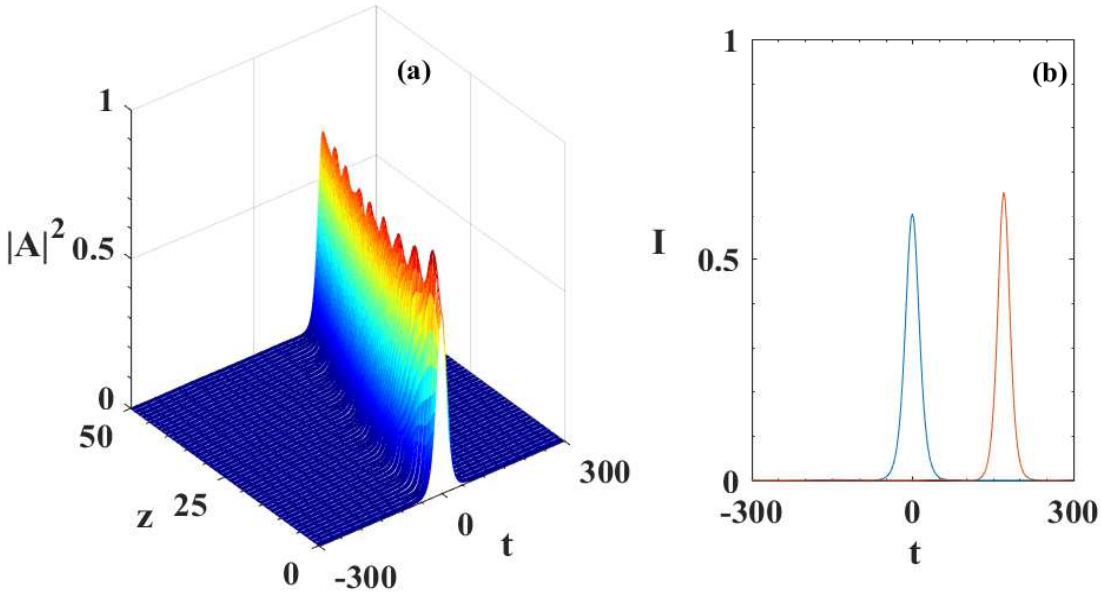

Fig. 6.11: (a)Generation of DS under the effect of TOD, IRS, 3PA and gain dispersion. (b) The corresponding initial (blue color) and final (blue color) pulse plots are given. Here parameters used are $\gamma = -0.01$, $d = 0.05$, $K = 0.01$, $\nu = 0.01$, $\beta = 0.01$, $T_R = 0.1$ and $K = 0$. Here excess gain $\Delta g = 5.440 \times 10^{-6}$.

6.4 Conclusion

DSs are formed in dissipative optical fiber laser cavity with higher order nonlinear and dispersive effects. The impact of TOD and IRS on the DSs is highlighted. Intriguing soliton switching phenomena by tuning initial temporal separation and phase are shown. The results may be utilized for experimental observations of DSs in fiber laser under TOS and IRS effects.

Chapter 7

Conclusions

7.1 Conclusion of the Thesis

This thesis presents theoretical studies on the generation and dynamics of optical dissipative solitons in semiconductor doped fiber laser cavity in presence of higher order dispersive and nonlinear effects. Stability of the optical dissipative solitons (DSs) is shown for a range of values of the system parameters. Variational method in conjugation with Rayleighs dissipative function is employed for analytical study. Numerically the system is solved by using split-step Fourier method (SSFM). Also, results of both the methods are compared. Particularly, interaction dynamics are investigated numerically.

The collective effects of various multiphoton absorption processes and gain dispersion on the pulse as well as dissipative soliton in cubic-quintic nonlinear optical fiber are studied. DSs are obtained by introducing different gains in highly nonlinear fiber with two-photon absorption (TPA), three-photon absorption (3PA) and combined case of TPA and 3PA. The DSs thus obtained are bistable in nature. The results obtained by both analytical and numerical methods come out to be in close agreement with each other. 3PA is found to have less detrimental effect on pulse as well as DS dynamics in comparison to TPA. Thus, shifting from TPA to 3PA wavelength is more beneficial. A material with negative valued imaginary susceptibility (χ^5) may lead to three-photon

emission (3PE), which is found to be effective for arresting pulse degradation. Effect of initial chirp on the dissipative soliton has also been studied.

A realistic model of doped fiber laser cavity experiences randomly varying GVD. Generation and stability of DS are investigated in a lossy fiber with such random dispersion as well as cubic-quintic nonlinearity, multiphoton absorption or emission and gain dispersion. In spite of the presence of the gain, the zero background around the soliton remains stable. DSs are obtained in an approximate form by means of the variational approximation and SSFM based direct simulations, with a conclusion that the quasi-analytical results produced by the variational approximation are in reasonable agreement with the numerical findings. An essential result is that the nonlinear amplification due to the quintic gain 3PE provides an efficient alternative gain mechanism for the stable DSs. Another notable outcome is the stability of DSs under the action of the perturbation due to random GVD and noise. The DSs are bistable, with two different soliton solutions of low- and high-amplitudes but of same width. The low-amplitude DS is stable in the presence of nonlinear gain, while its high-amplitude counterpart shows blow-up instability. The blow-up is removed by controlling loss of the system. Interactions between the DSs lead to periodic merger-splitting sequences for low-amplitude ones and fusion of high-amplitude solitons into breathers. Intriguing interaction dynamics leads to relative phase controlled switching of DSs.

The generation of stable DSs and their interaction dynamics are studied by including dispersion-management technique in doped fiber laser cavity. The fiber also contains cubic-quintic nonlinearity, gain dispersion and multiphoton absorption. Importantly, the dispersion map is perturbed with random dispersion. The dispersion-managed dissipative solitons (DMDS) exhibit breather like characteristics and are robust against certain level of noise. The interaction between two DMDSs having same phase may lead to either a bound state or multiple branches for a temporal separation below a threshold value. For non-zero phase difference the temporal separation

between the interacting DMDSs controls the speed of the bound state soliton. This eventually leads to temporal separation controlled all-optical switching. Phase controlled all-optical switching is also obtained. Switching observed by tuning temporal separation is found to be more prominent than phase-controlled switching.

Other than multiphoton absorption, gain dispersion, and random dispersion, the performance of nonlinear dissipative fiber laser in the ultra-short pulse regime is limited by higher order dispersive and nonlinear effects like third order dispersion (TOD) and intra pulse Raman scattering (IRS). DSs are formed in such optical fiber laser cavity in presence of TOD and IRS along with the other aforesaid dispersive and nonlinear effects. The impact of TOD and IRS on the DSs is highlighted. Initial temporal separation and phase controlled soliton switching phenomena are found.

7.2 Applications

The results presented in this thesis may be utilized for experimental realization of dissipative soliton fiber laser under different highly dispersive and nonlinear environments. The outcomes have potential applications in experimenting dispersion-managed dissipative soliton fiber laser too. Besides improving the performance of DS fiber lasers and DMDS fiber lasers, the findings may be helpful in all-optical switching devices, all-optical data processing, all-optical delay lines and optical communication links.

The proposed alternate gain mechanism by means of three photon emission may be explored experimentally in soliton fiber laser. It also seems promising for fiber amplifiers.

Since, the 3PA wavelength has greater penetration capability into biological cells with less damaging effect to the tissues; the corresponding results may be extended to biological and medical science applications, e.g., bio-imaging and light-activated therapy.

7.3 Future Scope

Doped fiber can be used for biomedical applications. If the cladding is removed and a graphene layer is applied on the core which enables the doped fiber to act like a bio medical sensor. The present work can be further extended to this direction. In fact, already the theoretical background is given in chapters 3-5. Graphene behaves like a nonlinear saturable absorber. In all these chapter of our thesis we consider cubic-quintic nonlinearity which is approximation of saturable nonlinearity. Therefore, one can extend the mathematical model, solution technique of the current thesis for graphene embedded doped fiber laser used for bio-medical sensing and beyond.

In the thesis, the effect of TPA has been discussed in details in the light of soliton. However, TPA is widely used in medical imaging. Therefore the result of the current work can be extended to this direction too. Similarly, the role of 3PA can be explored for biomedical imaging.

In this thesis, 3PE is proposed as an alternate gain mechanism. Experimentalist may reap benefit using this concept which may lead to some new intriguing findings. Material that enhances 3PE can be explore and synthesized for optical fiber fabrication. 3PE based fiber amplifiers and soliton lasers can be investigated.

BIBLIOGRAPHY

[1] N. Akhmediev and A. Ankiewicz, *Dissipative Solitons*, (Springer, Berlin Heidelberg, 2005).

[2] N. Akhmediev and A. Ankiewicz, *Dissipative Solitons: From Optics to Biology and Medicine*, (Springer, Berlin Heidelberg, 2008).

[3] W. H. Renninger, A. Chong and F. W. Wise, Phys. Rev. A **77**, 023814 (2008).

[4] E. A. Ultanir and G. I. Stegeman, Phys. Rev. Lett. **90**, 253903 (2003).

[5] J. Ross, S. C. Müller and C. Vidal, Science **240**, 460 (1998).

[6] G. P. Agrawal, *Nonlinear Fiber Optics*, (Academic press, San Diego, 2007).

[7] N. Bloembergen, *Nonlinear optics*, (World Scientific Press, Singapore, 1996).

[8] A. Biswas and S. Konar, *Introduction to Non-Kerr Law Optical Solitons* (Taylor & Francis, Boca Raton, 2006).

[9] R. W. Boyd, *Nonlinear Optics*, (Academic Press, San Diego, 2003).

[10] F. Abdullaev, S. Darmanyan and P. Khabibullaev, *Optical solitons*, (Springer, Verlag Berlin Heidelberg, 1993).

[11] F. Abdullaev, *Theory of solitons in inhomogeneous media*, (Wiley, Chichester, 1994).

[12] Y. S. Kivshar and G. P. Agarwal, *Optical Solitons: From Fibers to photonic Crystals*, (Academic Press, San Diego, 2003).

[13] S. Medhekar, R. K. Sarkar and P. P. Paltani, Opt. Appl. **37**, 243 (2007).

[14] R. K. Sarkar and S. Medhekar, Phys. Scr. **76**, 683 (2007).

[15] I. Gabitov and S. K. Turitsyn, Opt. Lett. **21**, 327 (1996).

[16] P. Manneville, *Dissipative Structures and Weak Turbulence*, (Academic press, Boston, 1990).

[17] J. D. Murry, *Mathematical Biology: Spatial models and biomedical applications*, (Springer, Berlin, 2003).

[18] R. Richter and I. V. Barashenkov, Phys. Rev. Lett. **94**, 184503 (2005).

[19] I. Müller, E. Ammelt and H.G. Purwins, Phys. Rev. Lett. **82**, 3428 (1999)

[20] H. Zhang, D. Tang, R. J. Knize and L. Zhao, Appl. Phys. Lett. **96**, 111112 (2010).

[21] Y. S. Kivshar and B. A. Malomed, Rev. Mod. Phys. **61**, 763 (1989).

[22] D. Mihalache, D. Mazilu, F. Lederer, Y. V. Kartashov, L. C. Crasovan, L. Torner and B. A. Malomed, Phys. Rev. Lett. **97**, 073904 (2006).

[23] N. N. Akhmediev and A. A. Ankiewicz, *Solitons: Nonlinear Pulses and Beams*, (Chapman and Hall, London, 1997).

[24] L. A. Lugiato and R. Lefever, Phys. Rev. Lett. **58**, 2209 (1987).

[25] G. S. Parmar and S. Jana, J. Electromagn. Waves Appl. **29**, 1410 (2015).

[26] S. Raghavan and G. P. Agrawal, Opt. Commun. **180**, 377 (2000).

[27] I. Aranson and L. Kramer, Rev. Mod. Phys. **74**, 99 (2002).

[28] W. van Saarlos and P. C. Hohenberg, Phys. Rev. Lett. **64**, 749 (1990).

[29] N. N. Akhmediev, A. Ankiewicz and J. M. S. Crespo, Phys. Rev. Lett. **79**, 4047 (1997).

[30] O. Thual and S. Fauve, J. Phys. (France) **49**, 1829 (1988).

[31] S. Fauve and O. Thual, Phys. Rev. Lett. **64**, 282 (1990).

[32] N. N. Akhmediev, V. V. Afanasjev and J. M. Soto-Crespo, Phys. Rev. E **53**, 1190 (1996).

[33] J. M. S. Crespo, N. Akhmediev and A. Ankiewicz, Phys. Rev. Lett. **85**, 2937 (2000).

[34] D. Artigas, L. Torner, and N. N. Akhmediev, Opt. Commun. **143**, 322 (1997).

[35] E. N. Tsoy and N. Akhmediev, Phys. Lett. A **343**, 417 (2005).

[36] A. I. Maimistov, J. Exp. Theor. Phys. **77**, 727(1993).

[37] L. C. Crasovan, B. A. Malomed and D. Mihalache, Phys. Lett. A **289**, 59 (2001)

[38] N. Akhmediev, J. M. S. Crespo and G. Town, Phys. Rev. E **63**, 056602 (2001).

[39] N. Akhmediev, J. M. S. Crespo and G. Town, Phys. Rev. E **63**, 056602 (2001)

[40] N. Akhmediev, J. M. S. Crespo, M. Grapinet and P. Grelu, Opt. Fiber Tech. **11**, 209 (2005).

[41] A. Schwache and F. Mitschke, Phys. Rev. E **55**, 7720 (1997).

[42] A. Ankiewicz, N. Akhmediev and N. Devine, Opt. Fiber Tech. **13**, 91 (2007).

[43] V. Skarka and N. B. Aleksic, Phys. Rev. Lett. **96**, 013903 (2006).

[44] N. B. Aleksić, V. Skarka, D. V. Timotijevic and D. Gauthier, Phys. Rev. A **75**, 061802 (2007).

[45] N. Akhmediev, A. Ankiewicz, J. S. Crespo and P. Grelu, Int. J. Bifurc. Chaos **19**, 2621 (2009).

[46] W. Chang, A. Ankiewicz, J. M. S. Crespo and N. Akhmediev, Phys. Rev. A **78**, 023830 (2008).

[47] L. Duan, X. Liu, D. Mao, L. Wang, and G. Wang, Opt. Express **20**, 265 (2012).

[48] P. Grelu and N. Akhmediev, Nat. Photonics **6**, 84 (2012).

[49] N. Akhmediev, A. Ankiewicz, and J. M. Soto-Crespo, J. Opt. Soc. Am. B **15**, 515 (1998).

[50] X. Liu, Phys. Rev. A **84**, 023835 (2011).

[51] L. Yun, X. Liu and D. Mao, Opt. Express **20**, 20992 (2012).

[52] Z. Luo, Q. Ning, H. Mo, H. Cui, J. Liu, L. Wu, A. Luo and W. Xu, Opt. Express **21**, 10199 (2013).

[53] H. Leblond, A. Niang, F. Amrani, M. Salhi and F. Sanchez, Phys. Rev. A **88**, 033809 (2013).

[54] N. A. Kolyada, B. N. Nyushkov, A. V. Ivanenko, S. M. Kobtsev, P. Harper, S. K. Turitsyn, V. I. Denisov and V. S. Pivtsov, Quantum Electron. **43**, 95 (2013).

[55] L. Zhang, Z. Pan, Z. Zhuo and Y. Wang, Internat. J. of Opt. **2014**, 169379 (2014).

[56] J. M. S. Crespo and N. Akhmediev, Phys. Rev. Lett. **66**, 066610 (2002).

[57] T. Miyaji, I. Ohnishi and Y. Tsutsumi, Physica D **239**, 2066 (2010).

[58] L. M. Zhao, D. Y. Tang, T. H. Cheng and C. Lu, Opt. Lett. **31**, 2957 (2006).

[59] L. M. Zhao, D. Y. Tang, T. H. Cheng, H. Y. Tam and C. Lu, Appl. Opt. **46**, 4768 (2007).

[60] D. Y. Tang and L. M. Zhao, Opt. Lett. **32**, 41 (2007).

[61] A. Chong, W. H. Renninger, and F. W. Wise, Opt. Lett. **33**, 1717 (2008).

[62] R. Gumenyuk, I. Vartiainen, H. Tuovinen and O. G. Okhotnikov, Opt. Lett. **36**, 609 (2011)

[63] T. H. Maiman, Nature **187**, 493 (1960).

[64] P. A. Franken, A. E. Hill, C. W. Peters and G. Weinreich, Phys. Rev. Lett. **7**, 118 (1961).

[65] J. A. Armstrong, N. Bloemberg, J. Ducuing and P. S. Pershar, Phys. Rev. **127**, 1918 (1962).

[66] R. Kohl, A. Biswas, D. Milovic and E. Zerrad, Opt. Laser Technol.**40**, 647 (2008).

[67] A. Biswas and D. Milovic, Commun. Nonlinear Sci. Numer. Simul. **15**, 1473 (2010).

[68] S. Mukhopadhyay, S. Mondal, S. P. Singh, A. Date, K. Hussain and P. K. Datta, Opt. Express **21**, 454 (2013).

[69] S. Biswas, S. Mukhopadhyay, Optik **125**, 1954 (2014).

[70] N. Mitra, S. Mukhopadhyay, Optik **122**, 1508 (2011).

[71] M. G. Mayer, Annals of Physics **9**, 273 (1931).

[72] W. Kaiser and C. G. B. Garrett, Phys. Rev. Lett. **7**, 229 (1961).

[73] A. Biswas, M. Fessak, S. Johnson, S. Beatrice, D. Milovic, Z. Jovanoski, R. Kohl and F. Majid, Opt. Laser Technol. **44**, 263 (2012).

[74] A. Biswas, Opt. Commun. **216**, 427 (2003).

[75] S. Singh and L. T. Bradley, Phys. Rev. Lett. **12**, 612 (1964).

[76] G. Keiser, *Optical Fiber Communications*, (Tata McGraw Hill, New Delhi, 2009).

[77] A. E. Willner, S. M. R. M. Nezam, L. Yan, Z. Pan and M. C. Hauer, J. Lightwave Technol. **22**, 106 (2004).

[78] M. Tajiri and M. Tuda, J. Phys. Soc. Jpn. **54**, 19 (1985)

[79] E. A. Kuznetsov, A. M. Rubenchik and V. E. Zakharov, Phys. Rep. **142**, 103 (1986).

[80] H. U. Bödeker, M. C. Röttger, A. W. Liehr, T. D. Frank, R. Friedrich and H. G. Purwins, Phy. Rev. E **67**, 056220 (2003).

[81] A. Hasegawa and F. Tappert, Appl. Phys. Lett. **23**, 142 (1973).

[82] A. Hasegawa and F. Tappert, Appl. Phys. Lett. **23**, 171 (1973).

[83] I. Gabitov, E. G. Shapiro, S. K. Turitsyn, Opt. Commun. **134**, 317 (1997).

[84] T. Yu, E. A. Golovchenko, A. N. Pilipetskii, and C. R. Menyuk, Opt. Lett. **22**, 793 (1997).

[85] K. Kieu and F. W. Wise, IEEE Photon. Tech. Lett. **21**, 128 (2009).

[86] O. G. Okhotnikov, T. Jouhti, J. Konttinen, S. Karirinne and M. Pessa, Opt. Lett. **28**, 364 (2003).

[87] A. Chong, J. Buckley, W. Renninger and F. Wise, Opt. Exp. **14**, 10095 (2006).

[88] F. W. Wise, A. Chong and W. H. Renninger, Laser Photonics Rev. **2**, 58 (2008).

[89] S. K. Turitsyn, B. G. Bale, M. P. Fedoruk, Phys. Reports **521**, 135 (2012).

[90] S. Waiyapot and M. Matsumoto, Opt. Commun. **188**, 167 (2001).

[91] D. Anderson, Phys. Rev. A **2**, 3135 (1983).

[92] V. E. Zakharov and A. B. Sabat, Sov. Phys. JETP **34**, 62 (1972).

[93] S. N. Vlasov, V. A. Petrischev and V. I. Talanov, Sov. Radiophysics **14**, 1062 (1971).

[94] N. A. Lemos, Amer. J. Phys. **59**, 660 (1991).

[95] V. M. Nair, S. Sarkar, S. K. Khijwania, IEEE Photon. Technol. Lett. **20**, 1381 (2008).

[96] G. Das and S. N. Sarkar, Opt. Eng. **35**, 3413 (1996).

[97] S. Gangopadhyay and S. N. Sarkar, Fiber Integrated Opt. **20**, 191 (2001).

[98] O. V. Sinkin, R. Holzlöhner, J. Zweck and C. R. Menyuk, J. Lightwave Technol. **21**, 61 (2003).

[99] V. Mizrahi, K. W. DeLong and G. I. Stegeman, Opt. Lett. **14**, 1140 (1989).

[100] G. P. Agrawal, Phys. Rev. E. **48**, 2316 (1993).

[101] Y. Silberberg, Opt. Lett. **15**, 1005 (1990).

[102] J. S. Aitchison, M. K. Oliver, E. Kapon, E. Colas and P. W. E. Smith, Appl. Phys. Lett.**56**, 1305 (1990).

[103] S. Jana S and S. Konar, J. Nonlinear Optic. Phys. Mat.**13**, 25 (2004).

[104] S. Konar, S. Jana and M. Mishra, Opt. Commun.**255**, 114 (2005).

[105] W. J. Firth and P. V. Paulau, Eur. Phys. J. D. **59**, 13 (2010).

[106] K. S. Bindra, H. T. Bookey, A. K. Kar, B. S. Wherrett, X. Liu and A. Jha, Appl. Phys. Lett. **79**, 1939 (2001).

[107] R. E. Slusher, G. Lenz, J. Hodelin, J. Sanghera, L. B. Shaw and I. D. Aggarwal, J. Opt. Soc. Am. B. **21**, 1146 (2004).

[108] G. S. He, P. P. Markowicz, T. C. Lin and P. N. Prasad, Nature **415**, 767 (2002).

[109] P. Cronstrand, Y. Luo, P. Norman and H. Agren, Chem. Phys. Lett. **375**, 233 (2003).

[110] S. Roy and S. Bhadra, Physica D **232**, 103 (2007).

[111] Z. X. Qiong, Z. X. Xia, C. Ke and X. An-Ping, Chinese Phys. B. **23**, 064207 (2014).

[112] G. P. Agrawal, IEEE J. Quan. Elec. **27**, 1843 (1991).

[113] M. J. Ablowitz, D. J. Kaup, A. C. Newell and H. Segur, Phys. Rev. Lett. **31**, 125 (1973).

[114] M. J. Ablowitz, D. J. Kaup, A.C. Newell and H. Segur, Studies in Appl. Math. **53**, 249, (1974).

[115] C. Rogers and W. K. Schief, *Bäcklund and Buckland and Darboux Transformations* (Cambridge University Press, Cambridge, 2002).

[116] R. Hirota, J. Math. Phys. **14**, 805 (1973).

[117] R. Hirota, J. Math. Phys. **14**, 810 (1973).

[118] M. Lakshmanan and S. Rajaseekar, *Nonlinear Dynamics: Integrability, Chaos and Patterns* (Springer Science and Business Media, Heidelberg, 2003).

[119] S. Roy and S. K. Bhadra, J. Lightwave Technol. **26**, 2301 (2008).

[120] A. Hasegawa, Pramana **57**, 1097 (2001).

[121] X. Gai, D. Choi and B. L. Davies, Opt. Exp. **22**, 9948 (2014).

[122] P. Mehta, N. Healy, N. F. Baril, P. J. A. Sazio, J. V. Badding and A. C. Peacock, Opt. Exp. **18**, 16826 (2010).

[123] Y. Arashida, Y. Ogawa and F. Minami, Phys. Rev. B **85**, 235318 (2012).

[124] A. Hayat, P. Ginzburg and M. Orenstein, Nat. Phot. **2**, 238 (2008).

[125] S. Y. Set, H. Yaguchi, Y. Tanaka and M. Jablonski, J. Light. Tech. **22**, 51 (2004).

[126] Q. Bao, H. Zhang, Y. Wang, Z. Ni, Y. Yan, Ze X. Shen, K. P. Loh and D. Y. Tang, Adv. Funct. Mater. **19**, 3077 (2009).

[127] http://www.industrial-lasers.com/articles/print/volume-30/issue-1/features/fiber-lasers-continue-growth-streak-in-2014-laser-market-revenues-increase-despite-mixed-global-manufacturing-growth.html.

[128] N. N. Rosanov, *Spatial Hysteresis and Optical Patterns* (Springer, Heidelberg, 2002).

[129] D. Mihalache, Rom. Rep. Phys. **67**, 1383 (2015).

[130] S. V. Suchkov, A. A. Sukhorukov, J. Huang, S. V. Dmitriev, C. Lee and Y. S. Kivshar, Laser Photonics Rev. **10**, 177 (2016).

[131] V. V. Konotop, J. Yang, and D. A. Zezyulin, Rev. Mod. Phys. **88**, 035002 (2016).

[132] B. A. Malomed, [Invited], J. Opt. Soc. Am. B **31**, 2460 (2014).

[133] J. Yao, J. Yao, Y. Wang, S.C. Tjin, Y. Zhou, Y. L. Lam, J. Liu and C. Lu, Opt. Commun. **191**, 341 (2001).

[134] L. Duan, X. Liu, D. Mao, L. Wang and G. Wang, Opt Exp. **20**, 265 (2011).

[135] B. A. Malomed, G. D. Peng and P. L. Chu, Opt. Lett. **21**, 330 (1996).

[136] G. D. Peng, B. A. Malomed and P. L. Chu, J. Opt. Soc. Am. B **15**, 2462 (1998).

[137] J. Wu, D. Y. Tang, L. M. Zhao and C. C. Chan, Phys. Rev. E **74**, 046605 (2006).

[138] M. E. Fermann, M. J. Andrejco and Y. Silberberg, Opt. Lett. **18**, 894 (1993).

[139] F. O. Ilday, J. R. Buckley, W.G. Clark and F.W. Wise, Phys. Rev. Lett. **92**, 213902 (2004).

[140] K. Guesmi, G. Semaan, M. Salhi, Y. Meng, F. Bahloul, H. Leblond and F.Sanchez, Rom. J. Phys. **61**, 1330 (2016).

[141] L. Talaverano, S. Abad and M. Lopez-Amo, J. of Light. Tech. **19**, 553 (2001).

[142] Hamamatsu Photonics K.K. Laser group, Nat. Photonics, 14 - 15 (2006).

[143] N. Akhmediev, A. Ankiewicz and J. M. Soto-Crespo, J. Opt. Soc. Amer. B **15**, 515 (1998).

[144] P. Grelu, F. Belhache, F. Gutty and J. M. Soto-Crespo, Opt. Lett. **27**, 966 (2002).

[145] B. A. Malomed, Phys. Rev. A **44**, 6954 (1991).

[146] V. V. Afanasjev, P. L. Chu and B. A. Malomed, Phys. Rev. E. **56**, 6020 (1997).

[147] D. Y. Tang, W. S. Man, H. Y. Tam and P. D. Drummond, Phys. Rev. A. **64**, 033814 (2001).

[148] Y. Gong, P. Shum, T. Hiang, Chen, Q. Wen and D. Tang, Opt. Comm. **200**, 389 (2001).

[149] P. Grelu and N. Akhmediev, Opt. Exp. **12**, 3184 (2004).

[150] V. Besse, H. Leblond, D. Mihalache and B. A. Malomed, Opt. Commun. **332**, 279 (2014).

[151] L. M. Zhao, D. Y. Tang and J. Wu, Opt. Lett. **31**, 1788 (2006).

[152] B. G. Bale, J. N. Kutz, A. Chong, W. H. Renninger and F. W. Wise, J. Opt. Soc. Am. B **25**, 1763 (2008).

[153] M. Chertkov, I. Gabitov and J. Moeser, PNAS **98**, 14208 (2001).

[154] M. Chertkov, I. Gabitov, P. M. Lushnikov, J. Moeser, and Z. Toroczkai, J. Opt. Soc. Am. B **19**, 2538 (2002)

[155] F. K. Abdullaev, D. V. Navotny and B. B. Baizakov, Physica D **192**, 83 (2004).

[156] M. J. Ablowitz and J. T. Moeser, Opt. Lett. **29**, 821 (2004).

[157] F. Quochi, F. Cordella, A. Mura, G. Bongiovanni, F. Balzer and H. G. Rubahn, Appl. Phys. Lett. **88**, 041106 (2006).

[158] C. J. S. de Matos, L. de S. Menezes, A. M. Brito-Silva, M. A. M. Gamerz, A. S. L. Gomes and C. B. de Araújo, Phys. Rev. Lett. **99**, 153903 (2007).

[159] S. A. Babin, A. E. El-Taher, P. Harper, E. V. Podivilov and S. K. Turitsyn, Phys. Rev. A **84**, 021805 (2011).

[160] Z. Xian-Qiong, Z. Xiao-Xia, C. Ke and X. An-Ping, Chin. Phys. B **23**, 064207 (2014).

[161] N. Akhmediev, J. M. Soto-Crespo and P. Grelu, Phys. Lett. A **372**, 3124 (2008).

[162] M. L. Quiroga-Teixeiro, A. Berntson and H. Michinel, J. Opt. Soc. Am. B **16**, 1697 (1999).

[163] J. Atai and B. A. Malomed, Phys. Lett. A **284**, 247 (2001).

[164] M. Stern, J. P. Heritage and E. W. Chase, IEEE J. of Quant Elec. **28**, 2742 (1992).

[165] B. Zsigri, J. Laegsgaard and A. Bjarklev, J. Opt. A: Pure and Appl. Opt. **6**, 717 (2004).

[166] J. M. Fini, M.D. Mermelstein, M. F. Yan, R.T. Bise, A.D. Yablon, P.W. Wisk and M. J. Andrejco, Opt. Lett. **31**, 2550 (2006).

[167] D. Nodop, C. Jauregui, F. Jansen, J. Limpert and A. Tnnermann, Opt. Lett. **35**, 2982 (2010).

[168] M. F. Saleh, W. Chang, P. Hlzer, A. Nazarkin, J. C. Travers, N. Y. Joly, P. St. J. Russell and F. Biancalana, Phys. Rev. Lett. **107**, 203902 (2011).

[169] M. Azhar, G. K. L. Wong, W. Chang, N. Y. Joly, and P. St. J. Russell, Opt. Exp. **21**, 4405 (2013).

[170] B. A. Malomed, Prog. Opt. **43**, 71 (2002).

[171] Z. Luo, Y. Li, M. Zhong, Y. Huang, X. Wan, J. Peng and J. Weng, Photon. Res. **3**, A79 (2015).

[172] J. S. Sanghera, L. B. Shaw and I. D. Aggarwal, IEEE J. Selec. Topi. Quan. Elec. **15**, 114 (2009).

[173] Y. S. Kivshar, D. E. Pelinovsky, T. Cretegny and M. Peyrard, Phys. Rev. Lett. **80**, 5032 (1998).

[174] W. Sch´opf and L. Kramer, Phys. Rev. Lett. **66**, 2316 (1991).

[175] O. V. Borovkova, V. E. Lobanov, and B. A. Malomed, EPL **97**, 44003 (2012).

[176] S. D. Jackson, Nat. Photonics **6**, 423 (2012).

[177] A. Chong, J. Buckley, W. H. Renninger and F. W. Wise, J. Opt. Soc. Am. B **25**, 140(2008).

[178] http://www.laserfocusworld.com/articles/print/volume-48/issue-04/features/the-state-of-the-art.html.

[179] https://www.industrial-lasers.com/articles/print/volume-30/issue-1/features/fiber-lasers-continue-growth-streak-in-2014-laser-market-revenues-increase-despite-mixed-global-manufacturing-growth.html.

[180] E. Ding, H. N. Chan, K. W. Chow, K. Nakkeeran and B. A. Malomed, EPL, **119**, 54002 (2017).

[181] X. Zhang , F. Li , K. Nakkeeran , J. Yuan, Z. Kang, J. N. Kutz and P. K. A. Wai, IEEE J. Sel. Top. Quantum **24**, 1101309 (2018).

[182] P. W. Smith, Proceedings of the IEEE **58**, 1342 (1970).

[183] J. Wang, X. Bu, R. Wang, L. Zhang, J. Zhu, H. Teng, H. Han, and Z. Wei, Appl. Opt. **53**, 5088 (2014).

[184] Y. H. Zhong, Z. X. Zhang, and X. Y. Tao, Laser Phys. **20**, 1756 (2010).

[185] Z. Wu, D. Liu, S. Fu, L. Li, M. Tang, and L. Zhao, Opt. Express **24**, 18764 (2016).

[186] D. Mao, B. Jiang, X. Gan, C. Ma, Y. Chen, C. Zhao, H. Zhang, J. Zheng, and J. Zhao, Photon. Res. **3**, A43 (2015).

[187] H. Zhang, D. Y. Tang, X. Wu, and L. M. Zhao, Opt. Express **17**, 12692 (2009).

[188] K. Wu, X. Zhang, J. Wang, and J. Chen, Opt. Lett. **40**, 1374 (2015).

[189] Q. Wang, Y. Chen, L. Miao, G. Jiang, S. Chen, J. Liu, X. Fu, C. Zhao, and H. Zhang, Opt. Express **23**, 7681 (2015).

[190] K. Tamura, E. P. Ippen, H. A. Haus, and L. E. Nelson, Opt. Lett. **18**, 1080 (1993).

[191] K. Tamura, E. P. Ippen, and H. A. Haus, Appl. Phys. Lett. **67**, 158 (1995).

[192] H. Lim, F. O. Ilday, and F. W. Wise, Opt. Express **10**, 1497 (2002).

[193] P. K. Datta, R Pradhan, L. Mishra and S. Saha, IET Optoelectron. **5**, 77 (2011).

[194] S. P. Singh, V. Mishra, P. K. Datta and S. K. Varshney, J. Lightwave Technol. **33**, 55 (2015).

[195] F. M. Knox, W. Forysiak, and N. J. Dorm, J. Lightwave Technol **13**, 1955 (1995).

[196] A. Hasegawa, Y. Kodama and A. Maruta, Opt. Fiber Tech. **3**, 197 (1997).

[197] S. K. Turitsyn, E. G. Shapiro, S. B. Medvedev, M. P. Fedoruk and V. K. Mezentsev, Comptes Rendus Physique **4**, 145 (2003).

[198] T. I. Lakoba, J. Yang, D. J. Kaup and B. A. Malomed, Opt. Commun. **149**, 366 (1998).

[199] B. A. Malomed, Opt. Lett. **23**, 1250 (1998).

[200] T. F. Carruthers, I. N. Duling III, M. Horowitz and C. R. Menyuk, Opt. Lett. **25**, 153 (2000).

[201] J. W. Nicholson and M. Andrejco, Opt. Express **14**, 8160 (2006).

[202] N. Nishizawa, Y. Nozaki, E. Itoga, H. Kataura and Y. Sakakibara, Opt. Express **19**, 21874 (2011).

[203] B. G. Bale, S. Boscolo, and S. K. Turitsyn, Opt. Lett. **34**, 3286 (2009).

[204] K. Porsezian, A. Hasegawa, V. N. Serkin, T. L. Belyaeva and R. Ganapathy, Phys. Lett. A **361**, 504 (2007).

[205] H. Zhang, D. Y. Tang, L. M. Zhao, X. Wu and H. Y. Tam, Opt. Express **17**, 455 (2009).

[206] B. A. Malomed and A. Berntson, J. Opt. Soc. Am. B **18**, 1243 (2001).

[207] S. Konar, M. Mishra and S. Jana, Fiber Integr. Opt. **24**, 537 (2005).

[208] R. Radhakrishnan, A. Kundu and M. Lakshmanan, Phys. Rev. E **60**, 3314(1999).

[209] K. Bhambri, G. S. Parmar, N. Gupta, D. Deb and S. Jana, Opt. Quant. Electron. **49**, 376 (1-21) (2017).

[210] S. Jana, Shivani, G. S. Parmar, B. Kaur, Q. Zhou, A. Biswas and M. Belic, Optoelec. Adv. Mat.-Rapid Commun. **10**, 143 (2016).

[211] G. S. Parmar, S. Jana and B. A. Malomed, J. Opt. Soc. Am. B **34**, 850 (2017).

[212] D. J. Kaup, B. A. Malomed and J. Yang, J. Opt. Soc. Am. B **16**, 1628 (1999).

[213] M. Mishra, S. Konar, PIER **78**, 301 (2008).

[214] Y. Kodama, M. Romagnoli, S. Wabnitz and M. Midrio, Optics Letters **19**, 165 (1994).

[215] Z. Xu, L. Li, Z. Li and G. Zhou, Optics Communication **210**, 375 (2002).

[216] S. Roy and S. Bhadra, Journal of Nonlinear Optical Physics & Materials **16**, 119 (2007).

[217] S. Zhang, G. Zhao, A. Luo and Z. Zhang, Applied Physics B **94**, 227 (2009).

[218] S. Roy, S. Bhadra and G. P. Agrawal, Phys. Rev. A **79**, 023824 (2009).

[219] D. Pal, S. G. Ali and B. Talukdar, Pramana **72**, 939 (2009).

[220] B. G. Bale and S. Boscolo, Journal of Optics **12**, 015202 (2010).

[221] M. Kolobov, A. Mussot, A. Kudlinski, E. Louvergneaux and M. Taki, Phys. Rev. A **83**, 035801 (2011).

[222] M. I. Carvalho and M. Facao, Physics Letters **376**, 950 (2012).

[223] J. Santhanam and G. P. Agrawal, Optics Communications **222**, 413 (2003).

[224] X. Shi, L. Li, R. Hao, Z. Li and G. Zhou, Optics Communication **241**, 185 (2004).

[225] L. Song, X. Shi, W. Xue, Z. Li and G. Zhou, Optics Communication **246**, 495 (2004).

[226] S. C. V. Latas and M. F. S. Ferreira, Optics Communications **251**, 415 (2005).

APPENDIX-I

Derivation of Goverening Equation

The governing equation of the systems considered in this thesis are complax (CGLE) which can be viewed as perturbed NLSE.

Following is the method to derivation of simple perturbed NLSE. The propagation of light pulse through optical fibers is governed by famous Maxwell's equations:

$$\vec{\nabla} \cdot \vec{D} = \rho_f \tag{A.1}$$

$$\vec{\nabla} \cdot \vec{B} = 0 \tag{A.2}$$

$$\vec{\nabla} \times \vec{E} = -\frac{\partial \vec{B}}{\partial t} \tag{A.3}$$

$$\vec{\nabla} \times \vec{H} = \vec{J} + \frac{\partial \vec{D}}{\partial t} \tag{A.4}$$

Where, $\vec{E}$ is the electric field vector and $\vec{H}$ is the magnetic field vector, $\vec{J}$ is the current density and ρ_f is the free charge density in the medium. The electric flux density $\vec{D}$, arising due to the electric field $\vec{E}$ of the propagating light pulse inside the medium, is given by:

$$\vec{D} = \epsilon_0 \vec{E} + \vec{P} \tag{A.5}$$

The magnetic flux density $\vec{B}$, arising due to magnetic field $\vec{H}$ of the propagating light pulse inside the medium, is given by:

$$\vec{B} = \mu_0 \vec{H} + \vec{M} \tag{A.6}$$

where, ϵ_0 is the vacuum permittivity, $\vec{P}$ is the electric polarization, μ_0 is the vacuum permeability and $\vec{M}$ is the magnetic polarization. Since there is no free charge in optical fiber, $\vec{J}$ and ρ_f are zero. The Maxwell's equations reduce to:-

$$\vec{\nabla} \cdot \vec{D} = 0 \tag{A.7}$$

$$\vec{\nabla} \cdot \vec{B} = 0 \tag{A.8}$$

$$\vec{\nabla} \times \vec{E} = -\frac{\partial \vec{B}}{\partial t} = -\mu_0 \frac{\partial \vec{H}}{\partial t} \tag{A.9}$$

$$\vec{\nabla} \times \vec{H} = \frac{\partial \vec{D}}{\partial t} \tag{A.10}$$

Now, taking curl of Maxwell Equation A.9,

$$\vec{\nabla} \times \vec{\nabla} \times \vec{E} = -\mu_0 \frac{\partial}{\partial t}(\vec{\nabla} \times \vec{H}) \tag{A.11}$$

$$\vec{\nabla} \times \vec{\nabla} \times \vec{E} = -\mu_0 \frac{\partial^2 \vec{D}}{\partial t^2} \tag{A.12}$$

Solving LHS of above equation

$$\vec{\nabla}(\vec{\nabla} \cdot \vec{E}) - \nabla^2 \vec{E} = -\mu_0 \frac{\partial^2 \vec{D}}{\partial t^2} \tag{A.13}$$

Using Eqn. (A.5),

$$\vec{\nabla}(\vec{\nabla} \cdot \vec{E}) - \nabla^2 \vec{E} = -\mu_0 \frac{\partial^2 (\epsilon_0 \vec{E})}{\partial t^2} + \mu_0 \frac{\partial^2 \vec{P}}{\partial t^2} \tag{A.14}$$

Due to centrosymmetric nature of SiO_2, the optical fiber material, even order terms of χ are absent. Most significant nonlinearity in optical fibers is kerr nonlinearity or third order nonlinearity ($\chi^{(3)}$). So, electric polarization $\vec{P}$ can be written as:

$$\vec{P} = \epsilon_0 \left[\chi^{(1)} \vec{E} + \chi^{(3)} \mid E \mid^2 E + ... \right]$$

Neglecting higher order nonlinear terms, and consider only kerr nonlinearity, we get

$$\vec{P} = \epsilon_0 \left[\chi^{(1)} \vec{E} + \chi^{(3)} \mid E \mid^2 E \right] \tag{A.15}$$

Now solving Eqn. (A.14),

$$\vec{\nabla}(\vec{\nabla} \cdot \vec{E}) - \nabla^2 \vec{E} = -\mu_0 \frac{\partial^2 (\epsilon_0 \vec{E})}{\partial t^2} + \mu_0 \frac{\partial^2 \vec{P_L}}{\partial t^2} + \mu_0 \frac{\partial^2 \vec{P_{NL}}}{\partial t^2} \tag{A.16}$$

Rearranging the equation,

$$\nabla^2 \vec{E} - \frac{1}{c^2} \frac{\partial^2 \vec{E}}{\partial t^2} = \mu_0 \frac{\partial^2 \vec{P_L}}{\partial t^2} + \mu_0 \frac{\partial^2 \vec{P_{NL}}}{\partial t^2} \tag{A.17}$$

The electric field $\vec{E}$ can be written as a product of amplitude part and phase part,

$$\vec{E}(\vec{r}, t) = \frac{1}{2} \hat{x} \left[E(\vec{r}, t) \times exp(-i\omega_0 t) + c.c. \right] \tag{A.18}$$

where, $\hat{x}$ is polarization vector, $E(\vec{r}, t)$ is slowly varying envelope, $exp(-i\omega_0 t)$ is rapidly varying part and *c.c.* stands for complex conjugate. The electric polarization can be written as: The electric field $\vec{E}$ can be written as a product of amplitude part and phase part,

$$\vec{P_L}(\vec{r}, t) = \frac{\hat{x}}{2} \left[\vec{P_L}(\vec{r}, t) \times exp(-i\omega_0 t) + c.c. \right] \tag{A.19}$$

$$\vec{P_{NL}}(\vec{r}, t) = \frac{\hat{x}}{2} \left[\vec{P_{NL}}(\vec{r}, t) \times exp(-i\omega_0 t) + c.c. \right] \tag{A.20}$$

For convenience we derive the propagation equation in Fourier domain. The Fourier

transform (FT) of electric field $\vec{E}(\vec{r},t)$ can be written as:

$$\tilde{E}(r,\omega-\omega_0)=\int_{-\infty}^{\infty}\vec{E}(\vec{r},t)\times exp\left[i(\omega-\omega_0 t)\right]dt \tag{A.21}$$

In frequency domain, the electric field i.e. Eqn. (A.17) can be written as:

$$\nabla^2\tilde{E}+{K_0}^2\tilde{E}=-\mu_0\omega^2\left[\vec{P}_L+\vec{P}_{NL}\right] \tag{A.22}$$

$$\nabla^2\tilde{E}+{K_0}^2\tilde{E}=-\mu_0\omega^2\epsilon_0\left[\chi^{(1)}\tilde{E}+\chi^{(3)}:\tilde{E}\tilde{E}\tilde{E}\right] \tag{A.23}$$

$$\nabla^2\tilde{E}+{K_0}^2\tilde{E}=-{K_0}^2\left[\chi^{(1)}\tilde{E}+\chi^{(3)}:\tilde{E}\tilde{E}\tilde{E}\right] \tag{A.24}$$

$$\nabla^2\tilde{E}+{K_0}^2\epsilon(\omega)\tilde{E}=0 \tag{A.25}$$

where, $K_0=\frac{\omega}{c}$ and $\epsilon(\omega)=1+\tilde{\chi}^{(1)}+\epsilon_{NL}=n^2$ and $\epsilon_{NL}=\frac{3}{4}\chi^{(3)}\mid E(r,t)\mid^2$. The above equation is known as Helmholtz equation, which can be solved using method of separation of variables. The Fourier transformed solution can be written as:

$$\tilde{E}(r,\omega_0)=F(x,y)\tilde{A}(z,\omega_0)exp(i\beta_0 z) \tag{A.26}$$

where, $F(x,y)$ is the mode structure and $\tilde{A}(z,\omega_0)$ is the temporal structure of pulse. Using this solution, Helmholtz equation can be solved as:

$$\nabla^2F(x,y)\tilde{A}(z,\omega_0)exp(i\beta_0 z)+{K_0}^2\epsilon(\omega)F(x,y)\tilde{A}(z,\omega_0)exp(i\beta_0 z)=0 \tag{A.27}$$

Solve this equation by adding and subtracting $\tilde{\beta}^2F(x,y)A(z,\omega-\omega_0)exp(i\beta_0 z)$, we get

$$F_x^{"}+F_y^{"}+\left[\epsilon(\omega){K_0}^2-\tilde{\beta}^2\right]F=0 \tag{A.28}$$

$$2i\beta_0{A_z}'(\omega-\omega_0)+(\tilde{\beta}^2-\tilde{\beta_0}^2)\tilde{A}=0 \tag{A.29}$$

Using first order perturbation theory, the dielectric constant ϵ can be written as:

$$\epsilon=(n+\Delta n)^2\approx n^2+2n\Delta n \tag{A.30}$$

Where, Δn is small perturbation to refractive index term and is written as:

$$\Delta n=n_2\mid E\mid^2+\frac{i\tilde{\alpha}}{2K_0} \tag{A.31}$$

Where, $\tilde{\alpha}$ is absorption coefficient. The eigen value wave number becomes

$$\tilde{\beta}(\omega)=\beta(\omega)+\Delta\beta \tag{A.32}$$

Where,

$$\Delta\beta=\frac{K_0\int\int_{-\infty}^{\infty}\Delta n\mid F(x,y)\mid^2 dxdy}{\int\int_{-\infty}^{\infty}\mid F(x,y)\mid^2 dxdy} \tag{A.33}$$

Fourier transform of $\tilde{E}(r,\omega-\omega_0)$ is

$$E(r,t)=\frac{\hat{x}}{2}\left\{F(x,y)A(z,t)exp(i(\beta_0 z-\omega_0 t))+c.c.\right\} \tag{A.34}$$

Following some little algebraic simplification on equation,

$$2i\beta_0\frac{\partial\tilde{A}}{\partial z}+(\tilde{\beta}^2-{\beta_0}^2)=0 \tag{A.35}$$

Using Eqn. (A.32), the above equation can be written as

$$\frac{\partial \tilde{A}}{\partial z} = i[\beta(\omega) + \Delta\beta - \beta_0]\tilde{A} \tag{A.36}$$

Using Taylor series expansion of frequency dependent wave number as:

$$\beta(\omega) = \beta_0 + (\omega - \omega_0)\beta_1 + \frac{1}{2}(\omega - \omega_0)^2\beta_2 + ... \tag{A.37}$$

where,

$$\beta_m = \left[\frac{d^m\beta}{d\omega^m}\right]_{\omega=\omega_0} (m = 1, 2, ...).$$

Substituting Eqn. A.37 in Eqn. A.36 and taking the inverse Fourier transform by using:

$$A(z,t) = \frac{1}{2\pi}\int_{-\infty}^{\infty} \tilde{A}(z, \omega - \omega_0)exp(-i(\omega - \omega_0)t)d\omega \tag{A.38}$$

Eqn. A.36 can be written as:

$$\frac{\partial A}{\partial z} = i\left[i\beta_1\frac{\partial}{\partial t} - \frac{\beta_2}{2}\frac{\partial^2}{\partial t^2} + \Delta\beta\right]A \tag{A.39}$$

$$\frac{\partial A}{\partial z} + \beta_1\frac{\partial A}{\partial t} + \frac{i\beta_2}{2}\frac{\partial^2 A}{\partial t^2} = i\Delta\beta A \tag{A.40}$$

Here $\Delta\beta$ contains both nonlinear and fiber loss effects. Subsituting Eqn. A.31 in Eqn. A.33 and substituting for $\Delta\beta$ in Eqn. A.40, we get

$$\frac{\partial A}{\partial z} + \beta_1\frac{\partial A}{\partial t} + \frac{i\beta_2}{2}\frac{\partial^2 A}{\partial t^2} + \frac{\alpha}{2}A = i\gamma \mid A \mid^2 A \tag{A.41}$$

where, γ is nonlinear parameter and is defined as $\gamma = \frac{\omega_0 n_2}{cA_{eff}}$. The parameter A_{eff} is known as effective core area and is given by

$$A_{eff} = \frac{(\int\int_{-\infty}^{\infty} \mid F(x,y) \mid^2 dxdy)^2}{\int\int_{-\infty}^{\infty} \mid F(x,y) \mid^4 dxdy} \tag{A.42}$$

The parameter A_{eff} depends on core radius and core-cladding index difference of fiber. As the pulse envelop propagates slowly along the fiber. Using a transformation $t' = t - z/v_g = t - \beta_1 z$, into Eqn. A.41, we get

$$\frac{\partial A}{\partial z} + \frac{i\beta_2}{2}\frac{\partial^2 A}{\partial t^2} + \frac{\alpha}{2}A = i\gamma \mid A \mid^2 A. \tag{A.43}$$

The above equation describes the propagation of optical pulse in a single-mode fiber. It is often referred as nonlinear Schrödinger equation. Here α is fiber loss, β_2 is GVD coefficient and γ is cubic-nonlinearity coefficient. If we consider higher order nonlinear terms as well. So Eqn. A.31 becomes

$$\Delta n = n_2 \mid E \mid^2 + \frac{i\tilde{\alpha}}{2K_0} + n_4 \mid E \mid^4, \tag{A.44}$$

and the corresponding NLSE can be written as

$$\frac{\partial A}{\partial z} + \beta_1 \frac{\partial A}{\partial t} + \frac{i\beta_2}{2}\frac{\partial^2 A}{\partial t^2} - i\gamma \mid A \mid^2 A + \frac{\alpha}{2}A - iQ \mid A \mid^4 A = 0 \tag{A.45}$$

where, Q is the quintic nonlinearity coefficient. If we consider the χ value in Eqn. A.15 as complex, the imaginary parts will lead to the nonlinear loss terms. The resultant equation will take the following form:

$$i\frac{\partial A}{\partial z} + \frac{1}{2}\frac{\partial^2 A}{\partial t^2} + \mid A \mid^2 A + \gamma \mid A \mid^4 A = i(g_0 - \alpha)A + iK \mid A \mid^2 A + i\nu \mid A \mid^4 A \tag{A.46}$$

where, K and ν represents the cubic and quintic nonlinear loss coefficients. The above equation is called perturbed cubic-quintic nonlinear Schrödinger equation.

APPENDIX-II

Formation of soliton from different initial pulse profile

Generally, theoretical investigation consider, ideal pulse shape like sech or Gaussian ones. A practical radiation source may not excite these ideal profiles at the very first hand. Rather, multimode source will radiate a profile close to super-Gaussian ones.

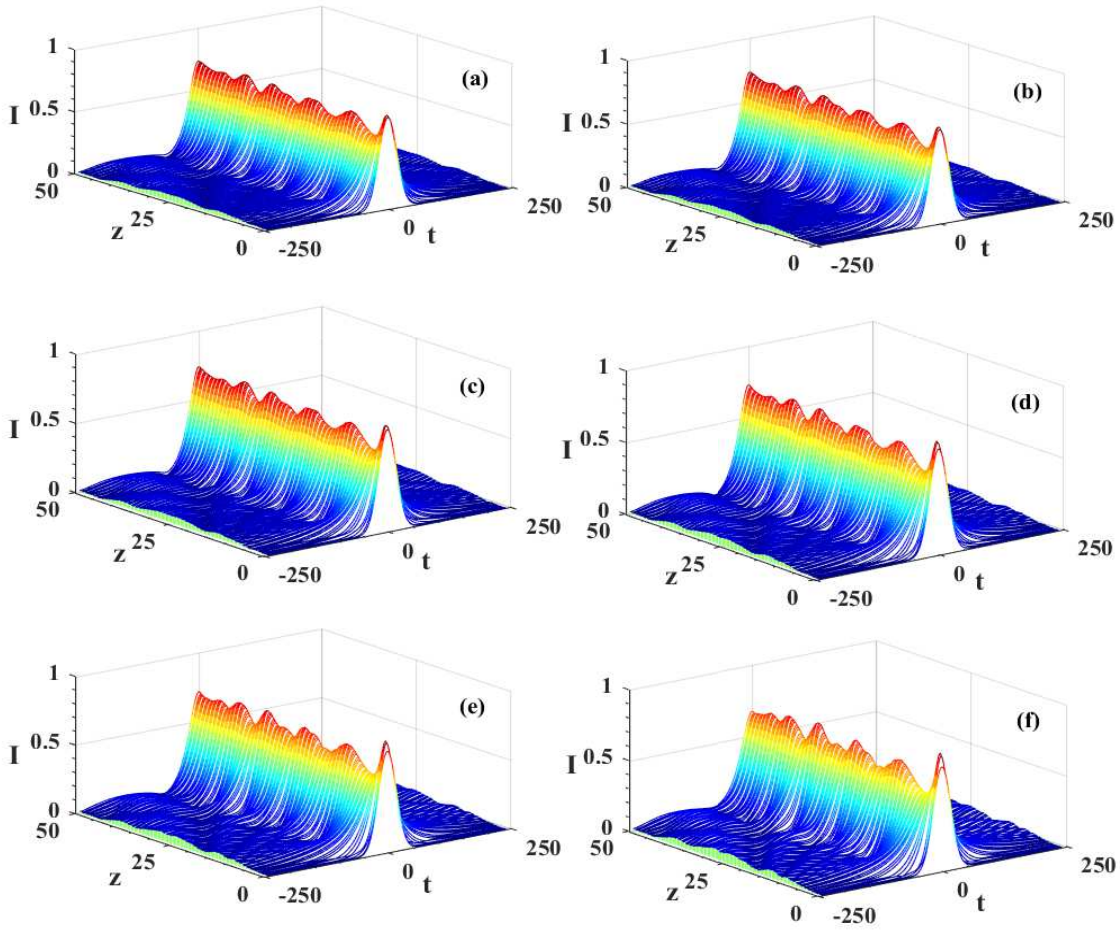

Fig. A.1: Evolution of solitonic Gaussian pulse ($m = 1$) under the combined effect of TPA, 3PA and gain dispersion for different values of chirp (c). For (a) c = 0.01, (b) c = 0.05, (c) c = 0.1 (d) c = 0.2 (e) c = 0.3 and (f) c = 0.4. The parameters are γ = -0.001, $d = 0.05$, $\nu = 0.01$ and $K = 0.01$.

Here we elaborate the soliton formation with different pulse shapes e.g., Gaussian, super-Gaussian, cosh-Gaussian and cosh super-Gaussian. To study the generation of soliton from a super-Gaussian pulse, we consider the super-Gaussian ansatz of following form:

$$E(z,t) = Aexp\left[-\frac{1+ic}{2}\left(\frac{t}{W}\right)^{2m}\right] \tag{A.47}$$

where, A, W and c represents pulse amplitude, temporal width and chirp respectively. Figures A.1, A.2 and A.3 depicts the soliton formation for TPA, 3PA and in presence of both TPA and 3PA.

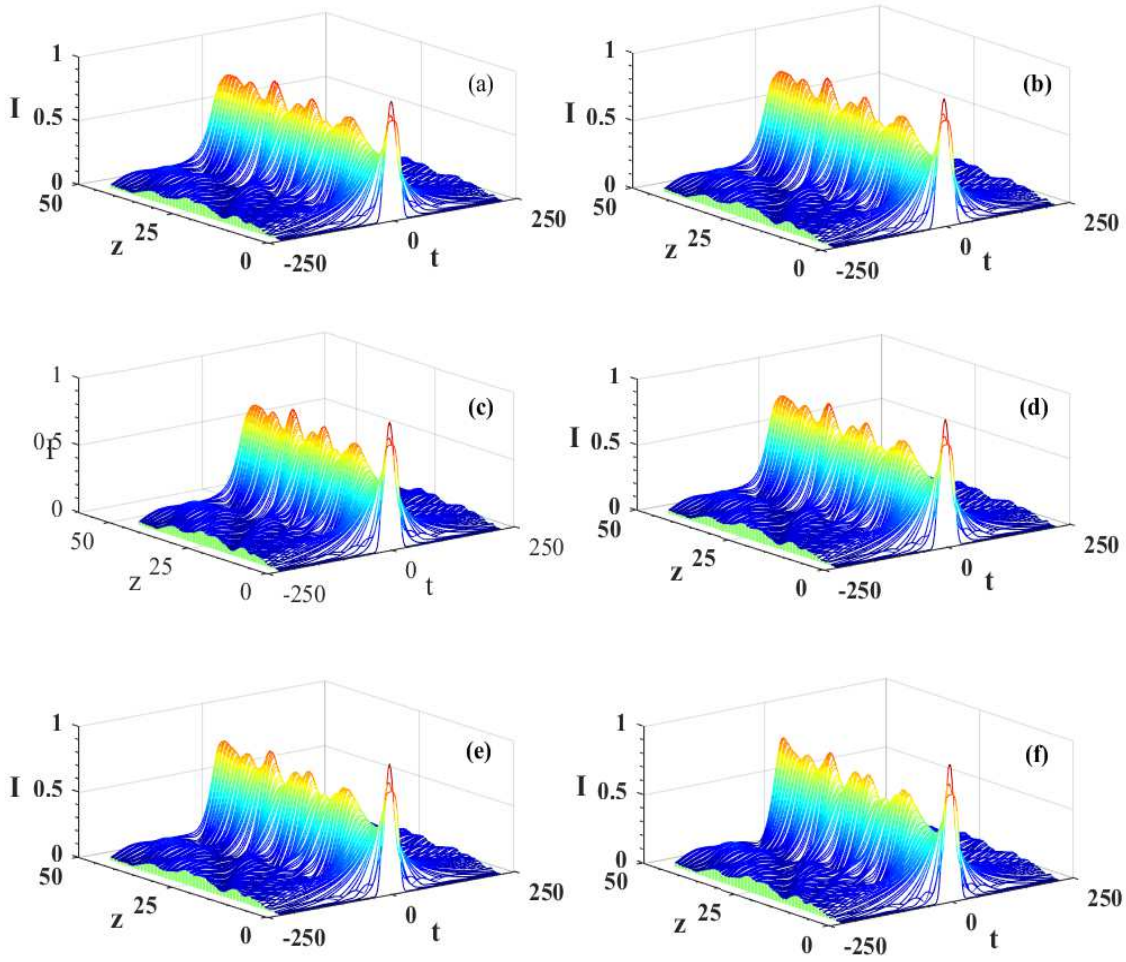

Fig. A.2: Evolution of super-Gaussian pulse ($m = 2$) under the combined effect of TPA, 3PA and gain dispersion for different values of chirp (c). For (a) c = 0.01, (b) c = 0.05, (c) c = 0.1 (d) c = 0.2 (e) c = 0.3 and (f) c = 0.4. The parameters are γ = -0.001, $d = 0.05$, $\nu = 0.01$ and $K = 0.01$.

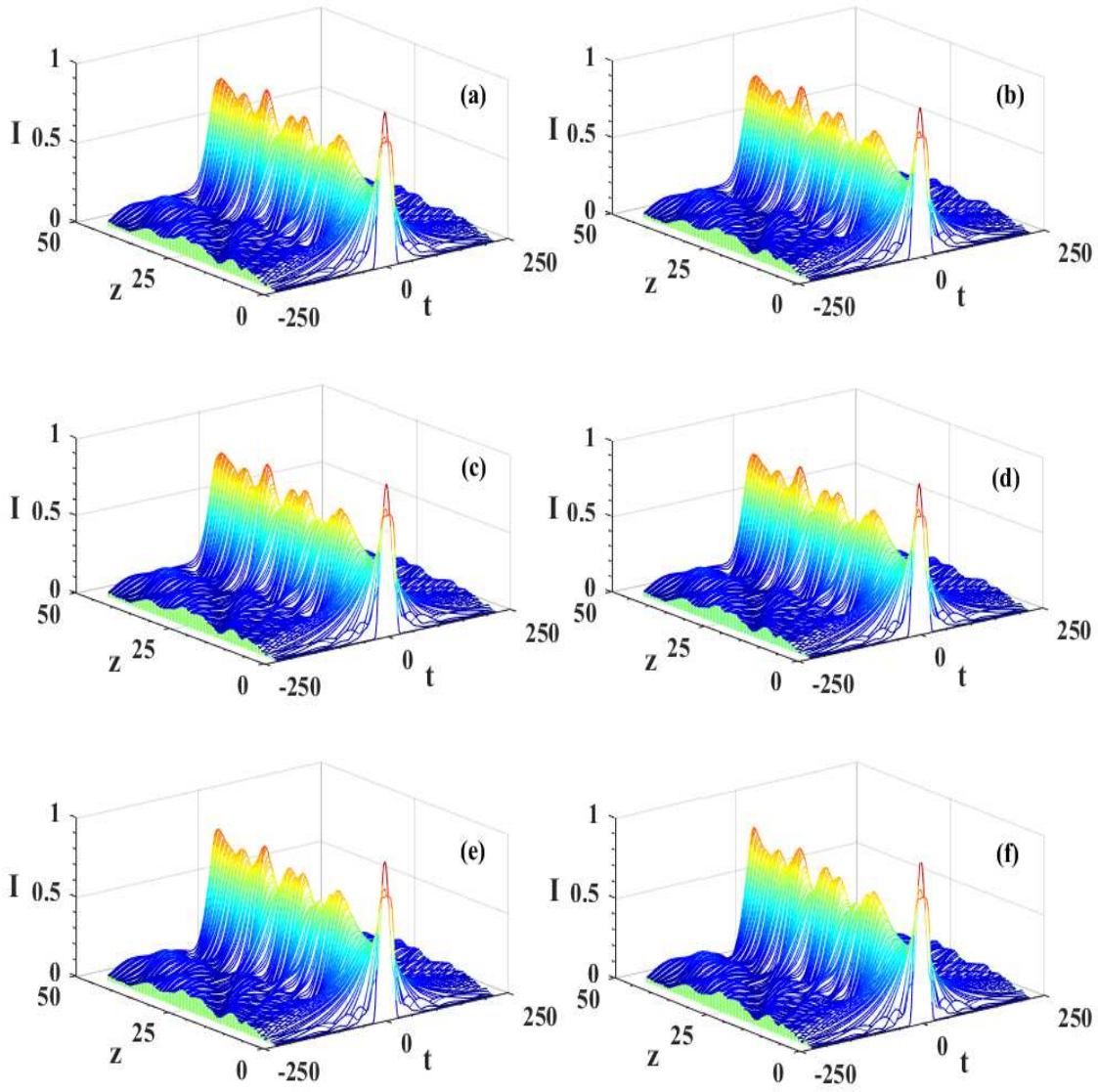

Fig. A.3: Evolution of super-Gaussian pulse ($m = 3$) under the combined effect of TPA, 3PA and gain dispersion for different values of chirp (c). For (a) c = 0.01, (b) c = 0.05, (c) c = 0.1 (d) c = 0.2 (e) c = 0.3 and (f) c = 0.4. The parameters are γ = -0.001, $d = 0.05$, $\nu = 0.01$ and $K = 0.01$.

It is evident from the figures that after an initial shape adjustment the incident pulse quickly attains bell-shaped solitonic shape and then executes steady state propagation with oscillations in the pulse amplitude. Higher order super-Gaussian pulses, which are of flat-top profiles, also first change to bell-shaped profile and thereafter propagate with oscillations in the pulse amplitude. The oscillations are result of the presence of quintic nonlinearity and chirp in the system. As we increase the value of chirp, oscillations in

pulse amplitude become more prominent also more gain supply it needed to sustain solitonic structure. As higher order pulse possesses more energy and hence requires more gain for soliton generation.

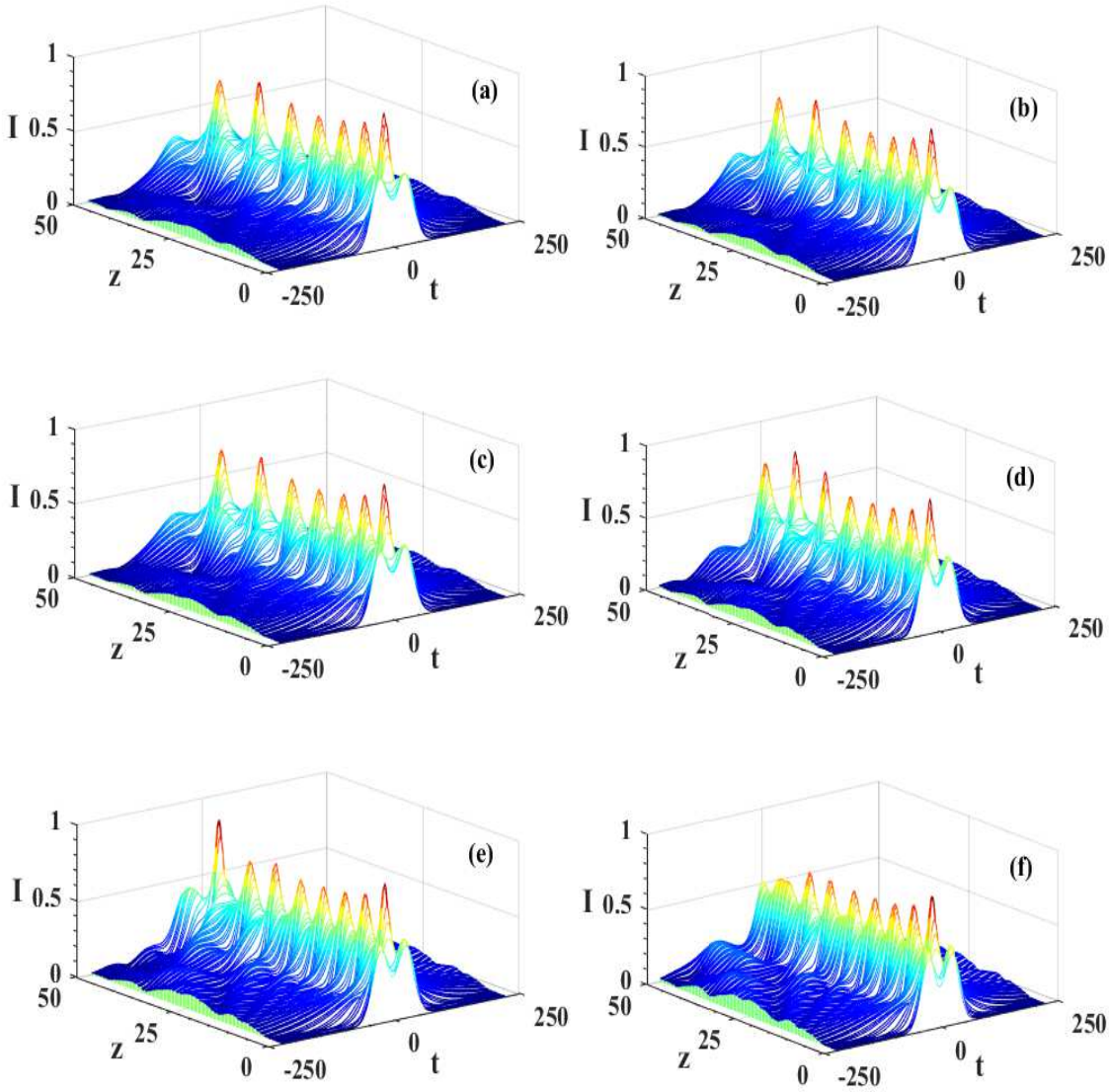

Fig. A.4: Evolution of cosh-Gaussian pulse ($m = 1$) under the combined effect of TPA, 3PA and gain dispersion for different values of chirp (c). For (a) c = 0.01, (b) c = 0.05, (c) c = 0.1 (d) c = 0.2 (e) c = 0.3 and (f) c = 0.4. The parameters are γ = -0.001, $d = 0.05$, $\nu = 0.01$ and $K = 0.01$.

Also, the incident pulse reshaping to a solitonic profile is accompanied by the excess energy radiations leading to the side band oscillations, which is prominent for all super-Gaussian cases. The greater the super-Gaussian parameter, i.e., greater difference from

the solitonic shape, the higher the radiation.

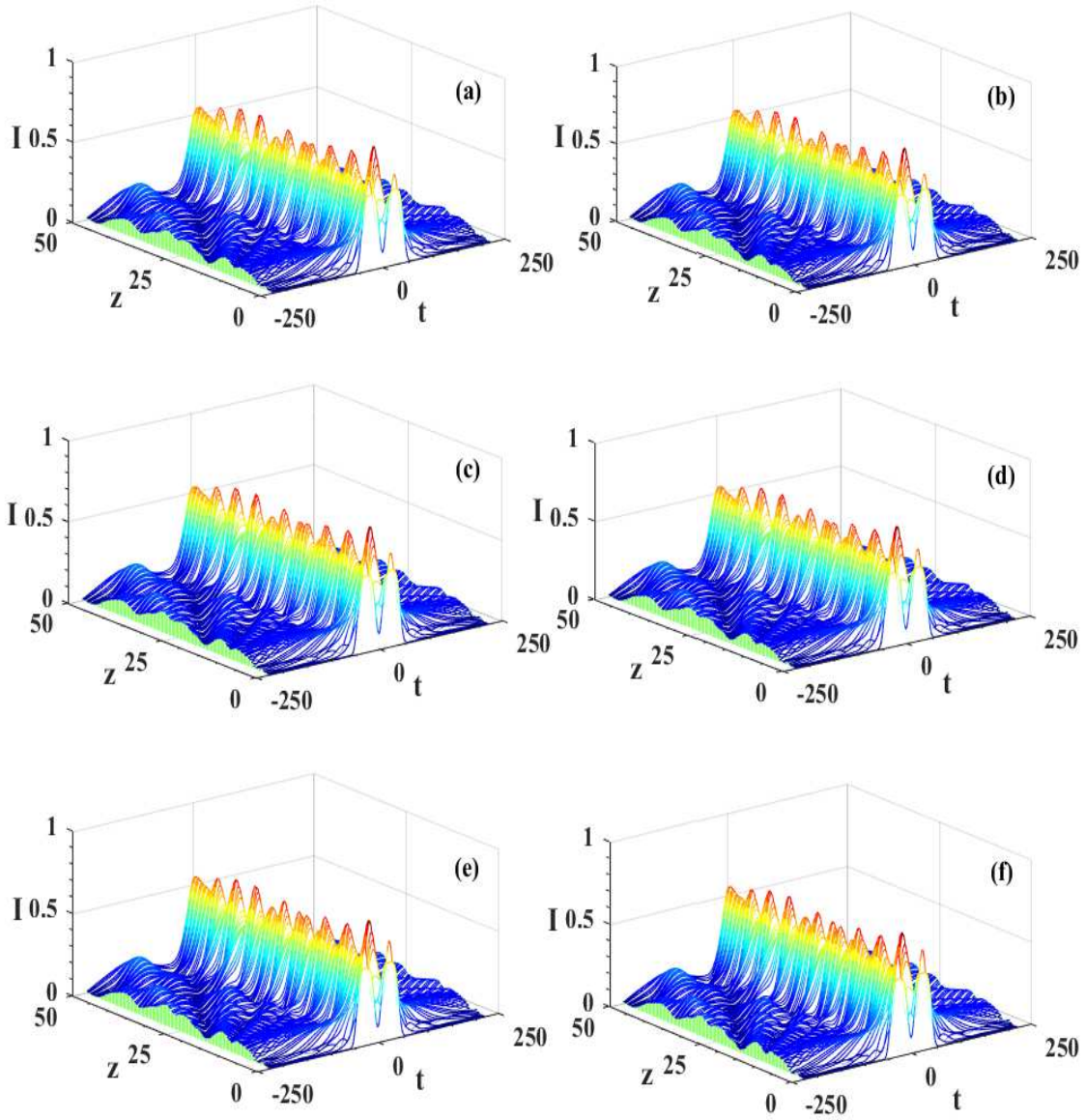

Fig. A.5: Evolution of cosh super-Gaussian pulse ($m = 2$) under the combined effect of TPA, 3PA and gain dispersion for different values of chirp (c). For (a) c = 0.01, (b) c = 0.05, (c) c = 0.1 (d) c = 0.2 (e) c = 0.3 and (f) c = 0.4. The parameters are γ = -0.001, $d = 0.05$, $\nu = 0.01$ and $K = 0.01$.

When two Gaussian (super-Gaussian) decentered pulses superpose, a cosh-Gaussian pulse (cosh super-Gaussian) is generated. A cosh-Gaussian pulse, when attempted to transform into a soliton pulse, first radiates some energy and accomodates its shape into a bell-shaped solitonic pulse (Fig. A.4). For cosh super-Gaussian pulse also, one can get soliton after significant amount of radiation as shown in Figs. A.5, A.6. However in

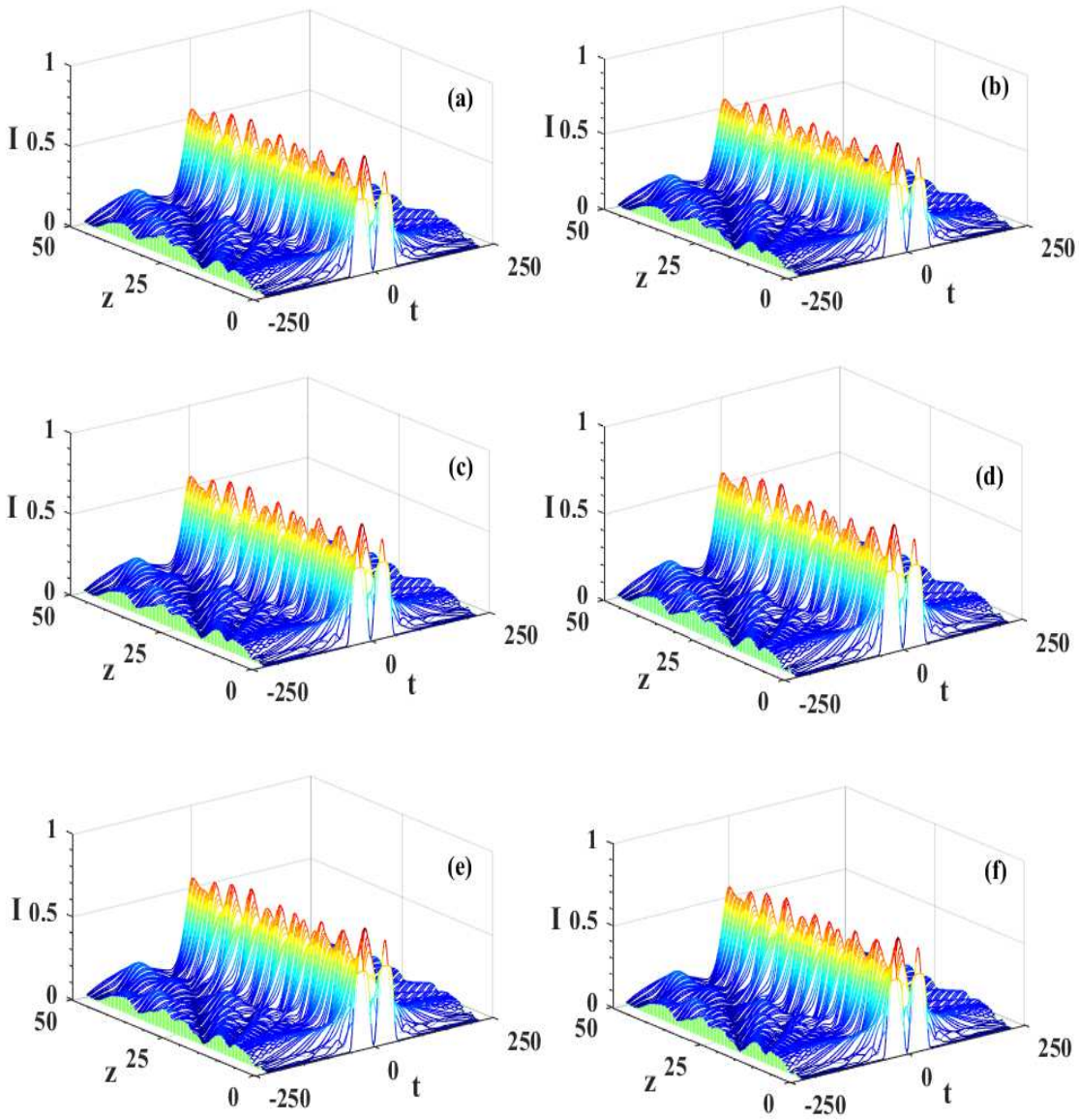

Fig. A.6: Evolution of cosh super-Gaussian pulse ($m = 3$) under the combined effect of TPA, 3PA and gain dispersion for different values of chirp (c). For (a) c = 0.01, (b) c = 0.05, (c) c = 0.1 (d) c = 0.2 (e) c = 0.3 and (f) c = 0.4. The parameters are γ = -0.001, $d = 0.05$, $\nu = 0.01$ and $K = 0.01$.

only few cases, a flattop soliton in both super-Gaussian and cosh-Gaussian cases can be observed (not shown here).